



THE HONG KONG
POLYTECHNIC UNIVERSITY

香港理工大學

Pao Yue-kong Library

包玉剛圖書館

Copyright Undertaking

This thesis is protected by copyright, with all rights reserved.

By reading and using the thesis, the reader understands and agrees to the following terms:

1. The reader will abide by the rules and legal ordinances governing copyright regarding the use of the thesis.
2. The reader will use the thesis for the purpose of research or private study only and not for distribution or further reproduction or any other purpose.
3. The reader agrees to indemnify and hold the University harmless from and against any loss, damage, cost, liability or expenses arising from copyright infringement or unauthorized usage.

IMPORTANT

If you have reasons to believe that any materials in this thesis are deemed not suitable to be distributed in this form, or a copyright owner having difficulty with the material being included in our database, please contact lbsys@polyu.edu.hk providing details. The Library will look into your claim and consider taking remedial action upon receipt of the written requests.

**OPERATING FUEL CELLS WITH AN
ELECTRICALLY RECHARGEABLE
LIQUID FUEL**

**OLADAPO CHRISTOPHER ESAN
PhD**

The Hong Kong Polytechnic University

2023

The Hong Kong Polytechnic University

Department of Mechanical Engineering

**Operating Fuel Cells with An Electrically
Rechargeable Liquid Fuel**

Oladapo Christopher Esan

**A thesis submitted in partial fulfilment of the
requirements for the degree of Doctor of Philosophy**

November 2022

CERTIFICATE OF ORIGINALITY

I hereby declare that this thesis is my own work and that, to the best of my knowledge and belief, it reproduces no material previously published or written, nor material that has been accepted for the award of any other degree or diploma, except where due acknowledgement has been made in the text.

Oladapo Christopher ESAN

Acknowledgements

I am most grateful to God, the custodian and giver of knowledge and wisdom, for seeing me through these memorable four years of my Ph.D. programme. I gratefully acknowledge the grace, blessings, and favor He bestowed upon me. Thanks be to God for the sound health and strength to successfully complete this journey.

My heartfelt gratitude goes to my Chief supervisor, Prof. Liang An, for introducing me to this field of study. Even though my progress was a bit slow at the beginning of this journey, his encouraging words and intentional dedication to my success made me realize that initial struggle is part of the learning process. His excellent and inspiring supervision has offered me comprehensive and thorough understanding necessary to gainfully explore the research field with richly rewarding experience. My Ph.D. research and thesis writing would not have been completed without his committed and consistent participation in every stage of the process. Thank you very much for your exemplary patience, immense support, intellectual guidance, and constructive criticism since the inception of my Ph.D. study. Thank you for always reading and correcting my research articles and the several beneficial opportunities you have exposed me to. Your fundamental and detailed approaches to research are inspiring and beyond comparison. You made the Ph.D. journey worthwhile and remarkable for me.

I also extend my gratitude to my Co-supervisor Prof. Hui Tang for his support during this Ph.D. programme. I am indebted to Prof. T.S. Zhao (Department of Mechanical and Aerospace Engineering, HKUST), for his

novel ideas and significant contributions to my research. I cannot but greatly appreciate Prof. Jiyun ZHAO (Department of Mechanical Engineering, CityU) and Prof. Chao Xu (Department of Energy Power and Mechanical Engineering, NCEPU) for the time taken to review my thesis, provide helpful comments and suggestions, and serve as members of my thesis examination committee.

Special thanks also go to the technical and administrative staffs of the Department of Mechanical Engineering at the Hong Kong Polytechnic University for their various support. I would like to particularly thank Mr. Benny Chi-kuen LEUNG for his friendly conversations and advice whenever I work in the laboratories. I would also like to appreciate Ms. Lily TAM, Mrs. Michelle LAI, Ms. Merlin WONG, and Ms. Yan WONG, for their eagerness to attend to my needs whenever I visit the departmental office.

My appreciation also goes to our research group members - Dr. Xiangyu SU, Dr. Zhefei PAN, Dr. Ruihan ZHANG, Dr. Guangzhe LI, Dr. Xingyi SHI, Mr. Yun LIU, Ms. Xiaoyu HUO, and all the newly recruited members for their enlightening discussions, various contributions, and assistance towards the success of my PhD research works. I must appreciate Dr. Xingyi SHI for the various helps and corrections regarding my research. I must also specifically thank Mr. Yun LIU and Ms. Xiaoyu HUO for their kind and amiable assistance.

I greatly appreciate the Student Affairs Office (SAO) and PolyU Student Halls of Residence for the awesome opportunity to serve as a Tutor and later

as the Senior Tutor in LiZhi Hall of Hung Hom Hall. Special thanks to the Hall Warden, Dr. Howard KWONG, for making the tutorship experience smooth and beautiful for me. I also appreciate the various Tutors and hall residents I have worked with during this period.

I sincerely appreciate all members of Association of Nigerian scholars in Hong Kong (ANSHK), particularly the ones studying or working in PolyU, for being a true family and supportive system. I also acknowledge the privilege to serve as a member the electoral committee during the 2020/2021 and 2022/2023 ANSHK elections. Thanks to my colleagues, the HK Friends group – Miracle, Olutomilayo, Tobi, Emmanuel, Kelvin, Kayode, Lekan, Mujib, Saka, Benjamin, and Dayo, for the numerous memorable times we shared together, notably the fun trip to Macao; and the Hiking and Cycling Club for teaching me how to ride bicycles and the opportunities to explore various tourist destinations in Hong Kong. I also appreciate my amiable friends – Kehinde OYETUNDE, Timothy AKINWANDE, and Ibrahim ADENIRAN for the all-round support and amazing moments. You all made my stay in Hong Kong beautiful and enjoyable.

To all members of the RCCG in Hong Kong, especially members of Christ Apostles group, I say thank you for the brotherly love. To the choir unit of the church, thank you for the privilege to serve and all the love and care shown unto me throughout my stay in Hong Kong. My special thanks also go to Dr. Tunde and Sis. Deola OGUNDELE, Dr. Philip and Sis. Omolara BODUNDE, Bro Benjamin and Dr. (Mrs.) Mayowa ADEGORIOLA. You

have all proven to me that having a loving family apart from one's immediate home is possible.

I cannot fail to deeply appreciate Pastor Isaiah BODUNWA and Dr. (Mrs.) Oluwatoyin BODUNWA for constantly checking up on me and praying for me in their closet, even though we are thousands of miles apart. I sincerely cherish all you do for me. Thank you for all the Godly advice, insightful discussions, and words of encouragement. Your impact in my life is seen and felt.

To my siblings, Pharm. Oluwatosin ESAN and Mrs. Yewande OMOLE, thank you for your love, care, and moral support. Most importantly, all thanks to my Parents, Mr. Lawrence Ajayi ESAN and Mrs. Elizabeth Funke ESAN for the prayers, love, encouragement, and all-round support. I cannot thank you enough for all the sacrifices of love and investment in my life over the years. Long life in sound health and prosperity you shall live. Thank you for being there for me all the time.

Finally, I appreciate those I have connected with during this journey. I also thank everyone who has contributed, in one way or the other, to the success of this my Ph.D. You are blessed. Amen!

Abstract

Fuel cells are electrochemical energy conversion devices as well as clean power sources as they offer practicable and smooth means to directly convert chemical energy, available in fuels, to electrical energy. The promising capability of fuel cell technology, particularly direct liquid fuel cells, have piqued increasing research interest over the years. However, the slow reaction kinetics of conventional liquid fuels on pricey metal catalysts at the anode has largely hindered the commercial market penetration of liquid fuel cells. To address this issue, a novel system which employs an electrically rechargeable liquid fuel (e-fuel) for renewable energy storage and power generation was recently proposed. The e-fuel can be obtained from diverse range of electroactive materials and not only metal ions. An e-fuel solution, which contains vanadium ions dissolved in sulphuric acid, is therefore employed to operate fuel cells. Unlike the conventional liquid fuels, the vanadium-based e-fuel possesses superior reactivity on carbon-based electrodes, consequently eliminating catalyst materials at the anode and improving the cost effectiveness of fuel cells. In addition, the e-fuel possesses low freezing point which allows the operation of fuel cells at wide temperature range. As a result of the fascinating properties and excellent potential of this e-fuel, this thesis is focused on the experimental and numerical investigations of e-fuel cells while exploring various oxidants at the cell cathode. Firstly, the performance of the e-fuel cell is experimentally examined with the use of air as oxidant, while taking the use of oxygen as performance benchmark. The cell attains an open-circuit voltage (OCV) of 1.25 V, which is comparable to an OCV of 1.26 V obtained when pure

oxygen is employed as oxidant. A peak power density of 168.3 mW cm^{-2} , at room temperature, is obtained with the use of air as oxidant. Furthermore, an energy efficiency of 26.4 % is achieved by the e-fuel cell. Secondly, to further boost the performance of the e-fuel cell and more importantly realize its application in airtight environments, hydrogen peroxide (H_2O_2) is considered as oxidant, in lieu of gaseous oxygen or ambient air. The novel e-fuel/ H_2O_2 fuel cell exhibits an impressive peak power density of $1456.0 \text{ mW cm}^{-2}$ at $60 \text{ }^\circ\text{C}$, which is 70 % higher than the use of oxygen as oxidant. A maximum current density exceeding 3000 mA cm^{-2} is also achieved by the cell. Furthermore, the cell achieved a stable performance after it was refueled 10 times under a constant current discharge. Thirdly, a mathematical model to describe the underlying theoretical and working principle of the e-fuel cells is presented. The model is first developed for the e-fuel cells using pure oxygen as oxidant. Afterwards, the modeling framework is extended to the e-fuel cells that employ hydrogen peroxide as oxidant, where mixed potential is considered in the cathodic reactions. Lastly, numerical simulation of the model is conducted to predict and optimize the performance of the e-fuel cells.

Table of Contents

Acknowledgements.....	iii
Abstract.....	vii
Table of Contents.....	ix
List of Figures.....	xvi
List of Tables.....	xx
Nomenclature.....	xxi
Chapter 1 Introduction.....	1
1.1 Background.....	1
1.2 Fuel cells.....	2
1.3 Direct liquid fuel cells.....	3
1.3.1 Features.....	3
1.3.2 Literature review.....	3
1.3.3 Performance progress.....	6
1.3.4 Applications.....	7
1.3.5 Challenging issues.....	7
1.3.6 Electrically rechargeable liquid fuels (e-fuel).....	8
1.3.7 Working principle.....	9
1.4 Thesis objectives.....	10
1.5 References.....	13
Chapter 2 Experimental setup and characterization platform.....	16

2.1 Introduction.....	16
2.2 Cell components and assembly	16
2.2.1 Flow field designs	17
2.2.2 Preparation of anode	17
2.2.3 Preparation of cathode	17
2.2.4 Preparation of membrane	18
2.2.5 Membrane electrode assembly.....	19
2.3 Preparation of electrolytes	19
2.3.1 Preparation of electrically rechargeable liquid fuel	19
2.3.2 Preparation of hydrogen peroxide solution.....	20
2.4 Experimental setup and instruments	20
2.4.1 Fuel supply system.....	21
2.4.2 Oxidant supply system.....	21
2.4.3 Temperature control system.....	21
2.4.4 Testing systems	21
2.5 Performance evaluation	22
2.5.1 Polarization curves	22
2.5.2 Constant-current discharge performance	23
2.5.3 Long-term stability performance	23
2.5.4 Efficiencies	24
2.6 Summary	24

2.7 References.....	26
Chapter 3 Operation of fuel cells using air/oxygen as oxidant.....	27
3.1 Introduction.....	27
3.2 Operation principle of the cell	29
3.3 Experimental details.....	30
3.3.1 Membrane electrode assembly.....	30
3.3.2 Preparation of e-fuel	30
3.3.3 Experimental set-up and instruments.....	31
3.4 Results and discussion	31
3.4.1 General performance and comparison	31
3.4.2 Influence of the oxidant flow rate.....	33
3.4.3 Influence of the operating temperature	35
3.4.4 Constant-current discharge performance	37
3.4.5 Energy efficiency	39
3.5 Summary	40
3.6 References.....	42
Chapter 4 Operation of fuel cells using hydrogen peroxide as oxidant.....	54
4.1 Introduction.....	54
4.2 Operation principle of the cell	57
4.3 Experimental details.....	58
4.3.1 Membrane electrode assembly.....	58

4.3.2 Preparation of electrolytes	59
4.3.3 Fuel cell set-up and instruments	59
4.4 Results and discussion	60
4.4.1 General cell performance	60
4.4.2 Effect of the hydrogen peroxide concentration.....	62
4.4.3 Effect of the sulfuric acid concentration.....	64
4.4.4 Effect of the vanadium ion concentration.....	66
4.4.5 Effect of the membrane thickness.....	68
4.4.6 Effect of the operating temperature	70
4.4.7 Constant-current discharge behavior	71
4.5 Summary	73
4.6 References.....	75
Chapter 5 Mathematical modelling of e-fuel cells.....	85
5.1 Introduction.....	85
5.2 Model formulation	87
5.2.1 Physicochemical processes	87
5.2.2 Model simplifications and assumptions.....	89
5.2.3 Computational domains	90
5.3 Governing equations	90
5.3.1 Anode compartment.....	90
5.3.1.1 Fluid flow.....	90

5.3.1.2 Mass transport.....	91
5.3.1.3 Charge transport.....	92
5.3.2 Membrane	93
5.3.3 Cathode compartment	94
5.3.3.1 Mass transport.....	94
5.3.3.2 Charge transport.....	95
5.3.4 Electrochemical kinetics	96
5.3.4.1 Anode.....	96
5.3.4.2 Cathode	97
5.3.5 Boundary conditions	99
5.3.5.1 Momentum balance.....	99
5.3.5.2 Mass balance	100
5.3.5.3 Charge balance.....	101
5.4 Cell voltage	103
5.5 Model validation	103
5.6 Summary	105
5.7 References.....	106
Chapter 6 Simulation and optimization of e-fuel cells using oxygen as oxidant.....	118
6.1 Introduction.....	118
6.2 Simulation tool.....	119

6.3 Results and discussion	119
6.3.2 Effect of operating parameters.....	119
6.3.2.1 Effect of the vanadium-ion concentration.....	119
6.3.2.2 Effect of the sulfuric acid concentration.....	123
6.3.2.3 Effect of the e-fuel flow rate	124
6.3.3 Effect of structural design parameters	126
6.3.3.1 Effect of the anode porosity	126
6.3.3.2 Effect of the anode thickness	128
6.3.3.3 Effect of the membrane thickness.....	130
6.3.3.4 Effect of the cathode catalyst layer thickness	131
6.3.4 Effect of electrochemical parameters.....	132
6.3.4.1 Effect of the anodic exchange current density	132
6.3.4.2 Effect of the cathodic exchange current density	133
6.4 Summary	135
6.5 References.....	136
Chapter 7 Simulation of e-fuel cells using H ₂ O ₂ as oxidant.....	140
7.1 Introduction.....	140
7.2 Simulation tool.....	140
7.3 Results and discussion	141
7.3.1 Effect of the hydrogen peroxide concentration.....	141
7.3.2 Effect of the sulfuric acid concentration.....	142

7.3.3 Effect of the membrane thickness	144
7.3.4 Effect of the anode active surface area	145
7.3.5 Effect of the cathode active surface area	146
7.4 Summary	147
7.5 References	148
Chapter 8 Conclusions and future work.....	150
8.1 Conclusions.....	150
8.2 Future work.....	153
Appendix I Publications during PhD study at The Hong Kong Polytechnic University.....	155

List of Figures

Figure 1.1 Working principle of a DLFC fed with the e-fuel.....	10
Figure 2.1 The various components of the fabricated home-made fuel cell.	16
Figure 2.2 Experimental set-up for the e-fuel cell.	20
Figure 2.3 A typical polarization curve for fuel cells [1].	22
Figure 3.1 (a) General performance of the e-fuel cell using air as oxidant and (b) Comparison of power density with data obtained from the open literature for direct liquid fuel cells.	32
Figure 3.2 Comparison of the e-fuel cell performance with air and pure oxygen as the oxidant.....	33
Figure 3.3 Performance of the e-fuel cell at different (a) air flow rates and (b) oxygen flow rates.	34
Figure 3.4 Comparison of the e-fuel cell performance at different operating temperatures using (a) air and (b) oxygen as the oxidant.	36
Figure 3.5 Comparison of the cell performance using pure oxygen at the cathode at an operating temperature of 23 °C and when using air at the cathode under an operating temperature of 60 °C.	37
Figure 3.6 Constant-current discharge performance of the e-fuel cell at various (a) air flow rates and (b) oxygen flow rates.	38
Figure 3.7 Faradic, Voltage, and Energy efficiencies of the e-fuel cell at various flow rates of (a) air and (b) pure oxygen.....	40
Figure 4.1 The operation principle of the e-fuel/ H ₂ O ₂ fuel cell.	58
Figure 4.2 Experimental set-up for the e-fuel/hydrogen peroxide cell [21].	60

Figure 4.3 (a) General performance of the H₂O₂-based fuel cell and (b) Comparison of power density with data obtained from the open literature for direct liquid fuel cells that employed H₂O₂ as oxidant.61

Figure 4.4 Effect of the hydrogen peroxide concentration on the cell performance.63

Figure 4.5 Effect of the sulfuric acid concentration on the cell performance.65

Figure 4.6 Effect of the vanadium ion concentration on the cell performance.67

Figure 4.7 Effect of the membranes thickness on the cell performance....69

Figure 4.8 Effect of the operating temperature on the cell performance. ..70

Figure 4.9 (a) Constant-current discharge performances and (b) Efficiencies of the cell under three different current densities – 50, 100, and 200 mA cm⁻².72

Figure 4.10 Durability of the cell showing its discharging behavior after refueling for 10 times.....73

Figure 5.1 (a) Schematic of the 3D domain for e-fuel flow at the anode; (b) Schematic of the 2D domain for the e-fuel cell.89

Figure 5.2 3D domain for hydrogen peroxide flow at the cathode..... 100

Figure 5.3 Model validation for the fuel cells using oxygen as oxidant [44]. 104

Figure 5.4 Model validation for the fuel cells using H₂O₂ as oxidant [16]. 104

Figure 6.1 Effect of the vanadium-ion concentration on the cell performance. 120

Figure 6.2 (a) Polarization curve of the cell using e-fuel of 0.1 M V^{2+} in 3.0 M H_2SO_4 . (b) Vanadium-ion concentration distributions at designated current densities – A. 20, B. 60, C. 100, D. 160, and E. 163 $mA\ cm^{-2}$ 121

Figure 6.3 (a) Polarization curve of the cell using e-fuel of 0.3 M V^{2+} in 3.0 M H_2SO_4 . (b) Vanadium-ion concentration distributions at designated current densities – A. 100, B. 200, C. 300, D. 423, and E. 431 $mA\ cm^{-2}$.
..... 122

Figure 6.4 (a) Polarization curve of the cell using e-fuel of 0.5 M V^{2+} in 3.0 M H_2SO_4 . (b) Vanadium-ion concentration distributions at designated current densities – A. 100, B. 300, C. 500, D. 650, and E. 680 $mA\ cm^{-2}$.
..... 122

Figure 6.5 Effect of the sulfuric acid concentration on the cell performance.
..... 123

Figure 6.6 Concentration distribution of H^+ ions at the anode under various sulfuric acid concentrations at a current density of 600 $mA\ cm^{-2}$ 124

Figure 6.7 Effect of the e-fuel flow rate on the cell performance..... 125

Figure 6.8 Vanadium-ion concentration distribution at the anode under different e-fuel flow rates at a current density of 150 $mA\ cm^{-2}$ 126

Figure 6.9 Effect of the anode porosity on the cell performance..... 127

Figure 6.10 Vanadium-ion concentration distribution at the anode under different porosities at a current density of 100 $mA\ cm^{-2}$ 127

Figure 6.11 Effect of the anode thickness on the cell performance. 129

Figure 6.12 Vanadium-ion concentration distribution at the anode under different thicknesses at a current density of 650 $mA\ cm^{-2}$ 129

Figure 6.13 Effect of the membrane thickness on the cell performance. 130

Figure 6.14 Effect of the cathode catalyst layer thickness on the cell performance.	132
Figure 6.15 Effect of the anodic exchange current densities on the cell performance.	133
Figure 6.16 Effect of the cathodic exchange current densities on the cell performance.	134
Figure 7.1 Effect of the hydrogen peroxide concentration on the cell performance.	141
Figure 7.2 Concentration distribution of H ₂ O ₂ at the cathode at a current density of 900 mA cm ⁻²	142
Figure 7.3 Effect of the sulfuric acid concentration on the cell performance.	143
Figure 7.4 Effect of the membranes thickness on the cell performance..	144
Figure 7.5 Effect of the anode active surface area on the cell performance.	145
Figure 7.6 Effect of the cathode active surface area on the cell performance.	147

List of Tables

Table 3-1 Comparison of peak power density among various direct liquid fuel cell that used either air or oxygen as oxidant.	50
Table 3-2 Comparison of the cost of e-fuel cell with other liquid fuel cells.	52
Table 3-3 Comparison of energy efficiency among various types of direct liquid fuel cell that employed either air or oxygen as oxidant.....	53
Table 4-1. Performance comparison with previous e-fuel cells using different oxidants.	82
Table 4-2. Performance comparison of direct liquid fuel cells that employed H ₂ O ₂ as oxidant.....	83
Table 5-1 Cell geometry properties and porous media parameters.	112
Table 5-2 E-fuel parameters and operating conditions for the cell using oxygen as oxidant.	113
Table 5-3 Electrolyte parameters and operating conditions for the cell using hydrogen peroxide as oxidant.	114
Table 5-4 Physicochemical parameters for the cell using oxygen as oxidant.	115
Table 5-5 Physicochemical parameters for the cell using H ₂ O ₂ as oxidant.	116
Table 5-6 Parameters for diffusion.	117

Nomenclature

List of Symbols

A	Cross sectional area (m^2)
a	Active surface area (m^2/m^3)
c	Concentration ($mol\ m^{-3}$)
D	Diffusion coefficient (m^2s^{-1})
d	Diameter (m)
E⁰	standard reduction potential (V)
E	potential (V)
F	Faraday's constant ($s\ A\ mol^{-1}$)
i	Exchange current density ($A\ m^{-2}$)
j	Local current density ($A\ m^{-2}$)
k	Reaction rate constant ($m\ s^{-1}$)
\vec{N}	Flux ($mol\ m^{-3}\ s^{-1}$)
n	number of electrons
Q	Flow rate ($mL\ min^{-1}$)
P	Pressure (Pa)
R	Universal gas constant ($J\ mol^{-1}K^{-1}$)
S	Source term ($mol\ s^{-1}\ m^{-3}$)

T	Operating temperature (<i>K</i>)
u	Mobility (mol s kg^{-1})
\vec{v}	Velocity (m s^{-1})
z	Charge/valence of ion

Greek

α	Transfer coefficient
\emptyset	Potential (V)
η	Overpotential (V)
ρ	Density (kg m^{-3})
σ	Conductivity (S m^{-1})
μ	Viscosity (Pa s)
δ	Thickness (m)
ε	Porosity

Subscripts

a	Anode
c	Cathode
i	Species

l Liquid

m Membrane

s Solid

Superscripts

eff Effective

eq Equilibrium

s Surface

Chapter 1 Introduction

1.1 Background

Energy is an indispensable requirement towards achieving virtually all the daily activities of humankind. Consequently, the global energy demand and consumption are on the increase in tandem with the rising global population, industrial expansion, and modernization process [1,2]. Interestingly, the U.S. Energy Information Administration (EIA) recently projected that the global energy demand will increase by nearly 50 % in 2050 [3]. This therefore provides stimulating insights to pursue sustainable energy for the future generations and accelerate the diversification of energy delivery across the world. However, the present outlook of the global energy profile clearly indicates that fossil or hydrocarbon fuels, such as natural gas, coal, and crude oil, remain the major energy sources even in this modern period [4]. The continuous use of fossil fuel-dependent energy directly contributes to the greenhouse gas emissions and these carbon footprints cause serious environmental pollution which are detrimental to human health and wellbeing. These fossil fuels are derived from limited reserves; hence they are exhaustible and nonrenewable in nature. The perpetual consumption of fossil fuels will lead to the steady depletion of these resources and pose negative effects on the global energy security [5-7]. It is thus of significant importance to explore energy sources that are sustainable and environmentally benign.

The quest to significantly cut down the massive dependence on the limited and inefficient conventional energy sources has therefore stimulated the

utilization of renewables as effective alternative to match up with the ever-increasing energy demands of the modern world. Following this, several power generation systems, including hydropower, thermoelectric power, solar photovoltaics, wind power, batteries, and fuel cells have been developed to supply efficient and sustainable energy for end use [8]. Among these systems, fuel cells are widely considered as one of the clean power source options and have thus attracted increasing research attention.

1.2 Fuel cells

Fuel cells are clean power source as they offer feasible and smooth means to directly convert chemical energy, available in fuels, to electrical energy through electrochemical reactions. Over the years, various fuel cells, based on the type of fuel or electrolyte employed, have been developed for various applications [9,10]. Beginning with the use of hydrogen, hydrogen fuel cells (HFCs), also referred to as proton exchange membrane fuel cells (PEMFCs), remains the most developed fuel cell technology and have received a broad array of applications, including the transportation sector [11]. However, the various risks of using gaseous hydrogen significantly limit the continuous application and large-scale deployment of hydrogen fuel cells. For instance, the flammability nature of hydrogen can cause explosions and therefore raises a major safety concern for its handling and applications. The stringent conditions for hydrogen production, high-pressure requirement for hydrogen storage, and transport difficulties of hydrogen also complicate the technical requirements and increase the running costs of HFCs [12]. These lingering issues therefore led to the introduction and application of liquid fuels to energize fuel cell systems.

1.3 Direct liquid fuel cells

1.3.1 Features

Direct liquid fuel cells (DLFCs) simply employ liquid fuel for their operations. Conventional DLFCs are therefore commonly fed with alcohol fuels, including methanol and ethanol, which are easier to handle and manage compared to hydrogen gas. As a result, DLFCs are among the common and promising types of fuel cell technology that is currently attracting increasing attention. Other compelling features of DLFCs include simple structural design, high energy density, noiseless operation, fuel flexibility, long operational cycles, excellent modularity, and diverse applications [13]. However, the sluggish reaction kinetics of liquid fuels relatively limit the power density and energy efficiency of DLFCs thereby hindering the commercial market penetration of these fuel cells. In addition, performance improvement of DLFCs often require high operating temperature such that a heating system is commonly incorporated into the cells which in turn leads to unwanted energy loss.

1.3.2 Literature review

Over the years, numerous research attention and efforts have been dedicated towards the design and development of DLFCs. Different types of liquid fuels have been employed for energizing DLFCs.

Among the existing DLFCs, the direct methanol fuel cells (DMFCs) are the most common and broadly studied due to the high electrochemical activity and higher energy density of methanol ($\sim 4.8 \text{ kWh L}^{-1}$) unlike hydrogen ($\sim 180 \text{ Wh L}^{-1}$) [11]. In addition, methanol is readily available, inexpensive,

and easy to store and transport, which makes it attractive as an ideal fuel. Several studies, including the development and use of different types of catalysts to enhance the oxidation reaction of methanol and improve the durability of DMFCs, have been conducted over the years. However, methanol is toxic and can be poisonous and thus requires adequate safety measure when employed in fuel cells.

Ethanol is another liquid fuel that has been commonly employed in fuel cell technology as a result of its intrinsic safety, sustainability, nontoxicity, and high energy density ($\sim 8 \text{ kWh kg}^{-1}$) [13]. Unlike methanol, ethanol can be efficiently produced from the fermentation of biomass. The relatively sluggish reaction kinetics of ethanol due to its strong C-C bond composition, however, is a major limitation to its further application in fuel cells. Operating the direct ethanol fuel cells (DEFCs) at high temperatures has been generally considered as one of the means to address this limitation. Membrane dehydration occurs at high temperature which would in turn significantly reduce the efficiency of the fuel cell.

Another liquid fuel that has received applications in DLFCs is ethylene glycol. Ethylene glycol comprises two hydroxyl groups and is commonly used as an antifreeze in the transportation sector. Ethylene-glycol possesses superior vapor pressure, in comparison to single-hydroxyl group alcohol fuel, which helps to reduce fuel loss during evaporation. The power density obtainable from direct ethylene glycol fuel cells (DEGFCs) is still low and therefore requires the fabrication of suitable catalysts to boost the cell performance.

Glycerol, a major byproduct during the production of biodiesel, is also considered as fuel option for DLFCs. Since glycerol is a waste product, it is therefore of very low price when compared to other fuels. One of the advantages of employing glycerol in fuel cells is that the production cost of its fuel cells are significantly reduced. Glycerol is non-toxic and bio-renewable, which make it suitable and easy to be employed in fuel cell. Glycerol also has a high energy density of $\sim 6.0 \text{ kWh L}^{-1}$ [14]. However, research and studies on direct glycerol fuel cells (DGFCs) are still in the early stage.

Dimethyl ether is another liquid fuel that has been used to energize fuel cells. Even though dimethyl ether naturally exists in gaseous state, one of its distinctive features is that it can also be used as a liquid fuel. Dimethyl ether is volatile, but not carcinogenic, and non-toxic. The theoretical cell voltage of direct dimethyl ether fuel cells (DDEFs) is $\sim 1.2 \text{ V}$ [15]. The oxidation process of the cell involves the transfer of 12 electrons, which doubles the 6 obtainable in DMFCs, thereby requires less fuel to generate power. DMFCs still require much research and development effort, such as improved feeding system and fabrication of suitable catalysts, to enhance their performance.

Sodium borohydride is another liquid fuel that have been proposed and employed to operate fuel cells. Similar to hydrazine, sodium borohydride is completely free of carbon atoms, hence it does not produce carbon substances that could contaminate or destroy the anode electrocatalyst. Some of the compelling attributes of direct borohydride fuel cells (DBFCs)

include high theoretical cell voltage (1.64 V), smooth electrooxidation of borohydride ion (BH_4^-) on non-precious metallic catalysts, and high-power density [16, 17]. However, the toxic nature of sodium borohydride and the high operating costs requirement of DBFCs pose major limitation for their commercialization.

1.3.3 Performance progress

Towards the performance improvement of the various DLFCs discussed in the previous section, several efforts, which include the fabrication and use of different catalysts for the electrooxidation of the liquid fuels, have been made by numerous researchers. Following this, the peak power density achieved by DMFCs, which is the most studied DLFC, is yet to reach 200 mW cm^{-2} even when operated at high temperatures up to $100 \text{ }^\circ\text{C}$. The peak power density demonstrated by DEFCs still falls below 60 mW cm^{-2} at room temperature. The highest power density attained by DEGFCs is around 300 mW cm^{-2} under an operating temperature of $130 \text{ }^\circ\text{C}$. The DFAFCs are able to produce a peak power density up to 200 mW cm^{-2} at room temperature. DDEFCs have been demonstrated to deliver a peak power density between 40 and 80 mW cm^{-2} . The reaction kinetics of the liquid fuels, the membrane used, cell configuration, catalyst employed, and operating temperature contribute to the performance differences achieved by different DLFCs. Apparently, the various performance obtained from these DLFCs are still far from the requirements for wide market penetration and commercialization.

1.3.4 Applications

DLFCs possess compelling characteristics and promising potential to achieve competitive spot in diverse markets for several applications. Due to their simple structural design, high energy density, noiseless operation, fuel flexibility, and excellent modularity, DLFCs cover various energy-demanding applications, including portable, stationary, and transportation [9]. For portable applications, DLFCs are suitable candidates for portable power generators, typically designed for different types of lighting, public display signs, and emergency power supply; and various electronic devices such as phones, radios, and laptops. DLFCs are also commonly employed as stationary power generation systems for residential and commercial purposes. Stationary fuel cell applications include power supply for remote-area, emergency back-up, and combined heat and power systems. The transportation applications of DLFCs include auxiliary power units, light- and heavy-duty fuel cell electric vehicles, light traction vehicles, marine and aerial propulsion.

1.3.5 Challenging issues

The progress made so far on the various conventional DLFCs indicate their potential for further improvement and applications. However, there are some challenges and limitations hindering the further development and commercialization of conventional DLFCs. Firstly, the conventional liquid fuels are not electrically rechargeable and thus can only be applied once, thereby increasing the financial cost incurred on fuel. Secondly, the slow reaction kinetics of the conventional liquid fuels require the use of expensive noble metal catalysts, which in turn increase the cell fabrication cost and

also limit the cell performance. Thirdly, the conventional DLFCs are commonly operated under high temperature to enhance performance, thereby increasing the system complexity and degrading the system efficiency. Another challenging issues with the some of the conventional DLFCs is the toxicity and flammability of the fuels which therefore raise safety and environmental concern. It is thus of significant importance to propose and employ an alternative and environmentally friendly fuel candidate towards achieving efficient and cost-effective liquid fuel cells.

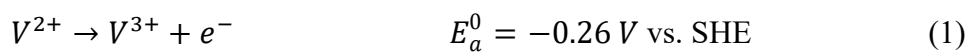
1.3.6 Electrically rechargeable liquid fuels (e-fuel)

Electrically rechargeable liquid fuel (e-fuel) is a newly introduced fuel for renewable energy storage and conversion and has piqued increasing research interest in recent years. In comparison to the alcohol fuels that has been employed in DLFCs over the years, e-fuels possess several superior advantages [19]. As an electrically rechargeable fuel, e-fuel can be recharged with the use of an e-fuel charger, thereby reducing the cost of the e-fuel production. In addition, e-fuels are obtainable from diverse range of electroactive materials, including metal ions, organic materials, and particle suspensions, indicating their broad material selectivity and flexibility. Furthermore, e-fuels possess superior electrochemical reactivity, even on carbon-based electrodes, and consequently eliminate the use of catalyst materials at the anode, thereby reducing the fabrication cost of fuel cells. Another advantage of an e-fuel is that it exhibits rapid reaction kinetics which is beneficial towards significantly increasing the performance of DLFCs. Other merits of e-fuel include low environmental footprint, easy handling, and effortless storage. As a result of the intriguing features of e-

fuels, an e-fuel solution which contains vanadium ions dissolved in sulfuric acid is prepared and employed to energize fuel cells. One of the unique features of this vanadium-based e-fuel is that it can be charged using a widely accepted technology known as all-vanadium redox flow cell. The vanadium-based e-fuel is thus considered to be a promising option and more efficient liquid fuel for operating DLFCs.

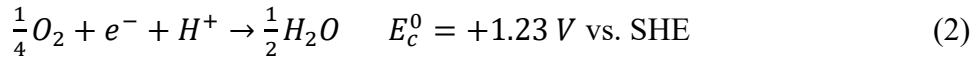
1.3.7 Working principle

As shown in Figure 1.1, the architectural feature of the fuel cell fed with e-fuel basically consists of a membrane electrode assembly (MEA). The MEA comprises a proton exchange membrane placed between a catalyst-free graphite-felt anode and a conventional cell cathode. During the operation of the e-fuel cell, the e-fuel containing vanadium ions is directly pumped, using a peristaltic pump, into the anode side where V^{2+} is oxidized to V^{3+} as given below [18]:



During this anodic reaction, electrons are released and transported to the cathode side through an external circuit while protons are transported through the membrane to the cathode side.

At the cathode side, pure oxygen is supplied through the flow channels and directly flows through the cathode diffusion layer to the cathode catalyst layer. On the cathode catalyst layer, the oxygen reacts with the electrons and protons, arriving from the anode, for oxygen reduction reaction as follows [19]:



The overall electrochemical reaction within the e-fuel cell is [20]:



This e-fuel cell apparently exhibits a theoretical voltage of 1.49 V, which is higher than those obtained from the conventional DLFCs including ethanol fuel cells (1.14 V) and methanol fuel cells (1.21 V). This therefore positions the e-fuel as a more promising and superior option for energizing DLFCs.

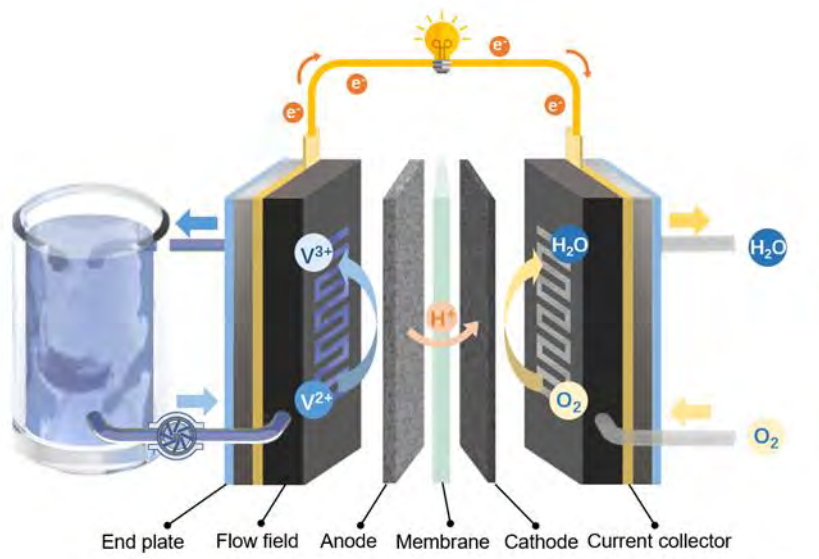


Figure 1.1 Working principle of a DLFC fed with the e-fuel.

1.4 Thesis objectives

The major objective of this thesis is to experimentally and numerically investigate the operation and performance of direct liquid fuel cells fed with an electrically rechargeable liquid fuel at the anode while exploring various oxidants at the cathode. Firstly, the operation of this e-fuel cell is experimentally examined using air as oxidant, while taking the use of oxygen as performance benchmark. This is to investigate the potential of air

as oxidant in the operation of e-fuel cells. A peak power density of 168.3 mW cm^{-2} was obtained when the cathode is fed with air. Secondly, in order to further boost the performance of the e-fuel cell and more importantly realize its application in air-tight environments, such as space propulsion and underwater power systems, hydrogen peroxide (H_2O_2) is considered as an alternative oxidant, in lieu of gaseous oxygen or ambient air, at the cathode. The novel e-fuel/ H_2O_2 fuel cell produces a peak power density of $1456.0 \text{ mW cm}^{-2}$ at $60 \text{ }^\circ\text{C}$, which is 70% higher than the use of oxygen. A maximum current density exceeding 3000 mA cm^{-2} is also achieved by the cell. Such impressive performance not only outperforms the e-fuel cells supplied with oxygen but also exceeds many liquid fuel cells that use H_2O_2 as oxidant. The performance of the cell at various operating conditions such as the concentration of the various species, operating temperature, membrane thickness, and its discharge behavior at constant currents are also investigated. Thirdly, to describe the underlying theoretical and working principle of the e-fuel cells, a two-dimensional mathematical model is developed. This is to better understand and garner more insights on the complex and highly coupled fluid flow, mass/charge transport processes, and electrochemical reactions which take place within the multi-layer porous structure of the cell. The model is first developed for the e-fuel cells using pure oxygen as oxidant. Afterwards, the modeling framework is extended to the e-fuel cells that employ H_2O_2 as oxidant, where mixed potential is considered in the cathodic reactions. The validation of the model developed for both cells through the comparison of the results with experimental data show a good agreement. Fourthly, to predict and optimize

the performance of the e-fuel cells that uses oxygen as oxidant, a computational platform is employed for the numerical simulation the model. The concentration distribution of the e-fuel at the anode under some designated current densities, which cannot be obtained by experimental approach, are presented to further provide substantial information useful for gaining in-depth insights into the operation and performance of the e-fuel cell. The simulation reveals that the mass transport loss of the e-fuel, particularly at high current densities, is a major factor limiting the cell performance. As for structural design parameters, an increase in anode porosity, anode thickness, and cathode catalyst layer thickness all boosts the cell performance, whereas the cell voltage is found to decrease with increasing membrane thickness. Increase of the exchange current density at the anode and the cathode is found to improve the performance of the e-fuel cell. Lastly, numerical simulation of the model established for the e-fuel cells that uses H_2O_2 as oxidant is performed. The simulation reveals the concentration distribution of H_2O_2 at the cathode, showing its limited mass transport at low concentration limits the cell performance. The concentration of the sulfuric acid at the cathode on the cell performance is also studied. The simulation result shows that cell performance increases with the sulfuric acid concentration. The cell voltage is found to increase with the use of thinner membranes. Furthermore, the active surface area of the anode and cathode are also presented to significantly influence the cell performance such that larger active surface area of the electrodes enhances electrochemical reactions and improve the overall cell performance.

1.5 References

1. J. Zhao, K. Dong, X. Dong and M. Shahbaz, How renewable energy alleviate energy poverty? A global analysis, *Renewable Energy*, 2022, 186, 299-311.
2. G. Luderer, S. Madeddu, L. Merfort, F. Ueckerdt, M. Pehl, R. Pietzcker, M. Rottoli, F. Schreyer, N. Bauer, L. Baumstark, C. Bertram, A. Dirnaichner, F. Humpenöder, A. Levesque, A. Popp, R. Rodrigues, J. Streffler and E. Kriegler, Impact of declining renewable energy costs on electrification in low-emission scenarios, *Nature Energy*, 2022, 7, 32-42.
3. S. Morrow, World energy demand will increase 50 % by 2050: EIA, <https://www.aa.com.tr/en/energy/oil/world-energy-demand-will-increase-50-by-2050-eia/33749>, (accessed September 15th, 2022).
4. S. Chu, Y. Cui and N. Liu, The path towards sustainable energy, *Nature materials*, 2017, 16, 16-22.
5. B. Pickering, F. Lombardi and S. Pfenninger, Diversity of options to eliminate fossil fuels and reach carbon neutrality across the entire European energy system, *Joule*, 2022, 6, 1253-1276.
6. K. R. Abbasi, M. Shahbaz, J. Zhang, M. Irfan and R. Alvarado, Analyze the environmental sustainability factors of China: The role of fossil fuel energy and renewable energy, *Renewable Energy*, 2022, 187, 390-402.
7. S. Chu and A. Majumdar, Opportunities and challenges for a sustainable energy future, *Nature*, 2012, 488, 294-303.
8. D. C. Walther and J. Ahn, Advances and challenges in the development of power-generation systems at small scales, *Progress in Energy and Combustion Science*, 2011, 37, 583-610.

9. O. Z. Sharaf and M. F. Orhan, An overview of fuel cell technology: Fundamentals and applications, *Renewable and sustainable energy reviews*, 2014, 32, 810-853.
10. S. Wang and S. P. Jiang, Prospects of fuel cell technologies, *National Science Review*, 2017, 4, 163-166.
11. N. Shaari, S. K. Kamarudin, R. Bahru, S. H. Osman and N. A. I. Md Ishak, Progress and Challenges: Review for Direct Liquid Fuel Cell, *International Journal of Energy Research*, 2021, 45, 6644-6688.
12. N. F. Barilo, S. C. Weiner and C. W. James, Overview of the DOE hydrogen safety, codes and standards program part 2: Hydrogen and fuel cells: Emphasizing safety to enable commercialization, *International Journal of Hydrogen Energy*, 2017, 42, 7625-7632.
13. B. Ong, S. Kamarudin and S. Basri, Direct liquid fuel cells: A review, *International Journal of hydrogen energy*, 2017, 42, 10142-10157.
14. Z. Zhang, L. Xin and W. Li, Supported gold nanoparticles as anode catalyst for anion-exchange membrane-direct glycerol fuel cell (AEM-DGFC), *International Journal of Hydrogen Energy*, 2012, 37, 9393-9401.
15. S. Basri and S. K. Kamarudin, Direct dimethyl ether fuel cells (DDMEFCs), in *Direct Liquid Fuel Cells*, Elsevier, 2021, pp. 177-189.
16. J. Ma, N. A. Choudhury and Y. Sahai, A comprehensive review of direct borohydride fuel cells, *Renewable and Sustainable Energy Reviews*, 2010, 14, 183-199.
17. L. An and C. Jung, Transport Phenomena in Direct Borohydride Fuel Cells, *Applied energy*, 2017, 205, 1270-1282.

18. H. Jiang, L. Wei, X. Fan, J. Xu, W. Shyy and T. Zhao, A Novel Energy Storage System Incorporating Electrically Rechargeable Liquid Fuels as the Storage Medium, *J Science Bulletin*, 2019, 64, 270-280.
19. X. Shi, X. Huo, Y. Ma, Z. Pan and L. An, Energizing fuel cells with an electrically rechargeable liquid fuel, *Cell Reports Physical Science*, 2020, 1, 100102.

Chapter 2 Experimental setup and characterization platform

2.1 Introduction

This chapter presents the various components, experimental set-up, and characterization platform of the e-fuel cell. The procedures for the preparation of the cell components, which includes the anode, cathode, and membrane, and the assembling of these components to achieve a membrane electrode assembly (MEA) are presented. The procedures involved in the preparation of the electrically rechargeable liquid fuel (e-fuel) are discussed. The experimental setup and the various instruments used during the experiments are also presented. The various performance evaluation tests, such as polarization curve, constant-current discharge, and performance stability for the e-fuel cell are introduced.

2.2 Cell components and assembly

The component materials for the design of the fabricated home-made fuel cell are displayed in Figure 2.1.

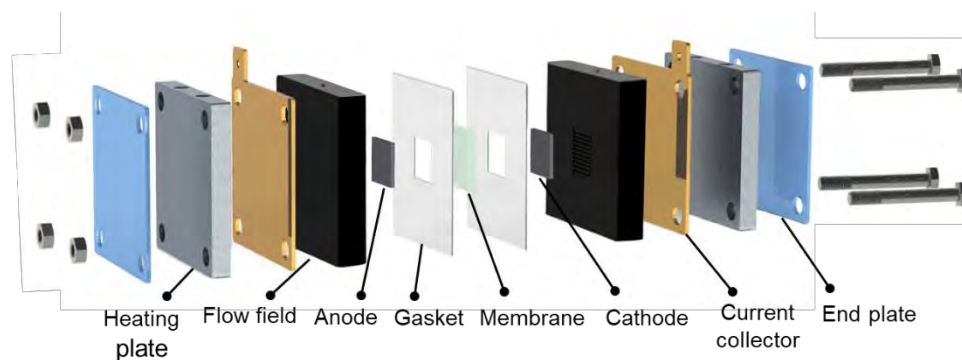


Figure 2.1 The various components of the fabricated home-made fuel cell.

The various components of the fuel cell include two heating plates, two graphite flow field structures etched with serpentine flow channel, two current collectors, two gaskets, an anode, a membrane, and a cathode. All

these elements are firmly fixed with bolts and nuts to avoid any form of leakage from the cell.

2.2.1 Flow field designs

The graphite flow field structure is designed with serpentine flow channel with a width and depth of 1.0 mm. The serpentine flow field serves as the route for the delivery and distribution of the electrolytes on the surface of the electrodes.

2.2.2 Preparation of anode

Catalyst-free graphite-felt anode is used throughout this study. The preparation procedures of this anode are as follows:

- 1) A large size of a graphite felt (AvCarb G100, Fuel Cell Store) is cut.
- 2) The graphite felt is placed inside a muffle furnace and heated for 5 hours in air at a temperature of 500°C to enhance its electrochemical reactivity and wettability.
- 3) The heated graphite felt is allowed to cool down and then taken out of the furnace.
- 4) The thermally treated graphite felt is then cut into smaller sizes of 2.0 cm × 2.0 cm in readiness to be used for the assembling of the cell.

2.2.3 Preparation of cathode

A home-made Pt/C coated carbon paper is used as the cathode in this study.

The procedures involved in the preparation of this cathode are as follows:

- 1) 60 wt. % Pt/C powder (Johnson Matthey Co., USA), 5 wt. % Nafion (Fuel Cell Store, USA), and ethanol are properly mixed together.
- 2) The mixed solution is placed into an ultrasonic bath for about 30

minutes to ensure the uniformity of the solution suitable for the catalyst ink.

- 3) A carbon paper of size 5.0 cm × 4.0 cm is fastened on a heating plate while exposing 4.0 cm × 4.0 cm surface area of the carbon paper.
- 4) The prepared catalyst ink is poured into a spray gun to uniformly spray the ink on the carbon paper.
- 5) The wet catalyst layer is allowed to dry up.
- 6) Steps 4) and 5) are repeated until the carbon paper attains the expected catalyst loading.
- 7) The coated carbon paper is thereafter cut into four pieces, each with a size of 2.0 cm × 2.0 cm, in readiness to be used for the assembling of the cell.

2.2.4 Preparation of membrane

For the various experimental investigations presented in this thesis, Nafion series membranes are used as the proton exchange membrane. The standard procedures followed for the preparation of these membranes are:

- 1) The purchased Nafion membrane is immersed into 3.0 wt.% hydrogen peroxide (H₂O₂) solution and placed in water bath to boil for an hour.
- 2) The membrane is removed from the H₂O₂ solution and then immersed into deionized water and placed in water bath to boil for an hour.
- 3) The membrane is removed from the deionized water and then immersed into 1.0 M H₂SO₄ and placed in water bath to boil for an hour.
- 4) The membrane is removed from the H₂SO₄ solution and again immersed into deionized water placed in water bath to boil for an hour.
- 5) The membrane is thereafter cut into a size of 3.0 cm × 3.0 cm and stored

in deionized water in readiness to be used during the assembling of the cell.

2.2.5 Membrane electrode assembly

After the preparation of the anode, cathode, and membrane, the membrane electrode assembly follows. The MEA with an active area of $2.0 \text{ cm} \times 2.0 \text{ cm}$ is prepared such that the commercial proton exchange membrane is sandwiched between the catalyst-free graphite felt anode and the conventional Pt/C coated carbon paper cathode.

2.3 Preparation of electrolytes

2.3.1 Preparation of electrically rechargeable liquid fuel

The fuel cell presented and investigated in this thesis is energized with an electrically rechargeable liquid fuel (e-fuel). The procedures involved in the preparation of this e-fuel fed into the anode of the cell are as follows:

- 1) Suitable amount of vanadyl sulfate (VO_2SO_4) powder is dissolved in sulfuric acid.
- 2) Deionized water is added to the solution and stirred to obtain uniform solution.
- 3) The prepared solution is allowed to cool down and thereafter transferred into a volumetric flask.
- 4) Deionized water is added to the solution inside the volumetric flask until the solution reaches the marked line for the desired volume.
- 5) The solution is then charged using a typical flow cell to obtain the desired e-fuel. The charging time is changed based on the e-fuel concentration required.

2.3.2 Preparation of hydrogen peroxide solution

Hydrogen peroxide is utilized as the oxidant for the experimental study presented in chapter 4. The procedures followed in the preparation of the hydrogen peroxide solution are given below:

- 1) Deionized water is poured into a big beaker after which an appropriate amount of sulfuric acid is added to the deionized water.
- 2) The solution is allowed to cool down and hydrogen peroxide is added, depending on the concentration required.
- 3) The acidified hydrogen peroxide solution is transferred into a volumetric flask.
- 4) Deionized water is added to the solution inside the volumetric flask until the solution reaches the marked line for the desired volume.
- 5) The acidified hydrogen peroxide solution is thereafter stored in clean and dry bottles.

2.4 Experimental setup and instruments

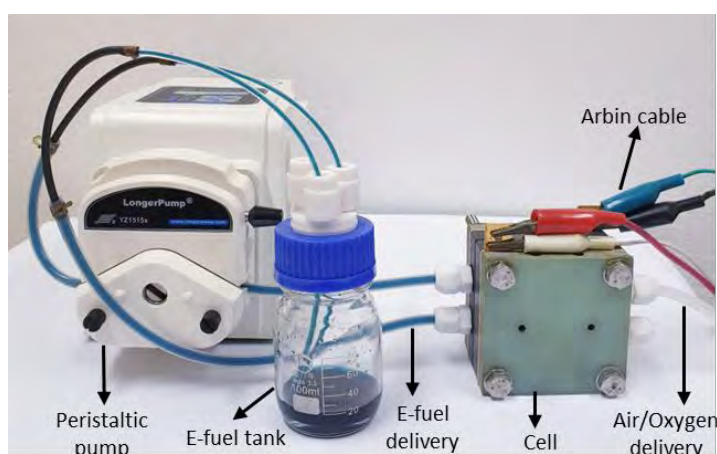


Figure 2.2 Experimental set-up for the e-fuel cell.

The experimental setup of the e-fuel cell system, which comprises a cell, pump, e-fuel, e-fuel tank and delivery, oxidant delivery, and Arbin cable, is

presented in Figure 2.2. Other instruments used during the experiments are introduced in subsequent sections.

2.4.1 Fuel supply system

The prepared e-fuel is drawn into a small tank for storage. A peristaltic pump is employed to deliver the e-fuel, at a set flow rate, to the anode side of the fuel cell.

2.4.2 Oxidant supply system

When oxygen or air are used as the oxidant, an oxygen or compressed air cylinder is connected to a mass flowmeter (Cole-Parmer, USA) to control the supply and flow rate of oxygen or air to the cathode side of the fuel cell.

When hydrogen peroxide is employed as the oxidant, a peristaltic pump is used to deliver the hydrogen peroxide solution, at a set flow rate, to the cathode.

2.4.3 Temperature control system

A proportional-integral-derivative (PID) temperature controller (Anhone Electronic Co. Ltd., China) is employed to heat the fuel cell when an operating temperature above the room temperature is required. The temperature controller consists of a pair of heating rods, inserted into the heating plates, for heating both sides of the cell; and a pair of K-typed thermocouples for monitoring the cell temperature.

2.4.4 Testing systems

A fuel cell testing system (Arbin BT2000, Arbin instrument Inc.) is used to perform the various experimental tests reported in Chapter 3 of this thesis while the experimental investigations reported in Chapter 4 were performed

and recorded using a fuel cell testing system (Neware Technology Limited, China).

2.5 Performance evaluation

2.5.1 Polarization curves

Polarization curve, also known as IV-curve, shown in Figure 2.3, presents the relationship between the applied current density and the voltage output of fuel cells. The polarization curve starts after the cell voltage falls below the cut-off voltage. The sources of the primary losses, such as the activation loss, ohmic loss, and mass transport loss, common in fuel cells can be clearly displayed and analyzed using polarization curves [1].

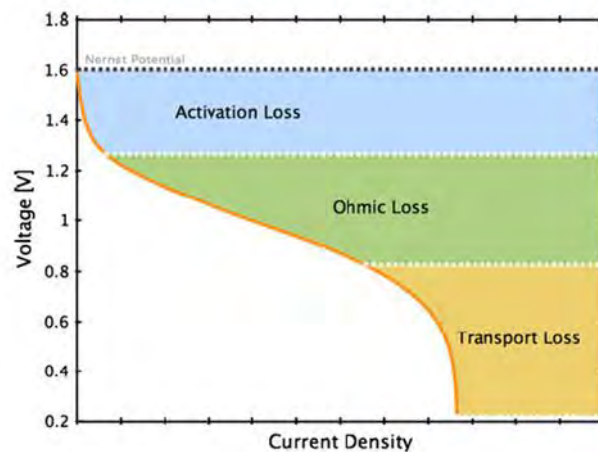


Figure 2.3 A typical polarization curve for fuel cells [1].

The activation loss, which is evident at the low operating current density range, occurs as a result of the sluggish charge transfer reaction at the electrode and electrolyte interface required to kickstart the electrochemical reaction. The ohmic loss, evident at the medium current density regions, is caused by the ohmic resistance of the cell components, which include the electrical resistance in the electrodes, ionic transport resistance through the

electrolyte and membrane, and contact resistance between the cell components. The mass transport loss, which is mostly obtained at the high current density range, occurs during the depletion of the reactants at the electrode surface. In addition to these, the open-circuit voltage (OCV) and the maximum current density of the cell can be obtained from the polarization curves. The peak power density that can be delivered by the cell can also be derived from the polarization curves by simply multiplying the cell voltages with their corresponding current densities.

2.5.2 Constant-current discharge performance

Constant-current discharge test is a performance evaluation method commonly conducted on power generation devices, such as fuel cells, to determine their performance characteristics during real and practical applications. In addition, constant-current discharge test provides the basis for evaluating the Faradic, voltage, and energy efficiencies of fuel cells to further examine their suitability for real-life operation. Constant-current discharge performance of a fuel cell is obtained by operating the cell under a constant current load while the voltage responses are generated.

2.5.3 Long-term stability performance

Long-term stability test is commonly conducted on fuel cells to determine their performance stability during an extended duration of operation. At the initial stage of the long-term stability test, the cell is subjected to a constant-current discharge mode to generate the voltage response. However, when the fuel is exhausted, the fuel tank is immediately replaced with fresh fuel to continue the cell operation. These procedures are continuously repeated until significant performance degradation from the cell is observed.

2.5.4 Efficiencies

The various efficiencies, which include the Faradic, voltage, and energy efficiencies, are also important performance indicators of DLFCs.

The Faradic efficiency, which is also referred to as the fuel utilization efficiency, can be calculated according to this equation [2]:

$$\text{Faradic efficiency (\%)} = \frac{\int i(t)dt}{VFc_{init}} \quad (1)$$

Where $i(t)$, V , F , and c_{init} denote the discharging current, volume of e-fuel, Faraday's constant, and the initial concentration of the e-fuel, respectively.

The voltage efficiency is calculated as follows [3]:

$$\text{Voltage efficiency (\%)} = \frac{E_{aver}}{E_{theo}} \quad (2)$$

$$\text{where } E_{theo} = \frac{\int_0^{c_{ini}} t[E^0 + \frac{RT}{F} \ln(\frac{c_{V^{2+}}}{c_{V^{3+}}})]dc}{c_{init}} \quad (3)$$

E_{aver} and E_{theo} denote the average discharging and theoretical voltage, respectively.

The energy efficiency is the multiplication of the Faradic efficiency and the voltage efficiency, expressed as:

$$\text{Energy efficiency (\%)} = \text{Faradic efficiency} \times \text{Voltage efficiency} \quad (4)$$

2.6 Summary

The various cell components and the assembly of the fuel cell are introduced in this chapter. The preparation methods of the anode, cathode, and membrane for the membrane electrode assembly are also presented. The

preparation methods of the electrolytes, which include the e-fuel and hydrogen peroxide, used in this study are also highlighted. The experimental setup, instrumentation, and performance evaluation of the e-fuel cell are also described.

2.7 References

1. D. Aaron, Z. Tang, A. B. Papandrew and T. A. Zawodzinski, Polarization curve analysis of all-vanadium redox flow batteries, *Journal of Applied Electrochemistry*, 2011, 41, 1175-1182.
2. J. Liu, T.-S. Zhao, R. Chen and C. W. Wong, Effect of methanol concentration on passive DMFC performance, *Fuel Cells Bulletin*, 2005, 2005, 12-17.
3. O. C. Esan, X. Shi, Y. Dai, L. An, and T. S. Zhao, Operation of Liquid E-fuel Cells Using Air as Oxidant, *Applied Energy*, 2022, 311, 118677.

Chapter 3 Operation of fuel cells using air/oxygen as oxidant

3.1 Introduction

The continuous increase in the global population, industrialization, and numerous human activities has inevitably resulted in the surge of energy and power demands. In addition, the significant consumption as well as the rapid depletion of the inefficient fossil energy has created severe energy crisis and insecurity across the globe [1,2]. In a bid to provide clean and sustainable power for the present energy-demanding modern lifestyles and the future generations, renewable energy sources have been largely explored and harnessed [3]. Following this, various renewable power generation and energy conversion systems, that are energy efficient as well as environmentally benign, have been developed and deployed for use in several applications. Fuel cells, in particular, are clean and alternative energy providers well known for the smooth conversion of chemical energy, stored in form of fuel, into electrical energy for end users [4,5]. The progress attained over the years on fuel cell technology has therefore gained the attention of many researchers for further studies, design, and development towards improved performance.

Direct liquid fuel cells are among the common and promising types of fuel cell technology that is currently attracting increasing attention due to their simple structural design, high energy density, safe handling, storage, and transport of fuel [6,7]. Liquid alcohols including methanol [8], ethanol [9], ethylene glycol [10], and even formic acid [11] have thus been commonly considered as choice of fuel to energize fuel cells. However, some of the peculiar challenges and shortcomings with the operation and application of

these direct liquid fuel cells include severe fuel crossover, high cost of catalyst, low power density, and low energy efficiency [12,13]. To tackle most of these challenges and ameliorate fuel cell performance and durability, alternative and more efficient liquid fuels are required.

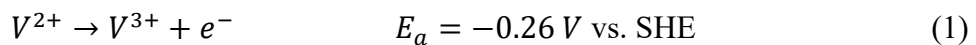
Recently, a novel energy storage system using electrically rechargeable liquid fuels was proposed and experimentally demonstrated [14]. Uniquely different from all the conventional energy storage systems, the innovative electrochemical system was developed such that the charge and discharge processes are independently achieved. The electrically rechargeable liquid fuels, known as e-fuels, which can be obtained from diverse range of electroactive materials, were mentioned as excellent options for the energy storage medium. E-fuel cell is one of the two major components, the other is an e-fuel charger, that constitutes the e-fuel energy storage system. While the e-fuel charger solely charges the discharged e-fuel to be stored as energy, the e-fuel cell primarily generates electrical energy using the charged and stored e-fuel. This latest system therefore characterizes a major step forward in the advancement of electrical energy storage and power generation systems. The e-fuel cell, in particular, has subsequently attracted increasing research attentions for power generation due to its unique features and advantages. As a result of the varieties of fuel that can be employed in the operation of the e-fuel cell, an e-fuel solution, which contains vanadium ions dissolved in sulphuric acid, is therefore employed to operate fuel cells. Superior reactivity, long cycle life, wide operating temperature range, low environmental footprint, easy storage, and catalyst-free materials were mentioned as some of the merits of using this vanadium-based e-fuel [15].

As a result of the proliferating interest in fuel cell electric vehicles, the feasibility of employing a power source that is easily re-fueled by simply supplying the fuel tank with rechargeable solution is an interesting idea that should receive enormous attention for further development.

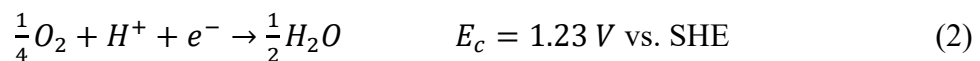
The successful operation of the e-fuel cell requires the supply of oxidant at its cathode. The oxidant is required to react with the protons and electrons from the anode to actualize reduction reaction at the cathode [16,17]. The use of air, on the other hand, would significantly reduce the design complexity and cost of the system. It is thus desired and of significant importance for the e-fuel cell to be workable using air as oxidant. Herein, the operation and behavior of the e-fuel cell is therefore examined with the use of air as oxidant, while taking the use of pure oxygen as performance benchmark. The experimental study shows that the cell exhibits a peak power density of 168.3 mW cm^{-2} at room temperature when air is employed as the oxidant. Such performance when air is used as the oxidant outperforms a number of conventional direct liquid fuel cells that are even fed with oxygen at the cathode.

3.2 Operation principle of the cell

An e-fuel solution which contains V^{2+} ions is supplied into the anode where the V^{2+} is oxidized to V^{3+} during the cell operation according to [15]:



The reduction reaction at the cathode is as follows [15]:



The overall reaction of the e-fuel cell is expressed as [15]:



As previously mentioned, the theoretical voltage (1.49 V) of this e-fuel cell is considerably higher in comparison to other types of direct liquid as well as hydrogen fuel cells.

3.3 Experimental details

3.3.1 Membrane electrode assembly

The membrane electrode assembly (MEA) adopted for this e-fuel cell was prepared by sandwiching a proton exchange membrane (Nafion 117) between a catalyst-free graphite-felt anode and a platinum/carbon coated carbon paper used as the cathode. While the dimension of the membrane is 3.0 cm × 3.0 cm, both the anode and the cathode are of size 2.0 cm × 2.0 cm. The anode was treated by heating in the air for 5.0 hours under a temperature of 500°C. Before use, the membrane was prepared and pretreated by following the standard preparation method as reported before [18]. The cathode, a platinum/carbon coated carbon paper with a metallic loading of ~0.50 mg cm⁻², was prepared by following the previously reported procedures [15].

3.3.2 Preparation of e-fuel

The e-fuel solution employed at the anode was produced by dissolving VOSO₄ powder in sulfuric acid and afterwards the solution is charged using a classic flow cell as reported before [19]. Thereafter, 20.0 mL of the e-fuel was drawn into the e-fuel tank and pumped into the fuel cell, at a flow rate of 20.0 mL min⁻¹, with the use of a peristaltic pump.

3.3.3 Experimental set-up and instruments

The experimental arrangement for this study consists of the assembled cell, an e-fuel tank, delivery pipes, and a peristaltic pump for the delivery of the e-fuel into the cell. The oxidant pipe is also fastened to the cathode side to deliver air/oxygen into the cell cathode such that the oxidant flow rate is regulated using a mass flowmeter. The polarization and the constant current discharge tests were implemented using a fuel cell testing system namely Arbin BT2000.

3.4 Results and discussion

3.4.1 General performance and comparison

The performance characteristics of the e-fuel cell with the use of air as oxidant for operating the e-fuel cell is presented in

Figure 3.1a. While the anode is supplied with an e-fuel solution (0.6 M V^{2+} dissolved in $3.0 \text{ M H}_2\text{SO}_4$) at a flow rate of 20.0 mL min^{-1} , air is supplied to the cathode side at a flow rate of 100 standard cubic centimeters per minute (sccm). It is found that the cell attains an open-circuit voltage (OCV) of 1.25 V with the use of air at the cathode which is comparable to an OCV of 1.26 V obtained when the cathode is fed with pure oxygen as shown in Figure 3.2. These values are apparently lower than the theoretical voltage of the e-fuel cell (1.49 V) as a consequence of the relatively high overpotential at the cathode due to the inevitable crossover of the e-fuel to the air side [15].

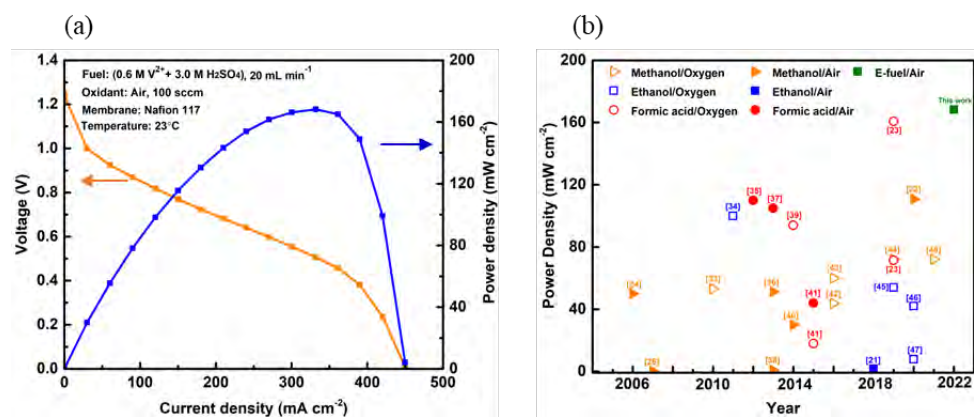


Figure 3.1 (a) General performance of the e-fuel cell using air as oxidant and (b) Comparison of power density with data obtained from the open literature for direct liquid fuel cells.

It can also be seen that a peak power density of 168.3 mW cm⁻² together with a maximum current density of approximately 450 mA cm⁻² are obtained when air is applied as the oxidant. As expected, the use of pure oxygen as oxidant in the e-fuel cell produces a higher peak power density of 254.6 mW cm⁻², as depicted in Figure 3.2, which is 51 % higher than the use of air at the cathode. This could be majorly ascribed to the fact that the air contains less concentration of oxygen (21 %) compared to that of pure oxygen [20]. However, the performance achieved by the e-fuel cell when air is utilized as the oxidant still outperforms a number of liquid fuel cells that are also fed with oxygen at the cathode as shown in

Figure 3.1b and Table 3-1. For instance, a close look at the comparisons shows that the operation of an ethanol fuel cell using air as oxidant could barely attain a power density of 2.0 mW cm⁻² at room temperature, despite the higher catalyst loading (Pt/C 4.0 mg cm⁻²) employed at the cathode [21]. A methanol fuel cell which also employed air as oxidant and operated at

higher temperature (90°C) could only achieve a peak power density of 110.77 mW cm⁻² [22]. Elsewhere, the peak power density, 160.7 mW cm⁻², of a formic acid fuel cell that was even operated with oxygen at higher temperature (60°C) [23] is still lower than the performance achieved in this study that is even conducted at room temperature. These therefore justify air as a suitable alternative for oxidant during the operation and more importantly future application of the e-fuel cell.

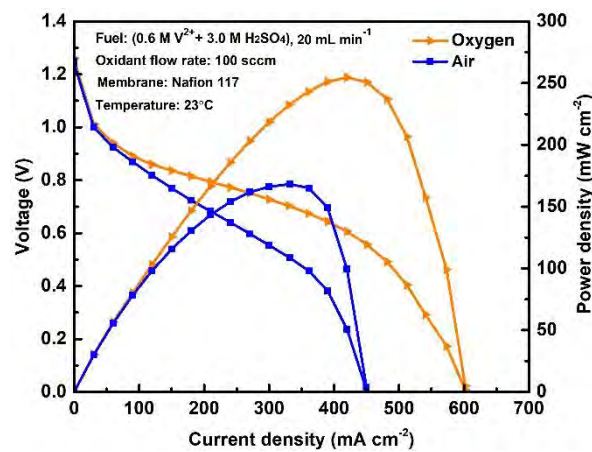


Figure 3.2 Comparison of the e-fuel cell performance with air and pure oxygen as the oxidant.

It is important to state that the excellent reactivity of the e-fuel which eliminate the need for noble metal catalysts at the anode, offers the fuel cell with a cost estimation of US\$737.30 kW⁻¹. In comparison to conventional liquid fuel cells as shown in Table 3-2, the e-fuel cell is cost-effective.

3.4.2 Influence of the oxidant flow rate

The flow rate of oxidant into the cathode is one of the significant factors which impact the performance outlook of the cell [21]. The availability and mass transport of oxidant at the cathode and the cell performance would therefore be affected by the oxidant flow rate. In this section, the influence

of various air flow rates starting from 10 to 100 sccm are investigated and compared as regards to the cell performance. The performance of the cell is seen to improve with increasing air flow rate from 10 to 100 sccm as shown in Figure 3.3a. This is primarily because increase in the air flow rate enhances the swift supply and spread of oxidant over the cathode thereby leading to the faster rate of the oxidant to the reaction sites at the cathode catalyst layer [8]. In more detail, the cell attains a peak power density of 97, 141.4, 159.5, 165, and 168.3 mW cm^{-2} at air flow rate of 10, 20, 30, 50, and 100 sccm, respectively. Whereas, as shown in Figure 3.3b, when pure oxygen is used as the oxidant in the e-fuel cell, serving as the benchmark, little variation in the performance of the cell is obtained at all the flow rates.

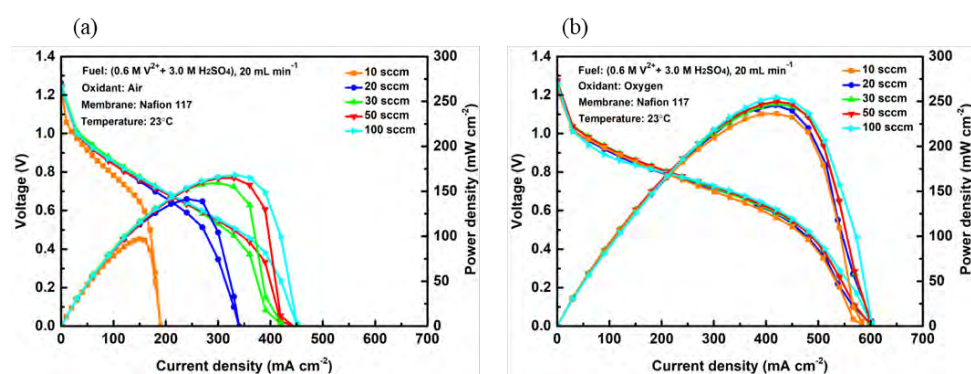


Figure 3.3 Performance of the e-fuel cell at different (a) air flow rates and (b) oxygen flow rates.

With the use of air at low air flow rates of 10 and 20 sccm, limited cell performance is well pronounced. This can be ascribed to the insufficient flow of air leading to oxygen starvation and increase in the mass transfer resistance of the oxygen component of air to the active sites of the cathode [24]. In contrast, at higher air flow rates of 50 and 100 sccm, very small difference in the peak power density, between 165 and 168.3 mW cm^{-2} is

demonstrated, which thereby indicates that a further increase in the air flow rate may not be vital for the seamless running of the e-fuel cell. Furthermore, it is considered that a further increase in the air flow rate would require the consumption of more power for the air delivery, which thereby could reduce the system efficiency [25]. While at low oxygen flow rate of 10 sccm, the supply of oxygen to the cathode is seen to be sufficient for achieving a high cell performance, further study is therefore suggested to develop catalyst with better catalytic reactivity for the cathodic reaction so that the e-fuel cell using air as oxidant could match-up with the performance of cell using oxygen.

3.4.3 Influence of the operating temperature

Operating temperature is a major parameter that should be considered in the operation and design of a fuel cell. This is because the operating temperature of the cell poses significant effect on the characteristics of the e-fuel, oxidant, membrane, and general cell performance [26,27]. Figure 3.4a displays the effect of operating temperature on the cell voltage and power density with the use of air as oxidant. Obviously, with the rise in the operating temperature from 23°C to 60°C, performance improvement in the e-fuel cell is achieved. The peak power density of the cell when fed with e-fuel/air and subjected to an operating temperature of 23°C is 143.3 mW cm⁻². This power density was increased by 26 % to attain 180.7 mW cm⁻² at 40°C. A further increase in the operating temperature to 60°C, the cell exhibits a peak power density of 199.5 mW cm⁻² which is about 40 % more than the performance at 23°C.

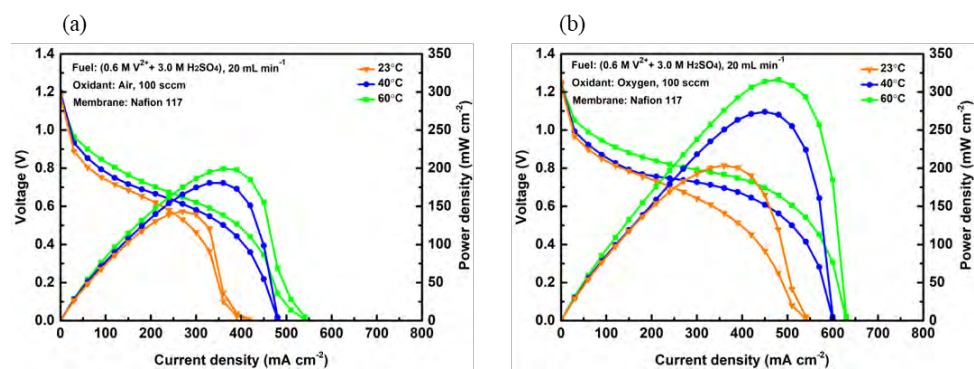


Figure 3.4 Comparison of the e-fuel cell performance at different operating temperatures using (a) air and (b) oxygen as the oxidant.

The increase in cell performance is accredited to the fact that increasing temperature enhances the reactions kinetics of the e-fuel oxidation and the cathodic reaction which therefore reduces activation losses during the cell operation, in accordance with Arrhenius equation [21,28]. Increasing temperature also facilitates the transport of reactants to their respective active sites, which thus reduces concentration loss [27]. The performance of the cell using pure oxygen as the oxidant in the e-fuel cell is displayed in Figure 3.4b. The peak power density obtained are 203.3, 273.9, and 315.9 mW cm⁻² when the cell is subjected to operating temperature at 23°C, 40°C, and 60°C, respectively. It was observed that when feeding the e-fuel cell with air at the cathode and operated at 60°C, the cell achieved nearly the same performance, a peak power density of approximately 200 mW cm⁻², in comparison to the performance of the cell fed with oxygen but operated at 23°C as presented in Figure 3.5.

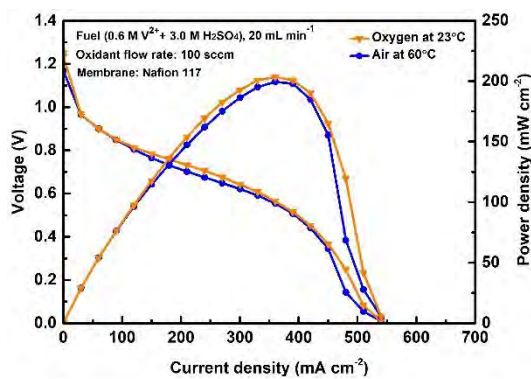


Figure 3.5 Comparison of the cell performance using pure oxygen at the cathode at an operating temperature of 23 °C and when using air at the cathode under an operating temperature of 60 °C.

This further emphasizes the potential of air in the future operation and application of the e-fuel cell. However, it is worth noting that, when operated at high temperature, the dehydration of Nafion 117 membrane could happen, which thus would lead to increase in the membrane resistance and thereby induce a larger ohmic loss limiting the cell performance [27,29, 30]. In addition, the cell is prone to high crossover of reactive species through the membrane at higher temperature which would also result in a larger mixed potential at the cathode [15]. Hence, the long-term performance of the e-fuel cell at high operating temperature is an important aspect that still requires further investigations.

3.4.4 Constant-current discharge performance

Constant-current discharge is an evaluation test method commonly conducted on power generation devices such as fuel cells to determine their performance characteristics during real and practical applications. In addition, constant-current discharge test provides the basis for evaluating the Faradic, voltage, and energy efficiencies of fuel cells to further examine

their suitability for real-life operation. In this study, the constant current discharge test of this e-fuel cell is tested at 10 mA cm^{-2} considering five different flow rates of the oxidants – 10, 20, 30, 50, and 100 sccm using air as oxidant as shown in Figure 3.6a. For comparison, the constant current discharge test of this e-fuel cell with the use of pure oxygen, which is the widely accepted basis is displayed in Figure 3.6b.

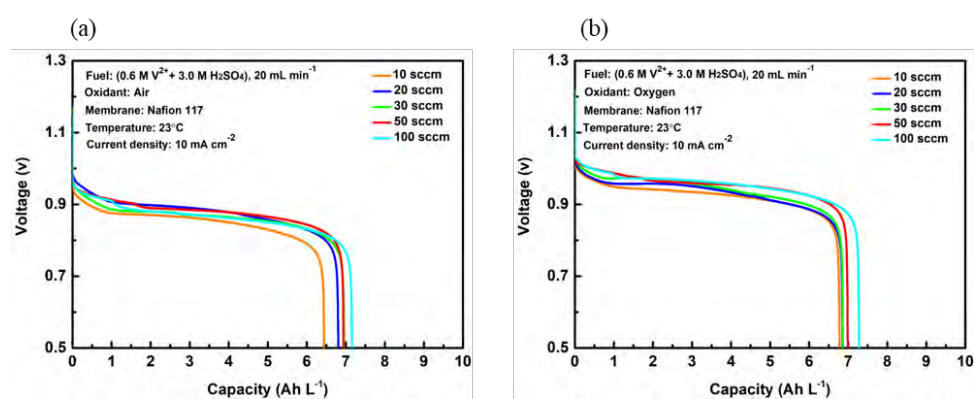


Figure 3.6 Constant-current discharge performance of the e-fuel cell at various (a) air flow rates and (b) oxygen flow rates.

As it can be seen, there is not much improvement in the voltage plateau with the increase in flow rate of both oxidants, at all the flow rates considered for air and oxygen. With the use of air, the discharge capacity of the cell slightly increases in tandem with the increasing air flow rate. In more detail, an improved discharge capacity performance from 6.44 to 7.16 Ah L⁻¹ is observed when the air flow rate is raised from 10 to 100 sccm. With the use of pure oxygen, the discharge capacity of the cell also increases from 6.77 to 7.28 Ah L⁻¹ as the oxygen flow rate increases. The primary reason for such increase in discharge capacity is that higher oxidant flow rate promotes fast distribution of the oxidant at the cathode catalyst layer which in turn reduces the concentration and activation losses that could affect the

discharge capacity [31,32]. Using air as the oxidant at all these flow rates, the cell is found to demonstrate its capability for stable operation.

3.4.5 Energy efficiency

The energy efficiency indicates the competence of the fuel cell regarding the efficient conversion of chemical energy to electrical energy. Here, the Faradic, voltage, and energy efficiencies of the cell considering various flow rates of air were calculated to further reveal the performance of the cell. As displayed in Figure 3.7a, it can be noticed that the energy efficiency of the cell when fed with air at a flow rate of 10 to 100 sccm is between 23.4 % and 26.4 %. In comparison, when the cathode is fed with pure oxygen, the energy efficiency of the cell as depicted in Figure 3.7b is slightly higher and ranges from 26.8 % to 29.6 %. The slight increment of the energy efficiency can be ascribed to the reality that pure oxygen possesses more oxygen concentration which brings about the reduction of activation loss [20]. However, the use of air is found to provide the cell with a similar performance with the use of oxygen in terms of achieving comparable energy efficiency. Furthermore, the efficiency attained by the e-fuel cell with the use of air as oxidant also outperforms some conventional direct liquid fuel cells that uses air as oxidant and operated under similar testing conditions as summarized in Table 3-3.

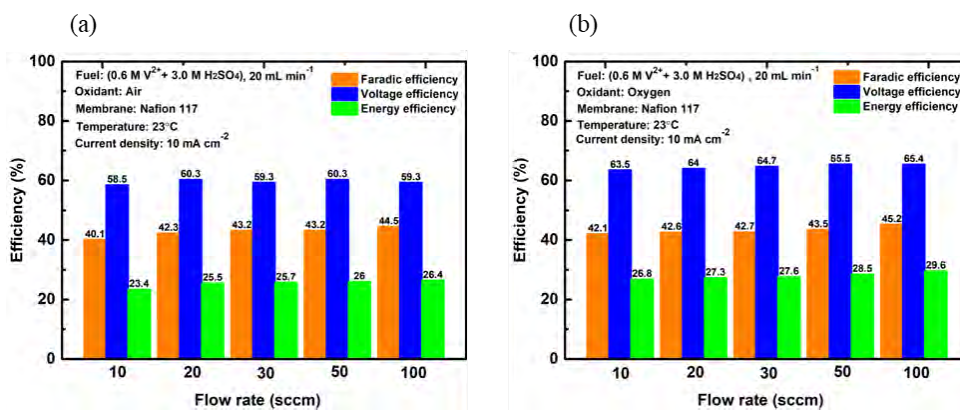


Figure 3.7 Faradic, Voltage, and Energy efficiencies of the e-fuel cell at various flow rates of (a) air and (b) pure oxygen.

All these therefore indicates air as a potential oxidant for the operation of the e-fuel cell. It is also essential to state that during the long-term running of the e-fuel cell, the oxidant flow rate also plays a major effect on removing the water generated at cathode and therefore still requires further investigation on determining the optimal oxidant flow rate after prolonged operation. Also, it is believed that by enhancing the cathode catalytic reactivity in order to ameliorate the slow oxygen reduction reaction at the cathode, towards reducing activation loss and thereby achieving a higher voltage efficiency, the energy efficiency of the e-fuel cell employing air as oxidant can be further improved.

3.5 Summary

The operation and performance of the e-fuel cell is explored with the use of air as oxidant, while taking the use of pure oxygen as performance benchmark. The experimental result shows that the cell is able to boost of a peak power density of 168.3 mW cm^{-2} which performs better than a number of the common direct liquid fuel cells, including those fed with oxygen at

the cathode. This therefore indicates the potential of air as oxidants in the operation of the e-fuel cell. The effects of a number of operating variables on the behavior and performance of the cell with respect to using air as the oxidant are examined. The cell performance is seen to improve with increasing the air flow rate as high air flow rate enhances the quick supply and spread of oxidant to the reaction sites at the cathode. Likewise, with the increase of the operating temperature from 23°C to 60°C, performance enhancement in the e-fuel cell is achieved. To further upgrade the cell performance obtainable with the use of air in comparison to pure oxygen, more research attention, such as the fabrication of catalyst with improved catalytic reactivity for the cathodic reaction, should be considered in the future. The influence of possible water flooding should also be investigated and studied. A numerical investigation to examine and analyze the influence of the use of air and pure oxygen as oxidant on the cell performance is also a potential direction for future studies.

3.6 References

1. S. Chu and A. Majumdar, Opportunities and challenges for a sustainable energy future, *Nature*, 2012, 488, 294-303.
2. T. M. Gür, Review of electrical energy storage technologies, materials and systems: challenges and prospects for large-scale grid storage, *Energy & Environmental Science*, 2018, 11, 2696-2767.
3. O. C. Esan, X. Shi, Z. Pan, X. Huo, L. An, and T. Zhao, Modeling and Simulation of Flow Batteries, *Advanced Energy Materials*, 2020, 10, 2000758.
4. X. Yan, C. Lin, Z. Zheng, J. Chen, G. Wei and J. Zhang, Effect of clamping pressure on liquid cooled PEMFC stack performance considering inhomogeneous gas diffusion layer compression, *Applied Energy*, 2020, 258, 114073.
5. J. P. Lemmon, Energy: Reimagine fuel cells, *Nature News*, 2015, 525, 447.
6. L. An, T. Zhao and L. Zeng, Agar chemical hydrogel electrode binder for fuel-electrolyte-fed fuel cells, *Applied energy*, 2013, 109, 67-71.
7. B. Ong, S. Kamarudin and S. Basri, Direct liquid fuel cells: A review, *International journal of hydrogen energy*, 2017, 42, 10142-10157.
8. T. Zhao, C. Xu, R. Chen and W. Yang, Mass transport phenomena in direct methanol fuel cells, *Progress in energy Combustion Science*, 2009, 35, 275-292.
9. L. An, T. Zhao, R. Chen and Q. Wu, A Novel Direct Ethanol Fuel Cell with High Power Density, *Journal of power sources*, 2011, 196, 6219-6222.

10. Z. Pan, Y. Bi and L. An, Performance Characteristics of a Passive Direct Ethylene Glycol Fuel Cell with Hydrogen Peroxide as Oxidant, *Applied Energy*, 2019, 250, 846-854.
11. L. An and R. Chen, Direct Formate Fuel Cells: A Review, *Journal of power sources*, 2016, 320, 127-139.
12. S. Wang and S. P. Jiang, Prospects of fuel cell technologies, *National Science Review*, 2017, 4, 163-166.
13. X. Yan, H. Li, C. Lin, J. Chen, A. Han, S. Shen, J. Zhang and Fuels, An inorganic-framework proton exchange membrane for direct methanol fuel cells with increased energy density, *Sustainable Energy & Fuels*, 2020, 4, 772-778.
14. H. Jiang, L. Wei, X. Fan, J. Xu, W. Shyy and T. Zhao, A Novel Energy Storage System Incorporating Electrically Rechargeable Liquid Fuels as the Storage Medium, *J Science Bulletin*, 2019, 64, 270-280.
15. X. Shi, X. Huo, Y. Ma, Z. Pan and L. An, Energizing Fuel Cells with an Electrically Rechargeable Liquid Fuel, *Cell Reports Physical Science*, 2020, 1, 100102.
16. J. Hou, M. Yang, C. Ke and J. Zhang, Control logics and strategies for air supply in PEM fuel cell engines, *Applied Energy*, 2020, 269, 115059.
17. O. S. Ijaodola, Z. El- Hassan, E. Ogungbemi, F. N. Khatib, T. Wilberforce, J. Thompson and A. G. Olabi, Energy efficiency improvements by investigating the water flooding management on proton exchange membrane fuel cell (PEMFC), *Energy*, 2019, 179, 246-267.
18. O. C. Esan, X. Shi, Y. Dai, L. An, and T. S. Zhao, Operation of Liquid E-fuel Cells Using Air as Oxidant, *Applied Energy*, 2022, 311, 118677.

19. H. Jiang, W. Shyy, M. Wu, L. Wei and T. Zhao, Highly Active, Bi-Functional and Metal-Free B₄C-Nanoparticle-Modified Graphite Felt Electrodes for Vanadium Redox Flow Batteries, *Journal of Power Sources*, 2017, 365, 34-42.
20. F. Laurencelle, R. Chahine, J. Hamelin, K. Agbossou, M. Fournier, T. Bose and A. Laperriere, Characterization of a ballard MK5-E proton exchange membrane fuel cell stack, *Fuel cells*, 2001, 1, 66-71.
21. A. M. I. N. Azam, S. H. Lee, M. S. Masdar, A. M. Zainoodin and S. K. Kamarudin, Parametric study on direct ethanol fuel cell (DEFC) performance and fuel crossover, *International Journal of Hydrogen Energy*, 2019, 44, 8566-8574.
22. X. Li, Z. Miao, L. Marten and I. Blankenau, Experimental measurements of fuel and water crossover in an active DMFC, *International Journal of Hydrogen Energy*, 2021, 46, 4437-4446.
23. F. Abd Lah Halim, T. Tsujiguchi, Y. Osaka and A. Kodama, Performance of direct formic acid fuel cell using transition metal-nitrogen-doped carbon nanotubes as cathode catalysts, *International Journal of Energy Research*, 2019, 43, 8070-8084.
24. A. Oedegaard and C. Hentschel, Characterisation of a portable DMFC stack and a methanol-feeding concept, *Journal of Power Sources*, 2006, 158, 177-187.
25. S. Z. Rejal, M. S. Masdar and S. K. Kamarudin, A parametric study of the direct formic acid fuel cell (DFAFC) performance and fuel crossover, *International journal of hydrogen energy*, 2014, 39, 10267-10274.

26. S. H. Seo and C. S. Lee, Effect of Operating Parameters on the Direct Methanol Fuel Cell Using Air or Oxygen As an Oxidant Gas, *Energy & Fuels*, 2008, 22, 1212-1219.
27. Z. Song, Y. Pan, H. Chen and T. Zhang, Effects of temperature on the performance of fuel cell hybrid electric vehicles: A review, *Applied Energy*, 2021, 302, 117572.
28. Y. Li and T. Zhao, A high-performance integrated electrode for anion-exchange membrane direct ethanol fuel cells, *International journal of hydrogen energy*, 2011, 36, 7707-7713.
29. J. Charvát, P. Mazúr, M. Paidar, J. Povedič, J. Vrána, J. Mrlík and J. Kosek, The role of ion exchange membrane in vanadium oxygen fuel cell, *Journal of Membrane Science*, 2021, 629, 119271.
30. C. Yang, P. Costamagna, S. Srinivasan, J. Benziger and A. B. Bocarsly, Approaches and technical challenges to high temperature operation of proton exchange membrane fuel cells, *Journal of Power Sources*, 2001, 103, 1-9.
31. F. Wandschneider, M. Küttinger, J. Noack, P. Fischer, K. Pinkwart, J. Tübke and H. Nirschl, A coupled-physics model for the vanadium oxygen fuel cell, *Journal of Power Sources*, 2014, 259, 125-137.
32. X. Ma, H. Zhang, C. Sun, Y. Zou and T. Zhang, An optimal strategy of electrolyte flow rate for vanadium redox flow battery, *Journal of Power Sources*, 2012, 203, 153-158.
33. Y. Wei, C. Shengzhou and L. Weiming, Oxygen reduction on non-noble metal electrocatalysts supported on N-doped carbon aerogel composites, *International Journal of Hydrogen Energy*, 2012, 37, 942-945.

34. L. An and T. Zhao, An alkaline direct ethanol fuel cell with a cation exchange membrane, *Energy & Environmental Science*, 2011, 4, 2213-2217.
35. A. M. Bartrom and J. L. Haan, The direct formate fuel cell with an alkaline anion exchange membrane, *Journal of Power Sources*, 2012, 214, 68-74.
36. S. H. Seo and C. S. Lee, Effects of dimethyl ether on the performance characteristics of a direct methanol fuel cell, *Energy conversion and management*, 2013, 70, 239-243.
37. A. M. Bartrom, J. Ta, T. Q. Nguyen, J. Her, A. Donovan and J. L. Haan, Optimization of an anode fabrication method for the alkaline Direct Formate Fuel Cell, *Journal of Power Sources*, 2013, 229, 234-238.
38. P. Kanninen, M. Borghei, O. Sorsa, E. Pohjalainen, E. I. Kauppinen, V. Ruiz and T. Kallio, Highly efficient cathode catalyst layer based on nitrogen-doped carbon nanotubes for the alkaline direct methanol fuel cell, *Applied Catalysis B: Environmental*, 2014, 156-157, 341-349.
39. L. Zeng, Z. K. Tang and T. S. Zhao, A high-performance alkaline exchange membrane direct formate fuel cell, *Applied Energy*, 2014, 115, 405-410.
40. M. M. Bruno, F. A. Viva, M. A. Petruccelli and H. R. Corti, Platinum supported on mesoporous carbon as cathode catalyst for direct methanol fuel cells, *Journal of Power Sources*, 2015, 278, 458-463.
41. T. Q. Nguyen, D. Minami, C. Hua, A. Miller, K. Tran and J. L. Haan, Ambient Temperature Operation of a Platinum-Free Direct Formate Fuel Cell, *Journal of Fuel Cell Science and Technology*, 2015, 12, 014501.

42. M. Ercelik, A. Ozden, E. Seker and C. O. Colpan, Characterization and performance evaluation of PtRu/CTiO₂ anode electrocatalyst for DMFC applications, *International journal of hydrogen energy*, 2017, 42, 21518-21529.
43. D. Sebastian, A. Serov, I. Matanovic, K. Artyushkova, P. Atanassov, A. Aricò and V. Baglio, Insights on the extraordinary tolerance to alcohols of Fe-NC cathode catalysts in highly performing direct alcohol fuel cells, *Nano Energy*, 2017, 34, 195-204.
44. C. Lo Vecchio, A. Serov, H. Romero, A. Lubers, B. Zulevi, A. S. Aricò and V. Baglio, Commercial platinum group metal-free cathodic electrocatalysts for highly performed direct methanol fuel cell applications, *Journal of Power Sources*, 2019, 437, 226948.
45. X. Sun, Y. Li and M.-J. Li, Highly dispersed palladium nanoparticles on carbon-decorated porous nickel electrode: An effective strategy to boost direct ethanol fuel cell up to 202 mW cm⁻², *ACS Sustainable Chemistry Engineering*, 2019, 7, 11186-11193.
46. V. S. Pinheiro, F. M. Souza, T. C. Gentil, A. N. Nascimento, P. Böhnstedt, L. S. Parreira, E. C. Paz, P. Hammer, M. I. Sairre and B. L. Batista, Sn-containing electrocatalysts with a reduced amount of palladium for alkaline direct ethanol fuel cell applications, *Renewable Energy*, 2020, 158, 49-63.
47. A. K. Choudhary and H. Pramanik, Enhancement of ethanol electrooxidation in half cell and single direct ethanol fuel cell (DEFC) using post-treated polyol synthesized Pt-Ru nano electrocatalysts supported on

HNO₃-functionalized acetylene black carbon, *International Journal of Hydrogen Energy*, 2020, 45, 574-594.

48. C. L. Vecchio, A. Serov, M. Dicome, B. Zulevi, A. Aricò and V. Baglio, Investigating the durability of a direct methanol fuel cell equipped with commercial Platinum Group Metal-free cathodic electro-catalysts, *Electrochimica Acta*, 2021, 394, 139108.

49. L. Mu, W. Cheng, L. Zhi-xiang and M. Zong-qiang, The development and performance analysis of all-China-made PEM fuel cell unit and 1 kW level fuel cell stack, *International Journal of Hydrogen Energy*, 2012, 37, 1106-1111.

50. Y. Zeng, T. Zhao, L. An, X. Zhou and L. Wei, A comparative study of all-vanadium and iron-chromium redox flow batteries for large-scale energy storage, *Journal of Power Sources*, 2015, 300, 438-443.

51. Y. Wang, G. Liu, M. Wang, G. Liu, J. Li and X. Wang, Study on stability of self-breathing DFMC with EIS method and three-electrode system, *International journal of hydrogen energy*, 2013, 38, 9000-9007.

52. S. Song, G. Wang, W. Zhou, X. Zhao, G. Sun, Q. Xin, S. Kontou and P. Tsiakaras, The effect of the MEA preparation procedure on both ethanol crossover and DEFC performance, *Journal of power sources*, 2005, 140, 103-110.

53. P. Hong, F. Luo, S. Liao and J. Zeng, Effects of Pt/C, Pd/C and PdPt/C anode catalysts on the performance and stability of air breathing direct formic acid fuel cells, *International Journal of Hydrogen Energy*, 2011, 36, 8518-8524.

54. V. Bambagioni, C. Bianchini, Y. Chen, J. Filippi, P. Fornasiero, M. Innocenti, A. Lavacchi, A. Marchionni, W. Oberhauser and F. Vizza, Energy Efficiency Enhancement of Ethanol Electrooxidation on Pd–CeO₂/C in Passive and Active Polymer Electrolyte-Membrane Fuel Cells, *ChemSusChem*, 2012, 5, 1266-1273.
55. J. Cao, L. Wang, L. Song, J. Xu, H. Wang, Z. Chen, Q. Huang and H. Yang, Novel cathodal diffusion layer with mesoporous carbon for the passive direct methanol fuel cell, *Electrochimica Acta*, 2014, 118, 163-168.
56. L. Wang, A. Lavacchi, M. Bevilacqua, M. Bellini, P. Fornasiero, J. Filippi, M. Innocenti, A. Marchionni, H. A. Miller and F. Vizza, Energy efficiency of alkaline direct ethanol fuel cells employing nanostructured palladium electrocatalysts, *ChemCatChem*, 2015, 7, 2214-2221.
57. Z. Yuan, W. Chuai, Z. Guo, Z. Tu and F. Kong, Investigation of self-adaptive thermal control design in passive direct methanol fuel cell, *Energy Storage*, 2019, 1, 64.

Tables

Table 3-1 Comparison of peak power density among various direct liquid fuel cell that used either air or oxygen as oxidant.

Year	Fuel	Membrane	Oxidant	Temp (°C)	Cathode Catalyst (mg cm ⁻²)	Peak power density (mW cm ⁻²)	Ref.
2006	Methanol	Nafion 117	Air	50	Pure Pt (4.0)	~50	24
2007	Methanol	Nafion 117	Air	80	Pt-black (4.0)	~0.16	26
2010	Methanol	Nafion 117	Oxygen	60	Co-CA-N (10.0)	53.16	33
2011	Ethanol	Nafion 211	Oxygen	60	Fe-Co (1.0)	100	34
2012	Formic acid	A201	Air	60	Pt/C (2.0)	~110	35
2013	Methanol	Nafion 115	Air	80	Pt-black (4.0)	51.2	36
2013	Formic acid	A201	Air	60	Pt/C (4.0)	105	37
2013	Methanol	Fumatech FAA3	Air	30	N-FWCNT (2.3)	0.73	38
2014	Formic acid	QAPSF membrane	Oxygen	60	Fe-Co (2.0)	~94	39
2014	Methanol	Nafion 212	Air	60	Pt/MC (3.0)	~30	40
2015	Formic acid	A201	Air	30	Fe-Co (0.75)	~44	41
2015	Formic acid	A201	Oxygen	20	Fe-Co (0.75)	18	41
2016	Methanol	Nafion 115	Oxygen	45	Pt/C (2.0)	43.75	42
2016	Methanol	Nafion 115	Oxygen	90	Fe-NCB (4.0)	60	43
2018	Ethanol	Nafion 117	Air	R.T.	Pt/C (4.0)	1.81	21
2019	Methanol	Nafion 115	Oxygen	90	Fe-N-C (6.0)	~72	44
2019	Ethanol	A201	Oxygen	20	Acta 4020 (2.0)	54	45
2019	Formic acid	NR212	Oxygen	60	Fe-NCNT (4.6)	71.5	23
2019	Formic acid	NR212	Oxygen	60	Co-NCNT (3.3)	160.7	23
2020	Ethanol	Nafion 117	Oxygen	80	Pt/C (1.0)	42	46
2020	Ethanol	Nafion 117	Oxygen	40	Pt/C (1.0)	7.86	47
2020	Methanol	Nafion 115	Air	90	Pt/C (1.25)	110.77	22
2021	Methanol	Nafion 115	Oxygen	90	Fe-N-C (6.0)	72	48

Year	Fuel	Membrane	Oxidant	Temp (°C)	Cathode Catalyst (mg cm⁻²)	Peak power density (mW cm⁻²)	Ref.
2022	E-fuel	Nafion 117	Air	23	Pt/C (~0.5)	168.3	This work

Table 3-2 Comparison of the cost of e-fuel cell with other liquid fuel cells.

Fuel Cells	Anode (USD m⁻²)	Membrane (USD m⁻²)	Cathode (USD m⁻²)	MEA (USD m⁻²)	PPD (mW m⁻²)	Cost (USD kW⁻¹)	Ref.
Methanol Fuel cell	\$11147 Pt-Ru black (4 mg cm ⁻²)	\$500 Nafion series	\$9171 Pt black (4 mg cm ⁻²)	\$20818	20.1	\$103572.14	[49-51]
Ethanol Fuel cell	\$8371 Pt-Ru black (3 mg cm ⁻²)	\$500 Nafion series	\$6889 Pt black (3 mg cm ⁻²)	\$15760	29.9	\$52709.03	[49,50,52]
E-fuel cell	\$70 Graphite felt	\$500 Nafion series	\$1307.17 Pt/C 60% (0.5 mg cm ⁻²)	\$1877.17	254.6	\$737.30	[49,50]

Table 3-3 Comparison of energy efficiency among various types of direct liquid fuel cell that employed either air or oxygen as oxidant.

Year	Fuel	Oxidant	Current Density (mA cm ⁻²)	Temp. (°C)	Energy Efficiency (%)	Ref.
2011	Formic acid	Air	5	R.T.	7.9	53
2012	Ethanol	Air	20	25	~12	54
2014	Methanol	Air	40	25	10.7	55
2015	Ethanol	Air	20	R.T.	6.6	56
2019	Methanol	Air	100	60	9.3	57
2022	E-fuel	Air	10	23	26.4	This work

Chapter 4 Operation of fuel cells using hydrogen peroxide as oxidant

4.1 Introduction

Depletion of resources and energy crisis in tandem with the increase in global population are undoubtedly some of the threatening challenges in our modern society. To significantly cut down the massive energy dependence on the limited and inefficient fossil fuels as well as their corresponding greenhouse gas emissions, the development and use of clean and renewable power sources are now of increasing importance and thus remain as one of the ultimate targets for researchers and scientists across the globe [1,2]. Over the years, fuel cell technology has emerged as an efficient and environmentally friendly energy conversion option as it converts the chemical energy available in fuel directly to electrical energy. Beginning with the use of hydrogen, a chemical energy carrier, hydrogen fuel cells have received a broad array of applications, including the transport sector. However, the high-pressure requirement, safety and flammability issues, storage as well as transport difficulties of hydrogen seriously limit the continuous application and large-scale deployment of hydrogen fuel cells [3]. This therefore necessitated the needs to introduce and employ alternative fuels for fuel cell systems.

Due to the modularity and flexibility of utilization of fuel cells, a number of liquid fuels, including alcohols such as methanol and ethanol, have been employed to operate fuel cells. These liquid fuel cells have also been demonstrated to offer several benefits, including high energy density, high safety, and easy storage, in comparison to hydrogen fuel cells [4,5]. However, the high catalyst cost, fuel crossover, short durability, limited

energy efficiency, and low power density associated with these direct liquid fuel cells later raised major concerns on the needs to utilize more efficient liquid fuels towards improving the cell performance. In response to this, the idea of using an electrically rechargeable liquid fuel (e-fuel) was recently proposed [6] and is currently receiving an increasing research attention. Interestingly, both organic and inorganic materials were stated as prospective and suitable candidates to produce e-fuels. Subsequently, an e-fuel solution which contains vanadium ions dissolved in H_2SO_4 was used to fuel the anode and thereafter showcased its promising capabilities for running a fuel cell system [7,8]. Addressing the fuel issues prevalent in hydrogen and alcoholic fuel cells, the use of this e-fuel offers several advantages including the elimination of catalyst material at the anode, thereby reducing the fabrication cost of the cell. This particular e-fuel has therefore been demonstrated to possess excellent potential and fascinating properties to remain dominant over a long term in fuel cell applications.

Generally, an oxidant is required at the cathode of fuel cells. Gaseous oxygen or ambient air has been mostly employed for this purpose. However, their utility and performance are largely limited in air/oxygen-free environments and similar special conditions, such as space propulsion, and underwater power systems. As an alternative and a realistic oxidant, hydrogen peroxide (H_2O_2) has been demonstrated to be workable in fuel cells under the above-mentioned air-independent systems and for high power applications. In addition, the use of H_2O_2 offers a number of advantages compared to oxygen [9,10]: (i) significantly increases the theoretical voltage of the fuel cell, (ii) offers low activation loss due to two-

electron transfer, (iii) avoids water flooding issue and simplifies heat removal as a result of its intrinsic liquid phase, (iv) offers higher current density due to its higher mass density compared to gas, and thus ultimately improves the performance of the fuel cell. Following these intriguing advantages, H_2O_2 has been employed as oxidant in the operation of fuel cells.

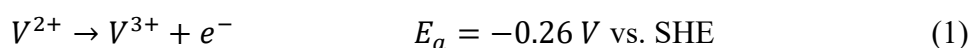
Interestingly, the reduction reaction of H_2O_2 can occur in either acidic or alkaline media [9]. However, to achieve high fuel cell performance, the reduction reaction is mostly preferred in acidic media as a result of its inherently higher potential (1.78 V) in comparison to alkaline media (0.87 V). In addition, hydrogen peroxide is less stable in alkaline solution leading to its high decomposition rate [9,10]. Conversely, the addition of sulfuric acid stabilizes the H_2O_2 solution and also enhances its electrochemical reduction [9]. While various fuels, including hydrazine [11] and ethylene glycol [12], have been paired with hydrogen peroxide for fuel cell operations, sodium borohydride is the mostly used fuel in H_2O_2 -based fuel cells with numerous studies, including the development of anode [13, 14] and cathode electrocatalysts [15,16], and bipolar interface membrane electrode assembly [17,18] with the aim to enhance the performance of the fuel cells. However, the toxic nature and safety concerns regarding the hydrogen evolution of the borohydride solution and the undesired disparity between the pH environment of the alkaline electrolyte at the anode and acid-based oxidant at the cathode have largely constrained the commercialization of direct borohydride/ H_2O_2 fuel cells.

Herein, the operation as well as the performance of H₂O₂-based e-fuel cell, as it combines an all-aqueous reactant and the superior advantages of both e-fuel (as anolyte) and H₂O₂ (as catholyte), is experimentally examined. The hydrogen peroxide aqueous solution used at the cathode is, however, directly acidified using sulfuric acid. The experimental investigation of this novel e-fuel/hydrogen peroxide fuel cell produced a peak power density of 1456.0 mW cm⁻² at 60 °C, which is 70% higher than the use of oxygen (857.0 mW cm⁻²) [7], and also indicates a maximum current density exceeding 3000 mA cm⁻². Such impressive performance not only outshines the e-fuel cells receiving oxygen as oxidant, but also exceeds many of the regular direct liquid fuel cells whose oxidant is H₂O₂. The performance of the cell by varying hydrogen peroxide concentration, sulfuric acid concentration, vanadium ion concentration, operating cell temperature, Nafion membrane thicknesses, and its constant-current discharge characteristics are also investigated. The details of the experiment and the various results obtained from the investigations are discussed in subsequent sections.

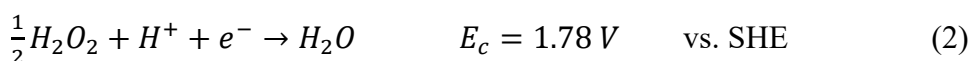
4.2 Operation principle of the cell

The operation principle of this e-fuel/H₂O₂ cell, schematically presented in Figure 4.1, is simply described below:

At the anode, the e-fuel is oxidized as follows [7]:



At the cathode, the reduction reaction of the hydrogen peroxide is as follows [12]:



The overall reaction of the e-fuel/ H_2O_2 cell is:

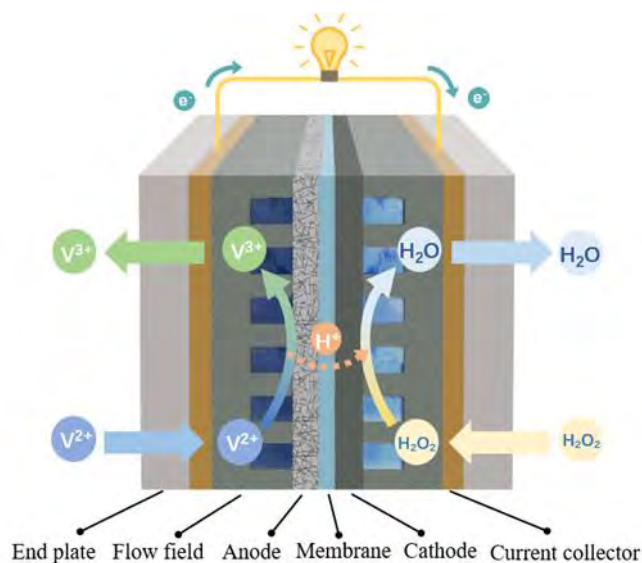


Figure 4.1 The operation principle of the e-fuel/ H_2O_2 fuel cell.

4.3 Experimental details

4.3.1 Membrane electrode assembly

For the membrane electrode assembly (MEA), a catalyst-free graphite-felt electrode having a surface area of 4.0 cm^2 and treated by heating for five hours in the air while subjected to a temperature of 500°C is used as the anode. A pretreated Nafion membrane, adopting the preparation method as reported before [19], of size 9.0 cm^2 is used for the experiment. A Pt/C coated carbon paper of 0.50 mg cm^{-2} loading produced by simply following the procedure used in one of our previous studies [20] is used as the cathode. Thereafter, these three aforementioned materials were assembled such that the Nafion membrane is properly placed in the middle of the anode and the cathode to achieve the MEA.

4.3.2 Preparation of electrolytes

The anolyte, known as the e-fuel, which fuels the anode was prepared as follows. VO_2 powder was first dissolved in H_2SO_4 , the resulting solution was thereafter subjected to a charging process in a classic flow cell as described before [21]. The catholyte, which is mostly referred to as oxidant in this study, is also an aqueous solution simply prepared by mixing sulfuric acid solution and hydrogen peroxide. After the preparation of both solutions, a 40.0 mL of both anolyte and catholyte was released into separate tanks for storage and in readiness for the cell operation.

4.3.3 Fuel cell set-up and instruments

The devices set-up for this experimental study is presented in Figure 4.2. A peristaltic pump was assigned to each side of the cell to circulate the electrolytes through the cell. A temperature controller device (Anhone Electronic Co. Ltd., China) which has two heating rods was later inserted, each for heating the anode and cathode sides, and thermocouples for monitoring the temperature of the cell was also employed during the cell operation. The various experimental tests reported in this study were performed and recorded using a fuel cell testing system (Neware Technology Limited, China).

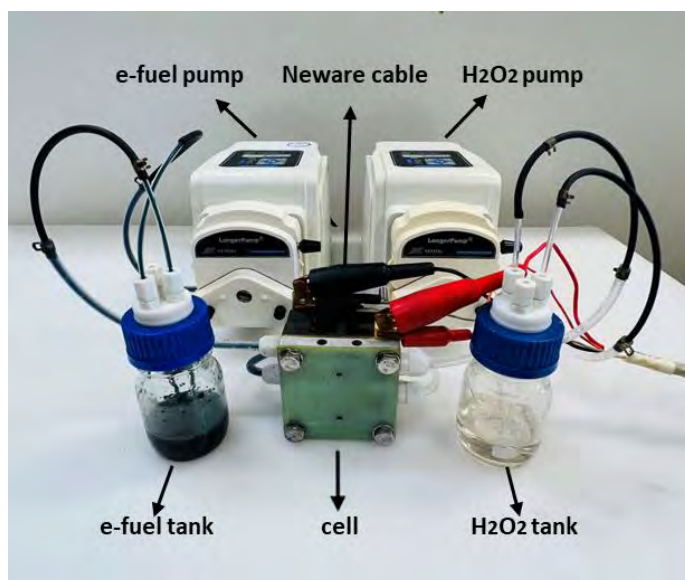


Figure 4.2 Experimental set-up for the e-fuel/hydrogen peroxide cell [21].

4.4 Results and discussion

4.4.1 General cell performance

The general performance of this H₂O₂-based fuel cell is presented in this section. The anolyte delivered into the cell is composed of 1.5 M V²⁺ in 4.0 M H₂SO₄ while the catholyte is a combination of 4.0 M H₂O₂ in 1.0 M H₂SO₄. Both anolyte and catholyte are pumped into the cell at a flow rate of 50.0 mL min⁻¹. The operating temperature of the cell is set at 60 °C. Under such an operating condition, the cell achieved a peak power density of 1456.0 mW cm⁻² and an open circuit voltage of 1.09 V as shown in Figure 4.3a. The peak power density of this H₂O₂-based fuel cell demonstrates an impressive improvement in comparison to previous studies where oxygen/air are employed as oxidant in the demonstration of the e-fuel cell at 60 °C as presented in Table 4-1. The considerable performance enhancement can be majorly attributed to the several benefits, including

higher theoretical voltage and lower cathode overpotential, of utilizing H_2O_2 as oxidant in the fuel cells.

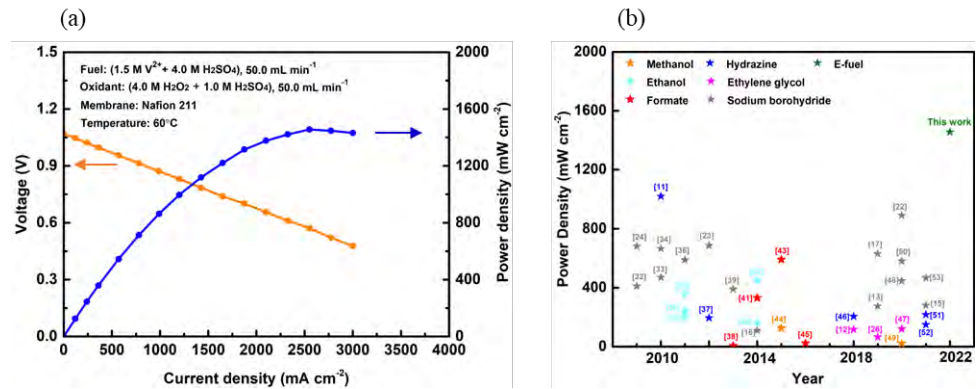


Figure 4.3 (a) General performance of the H_2O_2 -based fuel cell and (b) Comparison of power density with data obtained from the open literature for direct liquid fuel cells that employed H_2O_2 as oxidant.

In comparison to direct liquid fuel cells that also employed hydrogen peroxide as oxidant, the performance of this H_2O_2 -based e-fuel cell also substantially outperforms them all as presented in Figure 4.3b and Table 4-2. For instance, a hydrazine/ H_2O_2 fuel cell demonstrated at 60°C could only achieve a peak power density of 780 mW cm^{-2} [11], which is about half of the peak power density attained by the H_2O_2 -based fuel cell in this study. Even at a higher operating temperature (80°C), the peak power density exhibited by the hydrazine/ H_2O_2 fuel cell is 1020 mW cm^{-2} which is still lower than that of the e-fuel/hydrogen peroxide fuel cell. The widely studied direct borohydride/ H_2O_2 fuel cell demonstrated at 70°C has been reported to achieve a peak power density of 890 mW cm^{-2} after introducing bipolar interface membrane electrode assembly [22]. In another research group, the direct borohydride fuel cell with H_2O_2 as oxidant exhibited a peak power density of 685 mW cm^{-2} at an operating cell temperature of 60°C [23].

Elsewhere, the direct borohydride/H₂O₂ fuel cell demonstrated similar performance at 60 °C to yield a peak power density of 680 mW cm⁻² [24]. To the best of our knowledge, the peak power densities achieved by other fuel cells that employed H₂O₂ as oxidant all fall below 700 mW cm⁻², which further justify the superiority of this e-fuel/hydrogen peroxide fuel cell. Regarding open circuit voltage, the result achieved from this H₂O₂-based fuel cell is not only lower compared to when the cell was fed with oxygen at the cathode, but also lesser than its theoretical voltage. The voltage drop can be ascribed to the decomposition of the H₂O₂ to produce oxygen at the cathode which in turn decreases the cathode potential [12]. Moreover, the crossover of reactants from both sides of the cell, as both reactants are in liquid phase and can penetrate the Nafion membrane, can also reduce the open circuit voltage. In particular, the crisscross of the fuel to the cathode can cause large loss in the cathode potential because of mixed potential. While these issues are suggested to be addressed in future studies to increase the open circuit voltage, the impressive peak power density demonstrated by this e-fuel/hydrogen peroxide fuel cell positions it as a promising power generation system for air-free and high-power applications.

4.4.2 Effect of the hydrogen peroxide concentration

Concentration is generally considered to be of significant influence on the rate of decomposition of H₂O₂. Hence the effect of H₂O₂ concentration on the performance of this fuel cell is examined in this section. Here, various H₂O₂ concentrations varying from 1.0 to 6.0 M are considered with the concentration of the H₂SO₄ set as 1.0 M for the oxidant while the e-fuel solution at the anode is composed of 1.5 M V²⁺ in 4.0 M H₂SO₄. Figure 4.4

displays the cell performance obtained from the investigations at an operating temperature of 60 °C. As it can be seen, an upgrade in the performance of the cell is achieved all through the current density range when the H₂O₂ concentration is first increased from 1.0 M to 2.0 M. With an increase in the H₂O₂ concentration to 4.0 M, the cell performance was not only further enhanced but also displayed the highest performance.

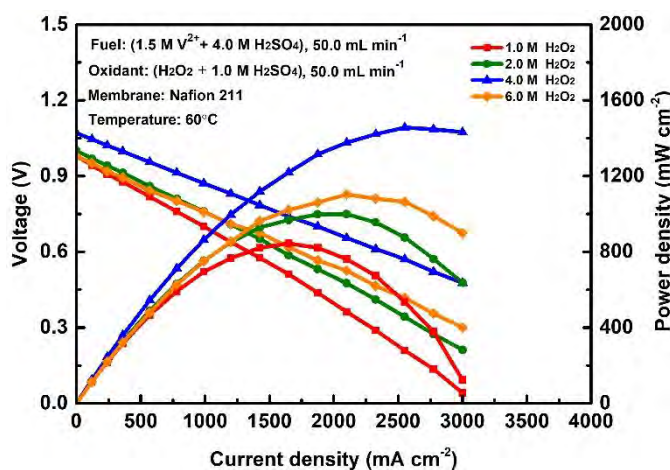


Figure 4.4 Effect of the hydrogen peroxide concentration on the cell performance.

The commensurate increase in the cell performance with increase in the hydrogen peroxide concentration is majorly due to the enhanced mass transport of the reactive species at the cathode which consequently reduces concentration polarization loss and further improves the cell performance [20]. A further increase in the hydrogen peroxide concentration to 6.0 M, however, decreases the cell performance below that of 4.0 M at all the current density regions. The general decrease in the performance of the cell when the H₂O₂ concentration was increased to 6.0 M can be said to be from the competitive adsorption that happens between H₂O₂ and H⁺ on the reactive spots of the cathode as a result of redundant H₂O₂ [12]. This

therefore facilitates the undesired concentration loss of H^+ and also heightens the internal resistance within the cell. In comparison to concentration at 2.0 M, the obtained cell voltage at the use of 6.0 M is also seen to fall below that of 2.0 M at the low current density regions and later increases above that of 2.0 M at higher current densities. At low current density, the reduced cell voltage can be attributed to higher crossover rate of hydrogen peroxide to the anode as the membrane is permeable to hydrogen peroxide [25]. The hydrogen peroxide that crossed over to the anode can react with the e-fuel and result to mixed potential at the anode which could raise the anode overpotential and hence decrease the cell voltage. At higher current density range, the reduced concentration loss as a result of high hydrogen peroxide concentration could be considered to have compensated for the mixed potential at the anode and thus only upgrade the cell performance above that of H_2O_2 concentration at 1.0 and 2.0 M but not that of 4.0 M. Overall, increasing the H_2O_2 concentration to 6.0 M is not beneficial to the cell voltage and its general performance, which therefore position an H_2O_2 concentration of 4.0 M as the optimal value to yield the best performance for the operation of this fuel cell.

4.4.3 Effect of the sulfuric acid concentration

In this study, the hydrogen peroxide used at the cathode is directly acidified using sulfuric acid. The concentration of the H_2SO_4 added to the hydrogen peroxide aqueous solution would definitely influence the properties of the oxidant at the cathode and thus the overall performance of the cell. We therefore investigate the influence of the sulfuric acid concentration on the cell performance in this section. Here, the e-fuel is composed of 1.5 M V^{2+}

in 4.0 M H₂SO₄ while 4.0 M H₂O₂ with varying sulfuric acid concentrations from 0 to 3.0 M are used as the oxidant. The cell performance derived from this investigation at an operating temperature of 60 °C are presented in Figure 4.5.

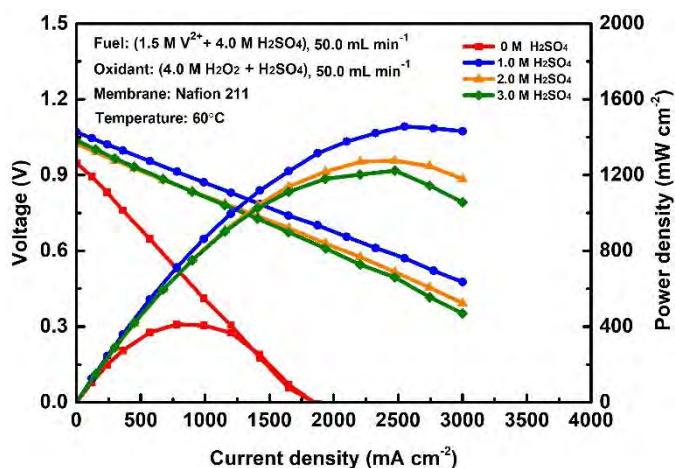


Figure 4.5 Effect of the sulfuric acid concentration on the cell performance.

At first, the cell was tested using a pure hydrogen peroxide solution, without adding sulfuric acid, as oxidant. It is seen that the cell performance obtained is very low with a peak power density slightly above 400 mW cm⁻². With the addition of 1.0 M H₂SO₄ to the H₂O₂ solution as the catholyte, the peak power density is seen to dramatically increase and exhibit the highest performance of the cell. The explanation for this is that the presence of sulfuric acid results in higher concentration of H⁺ at the cathode and also enhances its transport to the reactive area in the cathode catalyst layer, thereby accelerating the reduction reaction of the hydrogen peroxide [26]. Following this, the kinetic loss of the reduction reaction at cathode is reduced while the cathode potential and cell performance are improved. Afterwards, as the sulfuric acid concentration was further increased to 2.0 and 3.0 M, it can be seen that higher concentration of sulfuric acid does not

offer improvement to the cell performance but rather a decrease throughout the whole current density regions. The decrease in the cell voltage and power density with increase in the concentration of H_2SO_4 can be attributed to the blocking of the reactive area by the excessive sulfuric acid which leads to insufficient presence of H_2O_2 in the catalyst layer leading to its concentration loss at the cathode thereby degrading the cell performance [12,22]. In addition, higher concentration of sulfuric acid increases the catholyte viscosity which also impedes the transport of the reactants and in turn increases ohmic loss and degrade the cell performance [27]. The fuel cell therefore attains its best performance when the concentration of the sulfuric acid employed to acidify the hydrogen peroxide is 1.0 M.

4.4.4 Effect of the vanadium ion concentration

The effect of vanadium ion concentrations on the cell performance is also explored. In this case, the concentration of the H_2SO_4 in the anolyte is maintained at 4.0 M while various vanadium ion concentration of 0.1, 0.5, 1.0, and 1.5 M are used. The composition of the solution pumped into the cathode is 4.0 M H_2O_2 in 1.0 M H_2SO_4 . The various polarization and power density curves obtained from this particular test at 60 °C are shown in Figure 4.6. As it can be viewed, performance of the cell significantly improve all through the current density range when the vanadium ion concentration is increased from 0.1 M to 1.5 M. In more details, with the first increase of the vanadium ion concentration from 0.1 M to 0.5 M, the open circuit voltage, peak power density, and maximum current density of the cell is observed to increase from 0.75 V, 145.3 mW cm^{-2} , and 660 mA cm^{-2} to 0.89 V, 701.9 mW cm^{-2} , and 2550 mA cm^{-2} , respectively.

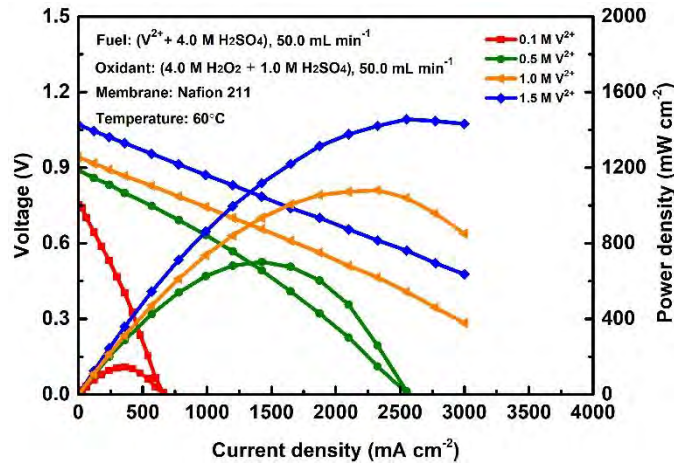


Figure 4.6 Effect of the vanadium ion concentration on the cell performance.

With a further increase of the vanadium ion concentration to 1.0 M and 1.5 M, it can be seen that the maximum current density of the cell apparently exceeds 3000 mA cm⁻² in both cases. Nevertheless, the highest performance of the cell with a peak power density of 1456.0 mW cm⁻² is achieved at a vanadium ion concentration of 1.5 M. The cell performance significantly improves with the increase of the vanadium ion concentration due to the increase in the amount and delivery of the reactive species to the active sites of the anode. This therefore enhances the mass transport of the reactant at the anode which beneficially lowers concentration loss [28]. Moreover, the increase of the vanadium ion concentration boosts the reaction kinetics at the anode which in turn reduces activation loss and augments the cell performance. However, it is undeniable that the increase of vanadium concentration would also increase the fuel viscosity and thereby limit the mass transport of the reactants and eventually deteriorate the cell performance [27]. Within the range tested in this study, however, a higher vanadium concentration up to 1.5 M yields the best performance.

4.4.5 Effect of the membrane thickness

Membrane is an indispensable element in fuel cell design which not only serves as a medium for ions transport between the two sides of the cell but also prevents reactants crossover. Nafion series have been mostly considered and adopted in the operation of fuel cells due to the excellent chemical stability in addition to the high proton conductivity of these membranes. A number of Nafion membranes – 117, 115, 212, and 211 are therefore incorporated into the setup of this cell. The effects of these membranes, particularly their thickness – 183.0, 127.0, 50.8, and 25.4 μm , respectively, on the performance of the cell at 60 °C are examined and the results are depicted in Figure 4.7. It is seen that the general performance of the cell increases with the decrease in the thickness of the membranes used in the cell operation. In terms of their peak power density, Nafion 117, 115, 212, and 211 membranes exhibit 615.13, 665.94, 1039.56, and 1456.0 mW cm^{-2} , respectively. With the use of Nafion 211, the thinnest membrane, the cell achieves a peak power density of 1456.0 mW cm^{-2} which is more than twice the peak power density (615.13 mW cm^{-2}) with the use of the thickest membrane, Nafion 117, in the cell. In addition, the maximum current density observed when the cell uses the thin membranes (Nafion 212 and 211) is apparently beyond 3000 mA cm^{-2} while the maximum current density realized with the use of thick membranes (Nafion 117 and 115) are lower at 2100 and 2325 mA cm^{-2} , respectively.

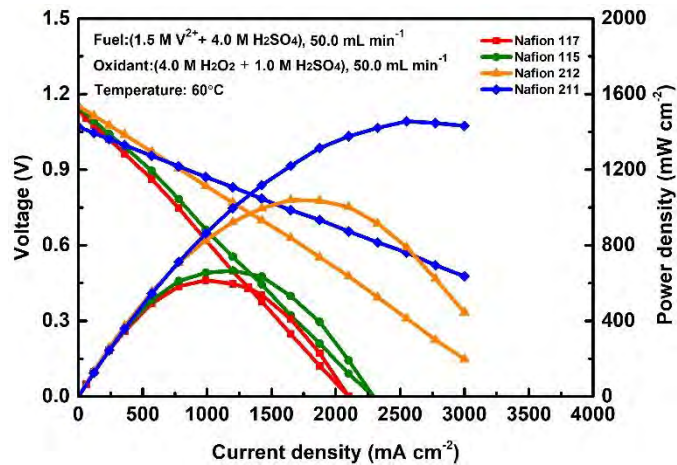


Figure 4.7 Effect of the membranes thickness on the cell performance.

The decrease in the cell performance as the membrane thickness increases can be explained by the higher internal resistance associated with thick membranes which often results in voltage loss [29]. However, the thick membranes are considered to be more suitable to prevent the crisscross of reactants to avoid mixed potential [7]. In other words, the use of thinner membrane leads to species crossover and cause mixed potential which could reduce the cell voltage. As seen in Figure 4.7, the cell voltage achieved at the low current density range with the use of Nafion 211, the thinnest membrane, is initially lower than others which can be ascribed to the crossover reactants. The thicker membranes therefore attain better performance in the low current density regions while the thinner membranes perform better at the high current densities. Overall, these findings suggest that the high internal resistance associated with thick membranes overrides the effects of species crossover on the cell performance to produce the best performance with the use of Nafion 211. This therefore justifies the use of thinner membranes, such as Nafion 211, for cell operations where high power density is of paramount importance.

4.4.6 Effect of the operating temperature

Operating temperature is a crucial parameter that is generally considered for the design and demonstration of liquid fuel cells. The operating temperature not only reflects the thermal range of the fuel cell and its various components but also reflects their thermal behavior and thereby provides useful insights on their thermal management. Furthermore, the chemical decomposition of the H_2O_2 used as the oxidant in this fuel cell is highly influenced by temperature and considered to be alleviated at lower temperatures [9]. This section therefore examines the performance of this H_2O_2 -based fuel cell under various operating temperature. The outcome of the investigation as displayed in Figure 4.8 clearly shows that both the cell voltage and power density increase in tandem with the temperature.

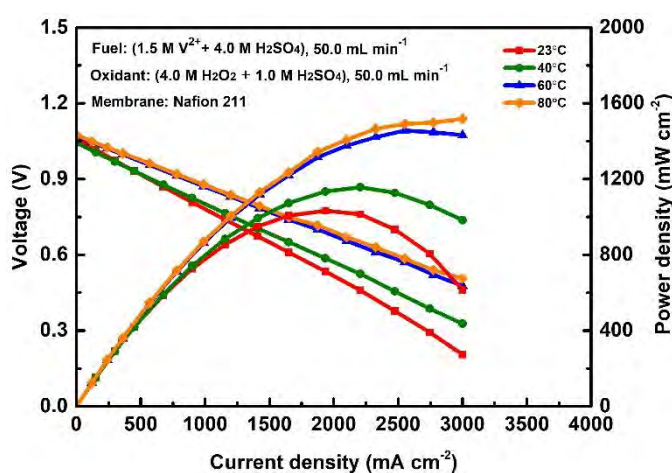


Figure 4.8 Effect of the operating temperature on the cell performance.

Starting with the operation of the cell at room temperature, taken as $23 \text{ }^\circ\text{C}$, a peak power density as high as $1033.6 \text{ mW cm}^{-2}$ is achieved. On increasing the cell temperature to $40 \text{ }^\circ\text{C}$, the peak power density of the cell increased by 12 % to reach $1157.6 \text{ mW cm}^{-2}$. The investigation of the cell performance at an operating temperature of $60 \text{ }^\circ\text{C}$ yields a peak power density of 1456.0

mW cm⁻² which is about 26 % higher than that of 40 °C. Increasing the cell temperature enhances the transport of the fuel and the delivery of H₂O₂ to their electrochemical reactive spots and further increases product removal rates, which beneficially reduces concentration loss [30]. In addition, activation loss of the cell is significantly lowered as the temperature of the cell increases due to the improvement in the electrochemical kinetics of the electrodes. Furthermore, an increase in the temperature boosts the conductivity of the membrane which thus lessens the undesired ohmic loss within the cell and ultimately improves the cell performance [7]. However, a further raise of the operating temperature from 60 °C to 80 °C could barely offer significant cell performance improvement as it can be seen in Figure 4.8. Such a high operating temperature speeds up the violent decomposition of H₂O₂ to oxygen, which consequently lowers the cathode potential [12]. Moreover, the cell is predisposed to severe reactant crossover at higher temperatures which degrades the electrode potential and thus deteriorates the cell performance [30]. Following this, 60 °C is considered as the optimal temperature suitable for the high performance of this cell.

4.4.7 Constant-current discharge behavior

The purpose of the constant-current discharge test is to evaluate the performance of the fuel cell similar to its real-life applications. In this study, the constant current discharge test is conducted at 50, 100, and 200 mA cm⁻² under an operating temperature of 60 °C. Results from the constant-current discharge test are further used to calculate the Faradic, voltage, and energy efficiencies of the cell. As shown in Figure 4.9a, it is clear that the voltage plateau and the discharge capacity of the cell increases with the constant

current. This therefore produced voltage efficiency of 46.7%, 47.8%, and 47.5%, under the three different currents considered as shown in Figure 4.9b. In addition, the discharge capacity of the cell under these three constant currents are 1.92, 6.67, and 12.5 Ah L⁻¹, respectively, which clearly increases with the constant currents. Such results thus demonstrate the increase of the constant discharge current could enable a better utilization of the reactants, where the energy efficiency of the cell, as shown in Figure 4.9b is also seen to increase from 2.3 % to 14.7 % as the operating current is increased from 50 to 200 mA cm⁻². Even though there is room for the improvement of the energy efficiency, this trend suggests that the cell has potential for higher energy efficiency when subjected to higher constant current.

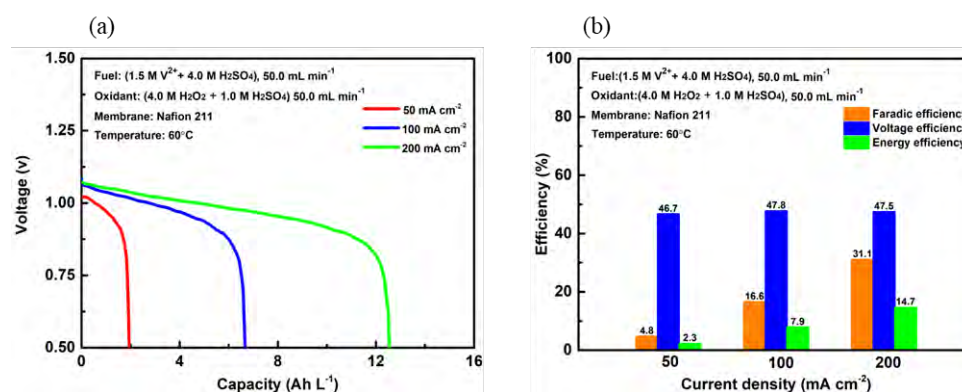


Figure 4.9 (a) Constant-current discharge performances and (b) Efficiencies of the cell under three different current densities – 50, 100, and 200 mA cm⁻².

Furthermore, to ascertain the ability of this system for long-term operations, it was refueled for 10 times while discharging at a constant current of 10 mA cm⁻² under an operating temperature of 60 °C (Figure 4.10) proving its good stability. However, during the cell operation, the e-fuel and hydrogen

peroxide could penetrate the membrane to the opposite side leading to the corrosion of the electrodes which in turn degrade the cell performance and thus require careful attention.

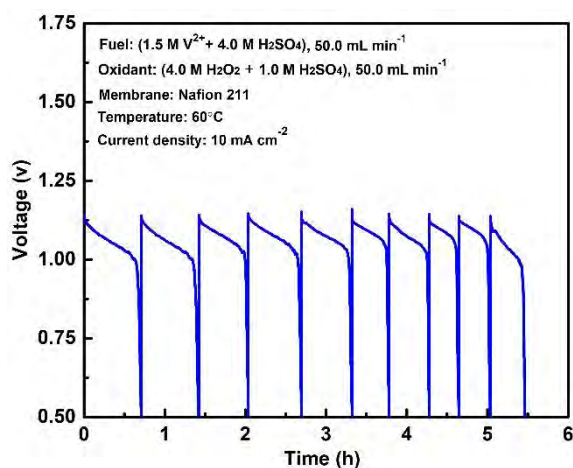


Figure 4.10 Durability of the cell showing its discharging behavior after refueling for 10 times.

4.5 Summary

This study presents the operation and performance of a high-performance H_2O_2 -based fuel cell for application in air-tight environments. As an alternative oxidant, instead of oxygen or ambient air, hydrogen peroxide is used at the cathode. The results obtained from the experimental study show that the application of H_2O_2 as oxidant substantially bolsters the performance of the cell to achieve a peak power density of 1456.0 $mW\ cm^{-2}$ at 60 °C and a maximum current density which exceeds 3000 $mA\ cm^{-2}$. This impressive performance not only outperforms the e-fuel cell fed with oxygen as oxidant but also exceeds most of the regular direct liquid fuel cells that also employ H_2O_2 as oxidant. Further investigations reveals that the cell performance increases with H_2O_2 concentration till 4.0 M, above which the performance starts to drop. Acidifying the H_2O_2 with sulfuric acid

concentration of 1.0 M yields the best cell performance. As for the vanadium ion, increasing its concentration from 0.5 M to 1.5 M contributes to the improvement of the cell performance. An operating temperature of 60 °C is considered suitable for the operation and high performance of this cell. Nafion 211 is demonstrated as the most suitable membrane for the cell operations as high-power density is of paramount importance for aerospace propulsion and underwater power systems. This study thus provides stimulating insights for future investigations towards improving the design and operating condition of this e-fuel/H₂O₂ fuel cell for advanced operations and applications.

4.6 References

1. M. Chen, Y. Zhang, G. Xing, S.-L. Chou and Y. Tang, Electrochemical Energy Storage Devices Working in Extreme Conditions, *Energy & Environmental Science*, 2021, 14, 3323-3351.
2. S. Chen, M. Zhang, P. Zou, B. Sun and S. Tao, Historical Development and Novel Concepts on Electrolytes for Aqueous Rechargeable Batteries, *Energy & Environmental Science*, 2022, 15, 1805-1839.
3. D. A. Cullen, K. C. Neyerlin, R. K. Ahluwalia, R. Mukundan, K. L. More, R. L. Borup, A. Z. Weber, D. J. Myers and A. Kusoglu, New Roads and Challenges for Fuel Cells in Heavy-duty Transportation, *Nature energy*, 2021, 6, 462-474.
4. V. S. Pinheiro, F. M. Souza, T. C. Gentil, A. N. Nascimento, L. S. Parreira, M. I. Sairre, B. L. Batista and M. C. Santos, Sn-containing electrocatalysts with a reduced amount of palladium for alkaline direct ethanol fuel cell applications, *Journal of Alloys and Compounds*, 2022, 899, 163361.
5. Y. Yang, X. Zhu, Q. Wang, D. Ye, R. Chen and Q. Liao, Towards Flexible Fuel Cells: Development, Challenge and Prospect, *Applied Thermal Engineering*, 2022, 203, 117937.
6. H. Jiang, L. Wei, X. Fan, J. Xu, W. Shyy and T. Zhao, A Novel Energy Storage System Incorporating Electrically Rechargeable Liquid Fuels as the Storage Medium, *J Science Bulletin*, 2019, 64, 270-280.
7. X. Shi, X. Huo, O. C. Esan, L. An and T. Zhao, Performance Characteristics of a Liquid E-fuel Cell, *Applied Energy*, 2021, 297, 117145.

8. X. Shi, Y. Dai, O. C. Esan, X. Huo, L. An and T. Zhao, A Passive Fuel Cell Fed with an Electrically Rechargeable Liquid Fuel, *ACS Applied Materials & Interfaces*, 2021, 13, 48795-48800.
9. L. An, T. Zhao, X. Yan, X. Zhou and P. Tan, The Dual Role of Hydrogen Peroxide in Fuel Cells, *Science Bulletin*, 2015, 60, 55-64.
10. X. Jing, D. Cao, Y. Liu, G. Wang, J. Yin, Q. Wen and Y. Gao, The Open Circuit Potential of Hydrogen Peroxide at Noble and Glassy Carbon Electrodes in Acidic and Basic Electrolytes, *Journal of electroanalytical chemistry*, 2011, 658, 46-51.
11. S. J. Lao, H. Y. Qin, L. Q. Ye, B. H. Liu and Z. P. Li, A development of direct hydrazine/hydrogen peroxide fuel cell, *Journal of Power Sources*, 2010, 195, 4135-4138.
12. Z. Pan, B. Huang and L. An, Performance of a Hybrid Direct Ethylene Glycol Fuel Cell, *International Journal of Energy Research*, 2019, 43, 2583-2591.
13. R. M. Hjelm, C. Lafforgue, R. W. Atkinson, Y. Garsany, R. O. Stroman, M. Chatenet and K. Swider-Lyons, Impact of the anode catalyst layer design on the performance of H₂O₂-direct borohydride fuel cells, *Journal of The Electrochemical Society*, 2019, 166, F1218.
14. K. Swider-Lyons, R. M. Hjelm, Y. Garsany, C. Lafforgue and M. Chatenet, Improved borohydride oxidation reaction activity and stability for carbon-supported platinum nanoparticles with tantalum oxyphosphate interlayers, *Journal of The Electrochemical Society*, 2020, 167, 164508.

15. T. H. Oh, Gold-based bimetallic electrocatalysts supported on multiwalled carbon nanotubes for direct borohydride–hydrogen peroxide fuel cell, *Renewable Energy*, 2021, 163, 930-938.
16. S. S. Yu, T. H. Lee and T. H. Oh, Ag–Ni nanoparticles supported on multiwalled carbon nanotubes as a cathode electrocatalyst for direct borohydride–hydrogen peroxide fuel cells, *Fuel*, 2022, 315, 123151.
17. Z. Wang, J. Parrondo, C. He, S. Sankarasubramanian and V. Ramani, Efficient pH-gradient-enabled microscale bipolar interfaces in direct borohydride fuel cells, *Nature Energy*, 2019, 4, 281-289.
18. C. G. Arges, V. Prabhakaran, L. Wang and V. Ramani, Bipolar polymer electrolyte interfaces for hydrogen–oxygen and direct borohydride fuel cells, *International Journal of Hydrogen Energy*, 2014, 39, 14312-14321.
19. B. Jiang, L. Wu, L. Yu, X. Qiu and J. Xi, A Comparative Study of Nafion Series Membranes for Vanadium Redox Flow Batteries, *Journal of Membrane Science*, 2016, 510, 18-26.
20. L. An and T. Zhao, Performance of an Alkaline-Acid Direct Ethanol Fuel Cell, *International journal of hydrogen energy*, 2011, 36, 9994-9999.
21. O. C. Esan, X. Shi, Z. Pan, Y. Liu, X. Huo, L. An and T. Zhao, A high-performance H₂O₂-based fuel cell for air-free applications, *Journal of Power Sources*, 2022, 548, 232114.
22. Z. Wang, S. Sankarasubramanian and V. Ramani, Reactant-transport engineering approach to high-power direct borohydride fuel cells, *Cell Reports Physical Science*, 2020, 1, 100084.
23. J. Ma and Y. Sahai, Cost-effective Materials for Direct Borohydride Fuel Cells, *ECS Transactions*, 2012, 42, 101.

24. G. H. Miley, R. Bernas, K.-J. Kim and N. Luo, Optimization of Catalyst Deposited Diffusion Layer for a Direct Sodium Borohydride Fuel Cell (DNBFC), *ECS Transactions*, 2009, 17, 525.
25. L. An, T. S. Zhao and J. B. Xu, A Bi-Functional Cathode Structure for Alkaline-Acid Direct Ethanol Fuel Cells, *International Journal of Hydrogen Energy*, 2011, 36, 13089-13095.
26. Z. Pan, Y. Bi and L. An, Performance Characteristics of a Passive Direct Ethylene Glycol Fuel Cell with Hydrogen Peroxide as Oxidant, *Applied Energy*, 2019, 250, 846-854.
27. Y. Zhao, L. Liu, X. Qiu and J. Xi, Revealing sulfuric acid concentration impact on comprehensive performance of vanadium electrolytes and flow batteries, *Electrochimica Acta*, 2019, 303, 21-31.
28. X. Shi, X. Huo, Y. Ma, Z. Pan and L. An, Energizing Fuel Cells with an Electrically Rechargeable Liquid Fuel, *Cell Reports Physical Science*, 2020, 1, 100102.
29. S. Won, K. Oh and H. Ju, Numerical Analysis of Vanadium Crossover Effects in All-Vanadium Redox Flow Batteries, *Electrochimica Acta*, 2015, 177, 310-320.
30. A. Uzundurukan, E. S. Akça, Y. Budak and Y. Devrim, Carbon Nanotube-Graphene Supported Bimetallic Electrocatalyst for Direct Borohydride Hydrogen Peroxide Fuel Cells, *Renewable Energy*, 2021, 172, 1351-1364.
31. O. C. Esan, X. Shi, Y. Dai, L. An and T. S. Zhao, Operation of Liquid E-fuel Cells Using Air as Oxidant, *Applied Energy*, 2022, 311, 118677.

32. S. Towne, M. Carella, W. Mustain, V. Viswanathan, P. Rieke, U. Pasaogullari and P. Singh, Performance of a Direct Borohydride Fuel Cell Stack, *ECS Transactions*, 2009, 25, 1951.
33. D. Santos and C. Sequeira, Zinc anode for direct borohydride fuel cells, *Journal of The Electrochemical Society*, 2009, 157, B13.
34. J. Ma, Y. Sahai and R. G. Buchheit, Direct borohydride fuel cell using Ni-based composite anodes, *Journal of Power Sources*, 2010, 195, 4709-4713.
35. L. An, T. Zhao, R. Chen and Q. Wu, A Novel Direct Ethanol Fuel Cell with High Power Density, *Journal of power sources*, 2011, 196, 6219-6222.
36. N. A. Choudhury, J. Ma, Y. Sahai and R. G. Buchheit, High Performance Polymer Chemical Hydrogel-Based Electrode Binder Materials for Direct Borohydride Fuel Cells, *Journal of Power Sources*, 2011, 196, 5817-5822.
37. X. Yan, F. Meng, Y. Xie, J. Liu and Y. Ding, Direct N_2H_4/H_2O_2 Fuel Cells Powered by Nanoporous Gold Leaves, *Scientific reports*, 2012, 2, 1-7.
38. A. Déctor, J. P. Esquivel, M. J. González, M. Guerra-Balcázar, J. Ledesma-García, N. Sabaté and L. G. Arriaga, Formic Acid Microfluidic Fuel Cell Evaluation in Different Oxidant Conditions, *Electrochimica Acta*, 2013, 92, 31-35.
39. W. Jin, J. Liu, Y. Wang, Y. Yao, J. Gu and Z. Zou, Direct $NaBH_4-H_2O_2$ fuel cell based on nanoporous gold leaves, *International journal of hydrogen energy*, 2013, 38, 10992-10997.

40. L. An, T. S. Zhao, L. Zeng and X. H. Yan, Performance of an Alkaline Direct Ethanol Fuel Cell with Hydrogen Peroxide as Oxidant, *International Journal of Hydrogen Energy*, 2014, 39, 2320-2324.
41. Y. Li, Y. He and W. Yang, A High-Performance Direct Formate-Peroxide Fuel Cell with Palladium–Gold Alloy Coated Foam Electrodes, *Journal of Power Sources*, 2015, 278, 569-573.
42. L. An, T. Zhao, X. Zhou, L. Wei and X. Yan, A High-Performance Ethanol–Hydrogen Peroxide Fuel Cell, *RSC Advances*, 2014, 4, 65031-65034.
43. Y. Li, H. Wu, Y. He, Y. Liu and L. Jin, Performance of Direct Formate-Peroxide Fuel Cells, *Journal of Power Sources*, 2015, 287, 75-80.
44. X. H. Yan, T. S. Zhao, L. An, G. Zhao and L. Shi, A Direct Methanol–Hydrogen Peroxide Fuel Cell with a Prussian Blue Cathode, *International Journal of Hydrogen Energy*, 2016, 41, 5135-5140.
45. Y. Li, A Liquid-Electrolyte-Free Anion-Exchange Membrane Direct Formate-Peroxide Fuel Cell, *International Journal of Hydrogen Energy*, 2016, 41, 3600-3604.
46. M. G. Hosseini, R. Mahmoodi and M. Abdolmaleki, High Performance Direct Hydrazine–Hydrogen Peroxide Fuel Cell using Reduced Graphene Oxide Supported Ni@M (M = Pt, Pd, Ru) Nanoparticles as Novel Anodic Electrocatalysts, *New Journal of Chemistry*, 2018, 42, 12222-12233.
47. Z. Pan, Y. Bi and L. An, A Cost-Effective and Chemically Stable Electrode Binder for Alkaline-Acid Direct Ethylene Glycol Fuel Cells, *Applied Energy*, 2020, 258, 114060.

48. G. Braesch, Z. Wang, S. Sankarasubramanian, A. G. Oshchepkov, A. Bonnefont, E. R. Savinova, V. Ramani and M. Chatenet, A high performance direct borohydride fuel cell using bipolar interfaces and noble metal-free Ni-based anodes, *Journal of Materials Chemistry A*, 2020, 8, 20543-20552.
49. B. Lu, W. Yuan, X. Su, Z. Zhuang, Y. Ke and Y. Tang, Passive Direct Methanol-Hydrogen Peroxide Fuel Cell with Reduced Graphene Oxide-Supported Prussian Blue as Catalyst, *Energy Technology*, 2020, 8, 1901360.
50. Z. Wang, M. Mandal, S. Sankarasubramanian, G. Huang, P. A. Kohl and V. K. Ramani, Influence of water transport across microscale bipolar interfaces on the performance of direct borohydride fuel cells, *ACS Applied Energy Materials*, 2020, 3, 4449-4456.
51. M. G. Hosseini, V. Daneshvari-Esfahlan, H. Aghajani, S. Wolf and V. Hacker, Palladium-Nickel Electrocatalysts on Nitrogen-Doped Reduced Graphene Oxide Nanosheets for Direct Hydrazine/Hydrogen Peroxide Fuel Cells, *Catalysts*, 2021, 11, 1372.
52. M. G. Hosseini, V. Daneshvari-Esfahlan, S. Wolf and V. Hacker, *RSC Advances*, Cobalt-Modified Palladium Nanocatalyst on Nitrogen-Doped Reduced Graphene Oxide for Direct Hydrazine Fuel Cell, 2021, 11, 39223-39232.
53. S. Saha, P. Gayen, Z. Wang, R. J. Dixit, K. Sharma, S. Basu and V. K. Ramani, Development of bimetallic PdNi electrocatalysts toward mitigation of catalyst poisoning in direct borohydride fuel cells, *ACS Catalysis*, 2021, 11, 8417-8430.

Tables

Table 4-1. Performance comparison with previous e-fuel cells using different oxidants.

Year	Fuel	Membrane	Oxidant	Temp. (°C)	Cathode catalyst (mg cm ⁻²)	Peak power density (mW cm ⁻²)	Ref.
2021	E-fuel	Nafion 117	Air	60	Pt/C (0.5)	199.5	31
2021	E-fuel	Nafion 211	Oxygen	60	Pt/C (4.0)	857.0	7
2022	E-fuel	Nafion 211	Hydrogen peroxide	60	Pt/C (0.5)	1456.0	This work

Table 4-2. Performance comparison of direct liquid fuel cells that employed H₂O₂ as oxidant.

Year	Fuel	Membrane	Temp (°C)	Cathode Catalyst (mg cm ⁻²)	Peak power density (mW cm ⁻²)	Ref.
2009	Sodium borohydride	Nafion 112	60	Pd (0.1)	680	24
2009	Sodium borohydride	Nafion membrane	80	Pt/C (1.8)	410	32
2010	Hydrazine	Nafion 112	80	Au/C (1.0)	1020	11
2010	Sodium borohydride	Nafion 117	22	Pt	470	33
2010	Sodium borohydride	Nafion 212	60	Pd (1.0)	665	24
2011	Ethanol	Nafion 117	60	PdNi/C (3.9)	240	35
2011	Ethanol	Nafion 211	60	Pt/C (4.0)	360	20
2011	Sodium borohydride	Nafion 117	70	Pd/C (1.0)	589	36
2011	Ethanol	Nafion 117	60	Au/C (1.2)	200	25
2012	Hydrazine	Nafion 115	80	Pt/C (0.1)	195	37
2012	Sodium borohydride	Chitosan hydrogel	60	Pd	685	23
2013	Formate	-	25	Pt/C (1.0)	4.9	38
2013	Sodium borohydride	Nafion 212	80	Nano porous gold leaves (0.12)	390	39
2014	Ethanol	A201	80	ACTA (1.0)	160	40
2014	Formate	Nafion 115	60	Pt/C (3.0)	331	41
2014	Ethanol	Nafion 117	60	-	450	42
2014	Sodium borohydride	Bipolar junction	70	Pt/C (1.0)	110	18
2015	Formate	Nafion 115	60	Pt/C (2.0)	591	43
2015	Methanol	Nafion 115	60	PB/CNT (20.0)	125	44
2016	Formate	A201	40	Pt/C (2.0)	23	45
2018	Hydrazine	Nafion 117	60	Pt/C (0.5)	204.8	46
2018	Ethylene glycol	Nafion 212	80	Au/C (2.66)	115.3	12
2019	Sodium borohydride	Nafion 117	25	Pt/C (0.3)	275	13
2019	Ethylene glycol	Nafion 211	60	Au/C (2.66)	65.8	26
2019	Sodium borohydride	Bipolar junction	70	Pt/C (3.0)	630	17

Year	Fuel	Membrane	Temp (°C)	Cathode Catalyst (mg cm⁻²)	Peak power density (mW cm⁻²)	Ref.
2020	Ethylene glycol	Nafion 211	60	Au/C (2.66)	120	47
2020	Sodium borohydride	Bipolar interface	70	Pt/C (1.0)	446	48
2020	Methanol	Nafion 115	85	PB (6.7)	20.5	49
2020	Sodium borohydride	Bipolar interface	25	Pt/C (3.0)	580	50
2020	Sodium borohydride	Bipolar interface	70	Pt/C (3.0)	890	22
2021	Hydrazine	Nafion 117	60	Pt/C (0.5)	216.71	51
2021	Hydrazine	Nafion 117	60	Pt/C (0.5)	148.58	52
2021	Sodium borohydride	Nafion 212	50	Au-Ni/MWCNTs (1.0)	279.5	15
2021	Sodium borohydride	Bipolar interface	25	Pt/C (3.0)	466	53
2022	E-fuel	Nafion 211	60	Pt/C (0.5)	1456.0	This work

Chapter 5 Mathematical modelling of e-fuel cells

5.1 Introduction

The quest for carbon-neutral energy options, in lieu of the inefficient and exhaustible conventional energy sources, has stimulated and accelerated the utilization of renewables as promising alternative to match up with the ever-increasing energy demands of the modern world [1-4]. Consequently, several power generation systems have been developed, explored, and deployed to supply efficient and reliable electricity for end use [5-8]. Notably is the fuel cell technology, which involves the conversion of fuels to electricity, identified to be among the promising power generation systems. This therefore led to the introduction and embracement of hydrogen fuel cells for diverse energy-related applications including electric vehicles [9-13]. Safety and energy efficiency concerns among other limitations of utilizing hydrogen as fuel, however, continue to reduce the suitability and competitiveness of hydrogen fuel cells.

Recently, a novel concept which involves energizing fuel cells with an electrically rechargeable liquid fuel (e-fuel), in lieu of hydrogen and liquid alcohols, was introduced [14]. Potential materials for the production of such e-fuel were mentioned to include inorganic and organic materials, as well as suspension of particles. Following this, vanadium ions dissolved in sulphuric acid has been employed as an e-fuel at the anode to demonstrate the operation and performance of e-fuel cells [15]. To further boost the performance of the e-fuel cell and more importantly realize its application in airtight environments, hydrogen peroxide (H_2O_2) has also been

considered as an alternative oxidant, in place of gaseous oxygen or ambient air [16].

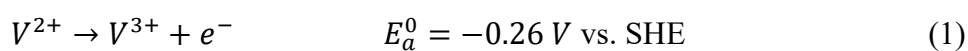
The physicochemical processes involved in the operation of these e-fuel cells include the transport of various charged species; transport of ionic and electronic current through the porous media; transport of ionic current through the membrane; and the electrochemical reactions on the active surface [17]. To better understand and garner more insights on the complex and highly coupled fluid flow, mass/charge transport processes, and electrochemical reactions which take place within the multi-layer porous structure of these e-fuel cells, mathematical modeling of is of paramount importance. In addition, modeling provides platform not only to explore the complex phenomena of the multi-variable cell components but also to optimize their design and operating parameters. In the open literature, Wandschneider et al. developed a two-dimensional model for a vanadium oxygen fuel cell [18]. Their modeling geometry, however, considered two membranes and an intermediate chamber between the anode and cathode half-cells. Apparently, this is not a typical fuel cell structure and may not be considered suitable to describe the transport behaviors and the simulation of the cell performance under real conditions and applications. Chen et al. also developed a one-dimensional model for a vanadium/oxygen redox fuel cell [19], which was achieved by simplifying the complexity of some phenomena that occur in the fuel cell system. Hence, the multi-dimensional effect of fluid flow and mass transport particularly at high current densities are not obtainable from the model.

In this chapter, a two-dimensional mathematical model to describe the transport behaviors and predict the performance of the e-fuel cell is presented using the actual structure of an e-fuel cell, eliminating catalyst and diffusion layers at the anode. The model is first developed for the e-fuel cells using pure oxygen as oxidant. Afterwards, the modeling framework is extended to e-fuel cells that employ hydrogen peroxide as oxidant, where mixed potential is considered in the cathodic reactions. The model involves fluid flow and species transport integrated with the involved electrochemical reactions. The mathematical model for both cells are thereafter validated by experimental data and the comparison shows a good agreement.

5.2 Model formulation

5.2.1 Physicochemical processes

The domain structure of the e-fuel cell as shown in Figure 5.1 basically consists of a proton exchange membrane placed between an anode and a cathode. The anode is a porous medium, while the cathode consists of a catalyst layer and a diffusion layer. During the operation of the cell, the e-fuel containing vanadium ions is directly fed into the anode flow channels. The e-fuel is thus transported to the matrix surface of the anode where the anodic reaction takes place. The electrochemical reaction at the anode is given as [20]:

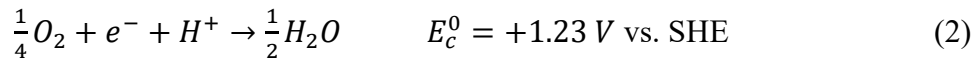


The consumption of V^{2+} at the anode during the oxidation reaction results in concentration gradients of the reacting species as the bulk e-fuel flows

from the channels to the surface of the anode. During the anodic reaction, electrons and protons are also released and transported to the cathode through an external electrical circuit and the membrane, respectively.

At the cathode side, the oxidant is supplied through the flow channels and directly flows through the cathode diffusion layer to the cathode catalyst layer. At the cathode catalyst layer, the oxidant reacts with the electrons and protons, arriving from the anode.

With the use of oxygen as oxidant, the oxygen reduction reaction (ORR) at the cathode is as follows [20]:



The overall electrochemical reaction occurring in the e-fuel cell is:



For the e-fuel cells using H_2O_2 as oxidant, the hydrogen peroxide reduction reaction (HPPR) at the cathode is [21]:



It is worth to mention that at such high potential of HPPR, hydrogen peroxide oxidation reaction (HPOR) can also occur at the cathode as follows [22]:



The overall reaction of the e-fuel/ H_2O_2 cell is:



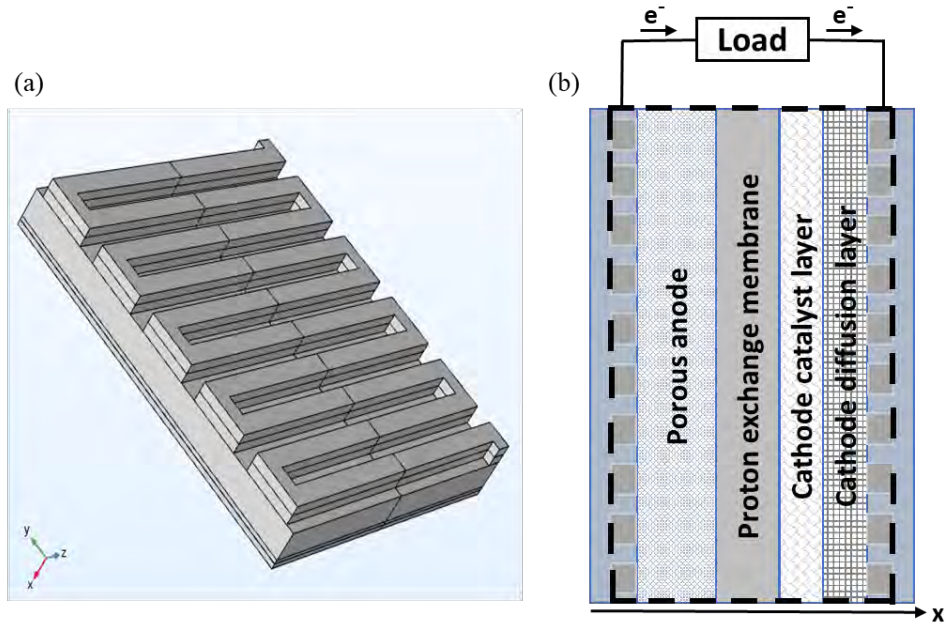


Figure 5.1 (a) Schematic of the 3D domain for e-fuel flow at the anode; (b) Schematic of the 2D domain for the e-fuel cell.

5.2.2 Model simplifications and assumptions

To simplify the computational modeling of the physicochemical processes that take place in the e-fuel cell, the following assumptions are taken into consideration:

1. Isotropic and homogeneous properties are assumed for the porous anode, membrane, and cathode.
2. Dilute-solution approximation describes the species transport at the anode, hence interactions among the ions in the e-fuel solution are neglected.
3. The e-fuel cell operations are assumed to be at steady-state conditions.
4. The e-fuel flow at the anode is taken as incompressible.
5. The crossover of the e-fuel, oxidant, and water via the membrane are not considered.

6. Side reactions are also ignored.

5.2.3 Computational domains

At this initial stage, many parameters which influence the performance and optimization of the e-fuel cell are yet to be numerically investigated. Therefore, applying a complex geometric dimensionality, such as 3D for the whole study, at this stage may not be suitable due to the significant computational time and huge computing facility required. Nonetheless, a 3D computational domain, shown in Figure 5.1a, is developed for the fluid flow process in the serpentine flow channel (2 cm x 2 cm) of the anode to obtain the pressure distribution of the fluid particularly in the flow channel. Thereafter, a 2D model is developed to capture the working principle of the whole e-fuel cell. Figure 5.1b shows the schematic of the 2D domain employed for the e-fuel cell in this study.

5.3 Governing equations

5.3.1 Anode compartment

5.3.1.1 Fluid flow

The flow of the e-fuel in the single serpentine flow channel is described by Navier–Stokes equation while the flow in the porous anode is governed by Brinkman equation as follows [23]:

$$\rho(\vec{v} \cdot \nabla)\vec{v} = \nabla \cdot [-PI + \mu(\nabla\vec{v} + (\nabla\vec{v})^T)] \quad (7)$$

$$\frac{1}{\varepsilon^2}\rho(\vec{v} \cdot \nabla)\vec{v} = \nabla \cdot \left[-PI + \frac{\mu}{\varepsilon}(\nabla\vec{v} + (\nabla\vec{v})^T) \right] - \frac{2\mu}{3\varepsilon}\nabla(\nabla \cdot \vec{v})I - \frac{\mu}{k}\vec{v} \quad (8)$$

The permeability, k , of the anode is described by Kozeny-Carman equation:

$$k = \frac{d^2 \varepsilon^3}{180(1-\varepsilon)^2} \quad (9)$$

Where d is the fibre diameter of the porous anode.

It is worth to mention that no specific boundary condition was formulated at the flow channel and the anode interface as a result of the mass and momentum continuity applied at this interface:

$$\rho \nabla \cdot \vec{v} = 0 \quad (10)$$

5.3.1.2 Mass transport

The mass transport at the anode of the e-fuel cell majorly involves the transport of the various charged species ($i = V^{2+}, V^{3+}, H^+$, and SO_4^{2-}) through the porous anode. The transport of each specie, i , is described by Nernst-Planck equation, where transport resulting from the interactions among the ions is ignored, such that the molar flux, \vec{N}_i , of each specie in the porous anode is given as [24]:

$$\vec{N}_i = -D_i^{eff} \nabla c_i - z_i c_i u_i F \nabla \phi_{a,l} + \vec{v} c_i \quad (11)$$

The effective diffusion coefficient, D_i^{eff} , of each specie according to Bruggemann correction is expressed as:

$$D_i^{eff} = \varepsilon^{1.5} D_i \quad (12)$$

Where D_i is the diffusion coefficient of species.

The effective mobility, u_i , of each specie according to Nernst-Einstein equation in relations to the effective diffusion coefficient, D_i^{eff} , is given as:

$$u_i = \frac{D_i^{eff}}{RT} \quad (13)$$

The conservation of mass for each charged specie in the porous anode at steady state is given as [25]:

$$\nabla \cdot \vec{N}_i = S_i \quad (14)$$

Where the electrochemical reaction source term, S_i , for the electroactive species is given as:

$$S_i = \frac{v_i}{nF} a_a j_a \quad (15)$$

Where v_i is the stoichiometric coefficient of each electroactive specie participating in the electrochemical reaction at the anode such that v_i is 1 and -1 for V^{2+} and V^{3+} , respectively (Equation 1), and j_a is the local current density at the porous anode.

5.3.1.3 Charge transport

The e-fuel solution, a mixture of vanadium ions and sulfuric acid, fed into the anode compartment of the e-fuel cell is considered to be electrically neutral such that the concentration of SO_4^{2-} from the dissociation of the sulfuric acid can be described by an electroneutrality condition as follows [24]:

$$\sum_i z_i c_i = 0 \quad (16)$$

The anode is subjected to both ionic and electronic conductions for the purpose of charge transfer between the anode and the e-fuel. Hence the charge leaving the e-fuel is expected to be balanced by the charge that is entering the anode according to charge conservation expressed as [26,27]:

$$\nabla \cdot \vec{i}_{a,l} = -\nabla \cdot \vec{i}_{a,s} = a_a j_a \quad (17)$$

Where the total ionic current, $\nabla \cdot \vec{i}_{a,l}$, due to the transfer of ions, i , in the e-fuel is expressed as:

$$\vec{i}_{a,l} = F \sum_i z_i \vec{N}_i \quad (18)$$

The electronic current, $\nabla \cdot \vec{i}_{a,s}$, in the porous anode described by ohm's law is expressed as:

$$\vec{i}_{a,s} = -\sigma_{a,s}^{eff} \nabla \phi_{a,s} \quad (19)$$

Where $\phi_{a,s}$ is the electric potential of the anode.

The effective electrical conductivity, $\sigma_{a,s}^{eff}$, of the anode is calculated according to Bruggemann correction expressed as:

$$\sigma_{a,s}^{eff} = (1 - \varepsilon)^{1.5} \sigma_{a,s} \quad (20)$$

Where $\sigma_{a,s}$ is the electrical conductivity of the anode.

5.3.2 Membrane

In this study, the proton exchange membrane is assumed to be permeable to only protons. Generally, membrane allows ionic but not electronic conduction, hence only ionic current exists in the membrane. The ionic current vector in the membrane, \vec{i}_m , is always in the direction of the proton flux, according to Faraday's law. However, current source is not produced in the membrane since charge consumption or generation via electrochemical reaction are not taking place in the membrane. The current conservation in the membrane is therefore expressed as [28]:

$$\nabla \cdot \vec{i}_m = 0 \quad (21)$$

Due to the absence of fluid flow and the fact that electroactive species crossover through the membrane is not considered in this model, the transport of protons through the membrane resulting from migration,

majorly driven by potential gradient, is represented by ohm's law as follows [29]:

$$\vec{i}_m = -\sigma_m \nabla \phi_m \quad (22)$$

The flux of proton, \vec{N}_{H^+} , through the membrane is therefore expressed as [26]:

$$\vec{N}_{H^+} = \frac{\vec{i}_m}{F} = -\frac{\sigma_m}{F} \nabla \phi_m \quad (23)$$

Where σ_m and ϕ_m represent the ionic conductivity and ionic potential of the proton exchange membrane, respectively.

5.3.3 Cathode compartment

5.3.3.1 Mass transport

A diffusion layer and a catalyst layer are considered as the porous media at the cathode compartment of the e-fuel cell. Oxidant is delivered into the cell at the cathode side through the flow channel to the diffusion layer and to the surface of the catalyst layer where the reduction reaction takes place.

With the use of oxygen as oxidant, the pure oxygen is assumed to be uniformly distributed at the cathode. Nonetheless, the cathode catalyst layer is still subjected to both ionic and electronic conductions.

With the use of H_2O_2 as oxidant, the mass transport of the species ($i = H_2O_2$ and H^+) at the cathode is described as [30]:

$$\vec{N}_i = -D_i^{eff} \nabla c_i + \vec{v} c_i \quad (24)$$

The effective diffusion coefficient, D_i^{eff} , of each specie according to Bruggemann correction is expressed as [31]:

$$D_i^{eff} = \varepsilon^{1.5} D_i \quad (25)$$

The conservation of mass for each charged specie at the cathode is given as [22]:

$$\nabla \cdot \vec{N}_i = 0 \quad (26)$$

5.3.3.2 Charge transport

The charge conservation at the cathode is expressed as [32]:

$$\nabla \cdot \vec{i}_{c,l} = -\nabla \cdot \vec{i}_{c,s} = a_{ccl} j_c \quad (27)$$

Where a_{ccl} is the active surface area of the cathode catalyst layer, and j_c is the local current density at the cathode.

The ionic current, $\nabla \cdot \vec{i}_{c,l}$, at the cathode catalyst layer is expressed as:

$$\vec{i}_{c,l} = -\sigma_{c,l} \nabla \phi_{c,l} \quad (28)$$

Where $\sigma_{c,l}$ is the ionic conductivity of the cathode catalyst layer and $\phi_{c,l}$ is the ionic potential at the cathode.

The electronic current, $\nabla \cdot \vec{i}_{c,s}$, at the cathode catalyst layer described by ohm's law is expressed as:

$$\vec{i}_{c,s} = -\sigma_{c,s} \nabla \phi_{c,s} \quad (29)$$

Where $\sigma_{c,s}$ is the electrical conductivity of the cathode catalyst layer and $\phi_{c,s}$ is the electronic potential of the cathode.

5.3.4 Electrochemical kinetics

5.3.4.1 Anode

The electrochemical reaction that occurs at the interface between the anode and the e-fuel solution is associated with the local current density, j_a , and activation overpotential, η_a , of the anode. This interfacial reaction kinetic is governed and mathematically expressed by the Butler-Volmer equation given as [23]:

$$j_a = Fk_a(c_{V^{2+}}^s)^{\alpha_{1,a}}(c_{V^{3+}}^s)^{\alpha_{1,c}} \left[\exp\left(\frac{\alpha_{1,a}F\eta_a}{RT}\right) - \exp\left(-\frac{\alpha_{1,c}F\eta_a}{RT}\right) \right] \quad (30)$$

The reference exchange current density, $i_{0,a}$, for the reaction at the anode is given as:

$$i_{0,a} = Fk_a(c_{V^{2+}}^s)^{\alpha_{1,a}}(c_{V^{3+}}^s)^{\alpha_{1,c}} \quad (31)$$

Where k_a is the rate constant of the anodic reaction, s is surface, $\alpha_{1,a}$ and $\alpha_{1,c}$ is the anodic and cathodic charge transfer coefficient at the anode, respectively.

The activation overpotential, η_a , for the reaction at the anode is described as:

$$\eta_a = \Phi_{a,s} - \Phi_{a,l} - E_a^{eq} \quad (32)$$

Where the anode potential, E_a , is given as:

$$E_a = \Phi_{a,s} - \Phi_{a,l} \quad (33)$$

The equilibrium potential, E_a^{eq} , for the electrochemical reaction at the anode, Equation (1), is determined using Nernst equation given as follows [24]:

$$E_a^{eq} = E_a^0 + \frac{RT}{F} \ln \left(\frac{c_{V^{3+}}}{c_{V^{2+}}} \right) \quad (34)$$

5.3.4.2 Cathode

For the e-fuel cell using oxygen as oxidant, a simplified Tafel equation is used to describe the local current density, j_c , at the cathode catalyst layer as follows [33]:

$$j_c = i_{0,c} \left[\exp \left(\frac{\alpha_{2,c} F \eta_c}{RT} \right) \right] \quad (35)$$

The activation overpotential, η_c , at the cathode is described as:

$$\eta_c = \phi_{c,s} - \phi_{c,l} - E_c^{eq} \quad (36)$$

Where the cathode potential, E_c , is given as:

$$E_c = \phi_{c,s} - \phi_{c,l} \quad (37)$$

Where $i_{0,c}$ is the reference cathodic exchange current density, $\alpha_{2,c}$ is the cathodic charge transfer coefficient, and E_c^{eq} is the equilibrium potential at the cathode.

For the e-fuel cell using H_2O_2 as oxidant, the local current density, j_c , is described by Tafel equation as follows [22]:

$$j_{HPRR} = i_{0,HPRR} \left(\frac{C_{H_2O_2}^{Cl}}{C_{H_2O_2}^{ref}} \right)^{\gamma_{HPRR}^{H_2O_2}} \left(\frac{C_{H^+}^{Cl}}{C_{H^+}^{ref}} \right)^{\gamma_{HPRR}^{H^+}} \exp \left(\frac{\alpha_{HPRR} F}{RT} \eta_{HPRR} \right) \quad (38)$$

$$\gamma_{HPRR}^{H_2O_2} = \begin{cases} 0 & C_{H_2O_2}^{Cl} > C_{H_2O_2}^{ref} \\ 1 & C_{H_2O_2}^{Cl} \leq C_{H_2O_2}^{ref} \end{cases} \quad (39)$$

$$\gamma_{HPRR}^{H^+} = \begin{cases} 0 & C_{H^+}^{Cl} > C_{H^+}^{ref} \\ 1 & C_{H^+}^{Cl} \leq C_{H^+}^{ref} \end{cases} \quad (40)$$

The anodic current density from the HPOR at the cathode is given as [22]:

$$j_{HPOR} = n_{HPOR} F k_{HPOR} \exp\left(\frac{\alpha_{HPOR} F}{RT} \eta_{HPOR}\right) \quad (41)$$

Where k_{HPOR} and α_{HPOR} are the rate constant and transfer coefficient of HPOR respectively.

Due to the simultaneous electrochemical reactions at the cathode, involving HPPR and HPOR, the consideration of mixed potential is necessary. The interfacial reaction kinetics at the cathode is therefore defined by both the cathodic current density of HPPR and the anodic current density resulting from HPOR given as [33]:

$$\begin{aligned} j_c &= j_{HPPR} + j_{HPOR} \\ &= i_{0,HPPR} \left(\frac{C_{H_2O_2}^{Cl}}{C_{H_2O_2}^{ref}}\right)^{\gamma_{HPPR}^{H_2O_2}} \left(\frac{C_{H^+}^{Cl}}{C_{H^+}^{ref}}\right)^{\gamma_{HPPR}^{H^+}} \exp\left[\frac{\alpha_{HPPR} F}{RT} (E_{HPPR}^0 - E_{mixed})\right] + \\ & n_{HPOR} F k_{HPOR} \exp\left[\frac{\alpha_{HPOR} F}{RT} (E_{mixed} - E_{HPOR}^0)\right] \end{aligned} \quad (42)$$

Where E_{mixed} is the mixed potential, C_i^{Cl} is the specie concentration at cathode catalyst layer, C_i^{ref} is the reference concentration of specie, γ is the reaction order with respect to species concentration, and E^0 is the theoretical potential.

It is worth noting that ORR may occur at the cathode as oxygen is produced. However, ORR and its corresponding current density are not considered in this model as the cathodic current density resulting from this ORR is almost equal to zero and therefore negligible [22]. The cathodic current density is

thus assigned to only HPPR, which is justified by its faster kinetics, as a result of its lesser electron transfer (two) compared to that of ORR (four).

5.3.5 Boundary conditions

5.3.5.1 Momentum balance

The boundary condition applied at the inlet and outlet of the 3D domain in Figure 5.1a for the anode flow channel of both fuel cells is as follows [24]:

$$\begin{cases} \vec{v} = v_{in} = Q_a/A \\ P = P_{out} = 0 \end{cases} \quad (43)$$

Where Q_a is the volumetric flow rate of the e-fuel, and A is the cross-sectional area of the flow channel.

In the 2D domain, pressure boundary condition is applied at each flow channel. The value of each pressure used in the 2D model is the average pressure obtained from each channel on the yz-planes as shown in Figure 5.1a from the 3D model of the fluid flow.

For the e-fuel cell using H_2O_2 as oxidant, a 3D domain as shown in Figure 5.2 is also developed to model to flow of the hydrogen peroxide solution. The boundary conditions in Equation (43) are also applied to the flow of hydrogen peroxide solution at the cathode.

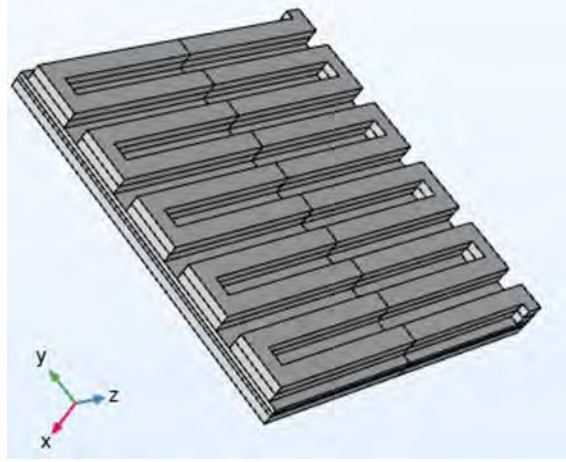


Figure 5.2 3D domain for hydrogen peroxide flow at the cathode.

5.3.5.2 Mass balance

The concentration of the e-fuel at the outlet of the 3D flow channel in Figure 5.1a is determined as follows:

$$c_{v^{2+}}^f = c_{v^{2+}}^0 - \frac{i_{cell}A_{cell}}{FQ_a} \quad (44)$$

Where $c_{v^{2+}}^f$ is the e-fuel concentration at the outlet, $c_{v^{2+}}^0$ is the initial e-fuel concentration at the inlet, and i_{cell} is the applied current density, A_{cell} is the area of the cell.

Hence, the overall concentration drop of the e-fuel, $\Delta c_{v^{2+}}$, in the 3D flow channel is:

$$\Delta c_{v^{2+}} = c_{v^{2+}}^0 - c_{v^{2+}}^f = \frac{i_{cell}A_{cell}}{FQ_a} \quad (45)$$

The e-fuel concentration drop at each section of the channel in the 3D flow model used in the 2D model is derived as follows:

$$\Delta c_{v^{2+}}^l = \Delta c_{v^{2+}} \times \frac{l}{L} \quad (46)$$

Where l is the length of each section of the channel from the inlet of the 3D flow model and L is the entire length of the 3D flow channel.

Thus, the e-fuel concentration at each section of the channel is calculated as:

$$c_{v^{2+}}^l = c_{v^{2+}}^0 - \Delta c_{v^{2+}}^l \quad (47)$$

For the e-fuel cell using H₂O₂ as oxidant, the concentration of the H₂O₂ at the outlet of the 3D flow channel in Figure 5.2 is determined as follows:

$$c_{\text{H}_2\text{O}_2}^f = c_{\text{H}_2\text{O}_2}^0 - \frac{i_{\text{cell}} A_{\text{cell}}}{F Q_a} \quad (48)$$

Where $c_{\text{H}_2\text{O}_2}^f$ is the H₂O₂ concentration at the outlet, $c_{\text{H}_2\text{O}_2}^0$ is the initial concentration of H₂O₂ at the inlet, and i_{cell} is the applied current density, A_{cell} is the area of the cell.

Hence, the overall concentration drop of H₂O₂, $\Delta c_{\text{H}_2\text{O}_2}$, in the 3D flow channel is:

$$\Delta c_{\text{H}_2\text{O}_2} = c_{\text{H}_2\text{O}_2}^0 - c_{\text{H}_2\text{O}_2}^f = \frac{i_{\text{cell}} A_{\text{cell}}}{F Q_a} \quad (49)$$

The H₂O₂ concentration drop at each section of the channel in the 3D flow model used in the 2D model is derived as follows:

$$\Delta c_{\text{H}_2\text{O}_2}^l = \Delta c_{\text{H}_2\text{O}_2} \times \frac{l}{L} \quad (50)$$

Where l is the length of each section from the inlet of the 3D flow channel and L is the entire length of the 3D flow channel.

Thus, the H₂O₂ concentration at each section of the channel is calculated as:

$$c_{\text{H}_2\text{O}_2}^l = c_{\text{H}_2\text{O}_2}^0 - \Delta c_{\text{H}_2\text{O}_2}^l \quad (51)$$

5.3.5.3 Charge balance

At the external boundary of the porous anode, the electric potential is taken as zero:

$$\phi_{a,s} = 0 \quad (52)$$

The boundary condition of the flux at the interface of the porous anode and the membrane is given as:

$$\begin{cases} \vec{N}_i = 0 \quad (i \neq H^+) \\ \vec{N}_{H^+} = -\frac{\vec{i}_{a,l}}{F} \end{cases} \quad (53)$$

At the porous anode and membrane interface, the ionic current density is regarded to be continuous:

$$\nabla \cdot \vec{i}_{a,l} = \nabla \cdot \vec{i}_m \quad (54)$$

The ionic potential at the porous anode and membrane interface, is taken to be continuous such that Donnan potential is not considered at this interface as follows:

$$\phi_{a,l} = \phi_m \quad (55)$$

Similarly, at the membrane and cathode catalyst layer interface, the ionic potential is expressed as:

$$\phi_{c,l} = \phi_m \quad (56)$$

To maintain the charge conservation, the electronic current density from the cathode is equal to the applied current density as follows:

$$\vec{i}_{c,s} = i \quad (57)$$

At the cathode catalyst layer and cathode diffusion layer interface, the boundary conditions for the species flux in relation to current density is given as:

$$N_{H_2O_2} = \frac{S_{HPRR}^{H_2O_2} j_{HPRR}}{n_{HPRR} F} + \frac{S_{HPOR}^{H_2O_2} j_{HPOR}}{n_{HPOR} F} \quad (58)$$

$$N_{H^+} = \frac{S_{HPRR}^{H^+} j_{HPRR}}{n_{HPRR} F} - \frac{S_{HPOR}^{H^+} j_{HPOR}}{n_{HPOR} F} \quad (59)$$

Where s , j , and n are stoichiometric coefficient, current density, and number of transferred electrons, respectively.

5.4 Cell voltage

The cell voltage, E_{cell} , is the electric potential difference between the cathode and the anode. It is therefore derived as follows:

$$E_{cell} = \phi_{c,s} - \phi_{a,s} \quad (60)$$

As mentioned earlier, the electric potential, $\phi_{a,s}$, at the external boundary of the porous anode is zero.

$$\text{Therefore, } E_{cell} = \phi_{c,s} \quad (61)$$

5.5 Model validation

For the e-fuel cell using oxygen as oxidant, the cell voltages at three different concentrations of V^{2+} ions are examined and compared with experimental data to validate the fidelity of the model. The e-fuel solution at 0.1 M, 0.3 M, and 0.5 M V^{2+} , each mixed with 3.0 M H_2SO_4 , are considered. The results, in comparison with experimental data, showing the polarization curves are displayed in Figure 5.3. The simulated cell polarization curves captures the trend of the experimental data. However, ignoring crossover seems to affect the accuracy of the results. This is evident as the observed deviation of the cell voltage between the model and experiment results becomes more obvious with the use of high e-fuel concentration as the current density increases.

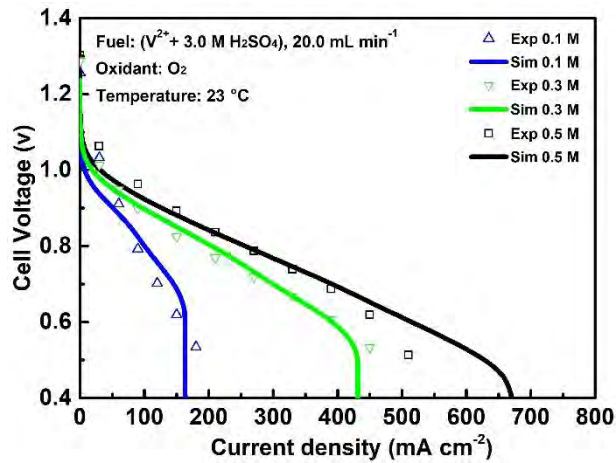


Figure 5.3 Model validation for the fuel cells using oxygen as oxidant [44].

For the model validation of the e-fuel cell using H_2O_2 as oxidant, mixed potential is considered in the modeling framework as the electrochemical reactions at the cathode simultaneously involve HPPR and HPOR. The model result when only HPPR is considered at the cathode is presented in blue line in Figure 5.4.

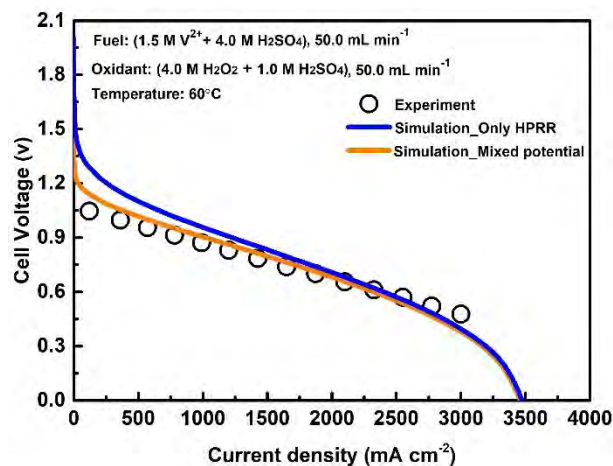


Figure 5.4 Model validation for the fuel cells using H_2O_2 as oxidant [16].

It is seen that the result, especially at the low current densities, is not consistent with the experimental data. With the consideration of mixed potential, by including HPOR at the cathode, larger voltage loss is observed at the low current densities, due to the mixed potential at the cathode, which

makes the predicted polarization curve of the cell to be in better fit with the experimental data. This therefore emphasizes the importance of considering mixed potential at the cathode during the modeling of e-fuel cells that use H_2O_2 as oxidant.

5.6 Summary

A two-dimensional mathematical model is presented to describe the transport behaviors and predict the performance of e-fuel cells. The model is first developed for the e-fuel cells that use pure oxygen as oxidant. Afterwards, the modeling framework is extended to the e-fuel cells that employ H_2O_2 as oxidant, where mixed potential is considered in the cathodic reactions. The model incorporates fluid flow and species transport coupled with electrochemical reactions and it is the first model framework to describe the underlying theoretical and working principle of these e-fuel cells using the exact domain structure of an e-fuel cell. The validation of the models through the comparison of the results from the model simulation with the experimental data obtained from the open literature is presented. This therefore provide suitable modeling framework for the simulation and optimization of the e-fuel cells to explore parameters that may be difficult to be examined via experimental studies.

5.7 References

1. D. Larcher and J.-M. Tarascon, Towards greener and more sustainable batteries for electrical energy storage, *J Nature chemistry*, 2015, 7, 19-29.
2. S. Chu, Y. Cui, and N. Liu, The path towards sustainable energy, *Nature materials*, 2017,16, 16-22.
3. R. C. Armstrong, C. Wolfram, K. P. De Jong, R. Gross, N. S. Lewis, B. Boardman, A. J. Ragauskas, K. Ehrhardt-Martinez, G. Crabtree and M. Ramana, The frontiers of energy, *Nature Energy*, 2016, 1, 1-8.
4. Y. Liu, O. C. Esan, Z. Pan and L. An, Machine learning for advanced energy materials, *Energy and AI*, 2021, 3, 100049.
5. Z. Yang, J. Zhang, M. C. Kintner-Meyer, X. Lu, D. Choi, J. P. Lemmon and J. Liu, Electrochemical energy storage for green grid, *Chemical reviews*, 2011, 111, 3577-3613.
6. J. W. Ager and A. A. Lapkin, Chemical storage of renewable energy, *Science*, 2018, 360, 707-708.
7. O. C. Esan, X. Shi, Z. Pan, X. Huo, L. An and T. Zhao, Modeling and Simulation of Flow Batteries, *Advanced Energy Materials*, 2020, 10, 2000758.
8. L. Carrette, K. Friedrich and U. Stimming, Fuel cells-fundamentals and applications, *Fuel cells*, 2001, 1, 5-39.
9. H. Chen, T. N. Cong, W. Yang, C. Tan, Y. Li and Y. Ding, Progress in electrical energy storage system: A critical review, *Progress in natural science*, 2009, 19, 291-312.

10. S. Changizian, P. Ahmadi, M. Raeesi and N. Javani, Performance optimization of hybrid hydrogen fuel cell-electric vehicles in real driving cycles, *International Journal of Hydrogen Energy*, 2020.
11. S. T. Thompson, B. D. James, J. M. Huya-Kouadio, C. Houchins, D. A. DeSantis, R. Ahluwalia, A. R. Wilson, G. Kleen and D. Papageorgopoulos, Direct hydrogen fuel cell electric vehicle cost analysis: System and high-volume manufacturing description, validation, and outlook, *Journal of Power Sources*, 2018, 399, 304-313.
12. D.-Y. Lee, A. Elgowainy, A. Kotz, R. Vijayagopal and J. Marcinkoski, Life-cycle implications of hydrogen fuel cell electric vehicle technology for medium-and heavy-duty trucks, *Journal of Power Sources*, 2018, 393, 217-229.
13. M. Granovskii, I. Dincer and M. A. Rosen, Economic and environmental comparison of conventional, hybrid, electric and hydrogen fuel cell vehicles, *Journal of Power Sources*, 2006, 159, 1186-1193.
14. H. Jiang, L. Wei, X. Fan, J. Xu, W. Shyy and T. Zhao, A Novel Energy Storage System Incorporating Electrically Rechargeable Liquid Fuels as the Storage Medium, *J Science Bulletin*, 2019, 64, 270-280.
15. O. C. Esan, X. Shi, Y. Dai, L. An and T. S. Zhao, Operation of Liquid E-fuel Cells Using Air as Oxidant, *Applied Energy*, 2022, 311, 118677.
16. O. C. Esan, X. Shi, Z. Pan, Y. Liu, X. Huo, L. An and T. Zhao, A high-performance H₂O₂-based fuel cell for air-free applications, *Journal of Power Sources*, 2022, 548, 232114.

17. X. Su, Z. Pan, L. An and Y. Yu, Mathematical modeling of direct Formate fuel cells incorporating the effect of ion migration, *International Journal of Heat and Mass Transfer*, 2021, 164, 120629.
18. F. Wandschneider, M. Küttinger, J. Noack, P. Fischer, K. Pinkwart, J. Tübke and H. Nirschl, A coupled-physics model for the vanadium oxygen fuel cell, *Journal of Power Sources*, 2014, 259, 125-137.
19. C. L. Chen, H. K. Yeoh and M. J. E. T. Chakrabarti, One Dimensional Mathematical Modelling of the All-Vanadium and Vanadium/Oxygen Redox Flow Batteries, *ECS Transactions*, 2015, 66, 1.
20. J. Noack, C. Cremers, D. Bayer, J. Tübke and K. Pinkwart, Development and characterization of a 280 cm² vanadium/oxygen fuel cell, *Journal of Power Sources*, 2014, 253, 397-403.
21. Z. Pan, B. Huang and L. An, Performance of a Hybrid Direct Ethylene Glycol Fuel Cell, *International Journal of Energy Research*, 2019, 43, 2583-2591.
22. L. An, T. Zhao, Z. Chai, L. Zeng and P. Tan, Modeling of the mixed potential in hydrogen peroxide-based fuel cells, *International journal of hydrogen energy*, 2014, 39, 7407-7416.
23. B. Zhang, Y. Lei, B. Bai and T. Zhao, A two-dimensional model for the design of flow fields in vanadium redox flow batteries, *International Journal of Heat and Mass Transfer*, 2019, 135, 460-469.
24. A. Shah, M. Watt-Smith and F. Walsh, A dynamic performance model for redox-flow batteries involving soluble species, *Electrochimica Acta*, 2008, 53, 8087-8100.

25. M. Messaggi, P. Canzi, R. Mereu, A. Baricci, F. Inzoli, A. Casalegno and M. Zago, Analysis of flow field design on vanadium redox flow battery performance: Development of 3D computational fluid dynamic model and experimental validation, *Applied energy*, 2018, 228, 1057-1070.
26. X. Zhou, T. Zhao, L. An, Y. Zeng and X. Yan, A vanadium redox flow battery model incorporating the effect of ion concentrations on ion mobility, *Applied Energy*, 2015, 158, 157-166.
27. K. Knehr, E. Agar, C. Dennison, A. Kalidindi and E. Kumbur, A transient vanadium flow battery model incorporating vanadium crossover and water transport through the membrane, *Journal of The Electrochemical Society*, 2012, 159, A1446.
28. M. Vynnycky, Analysis of a model for the operation of a vanadium redox battery, *Energy*, 2011, 36, 2242-2256.
29. S. Smith, I. Firdous, Q. Wang, S. Esmalla and W. A. Daoud, A two-dimensional model of the vanadium–cerium redox flow battery, *Electrochimica Acta*, 2019, 328, 135019.
30. R. O. Stroman and G. S. Jackson, Modeling the performance of an ideal $\text{NaBH}_4\text{--H}_2\text{O}_2$ direct borohydride fuel cell, *Journal of Power Sources*, 2014, 247, 756-769.
31. R. Chen and T. Zhao, Mathematical modeling of a passive-feed DMFC with heat transfer effect, *Journal of Power Sources*, 2005, 152, 122-130.
32. Y. Wang, D. Sauer, S. Koehne and A. Ersoez, Dynamic modeling of high temperature PEM fuel cell start-up process, *International journal of hydrogen energy*, 2014, 39, 19067-19078.

33. Z. Pan, Y. Bi and L. An, Mathematical modeling of direct ethylene glycol fuel cells incorporating the effect of the competitive adsorption, *Applied Thermal Engineering*, 2019, 147, 1115-1124.
34. X. Shi, X. Huo, Y. Ma, Z. Pan and L. An, Energizing Fuel Cells with an Electrically Rechargeable Liquid Fuel, *Cell Reports Physical Science*, 2020, 1, 100102.
35. Y. Wang and S. C. Cho, Analysis and three-dimensional modeling of vanadium flow batteries, *Journal of The Electrochemical Society*, 2014, 161, A1200.
36. M. Li, N. Bevilacqua, L. Zhu, W. Leng, K. Duan, L. Xiao, R. Zeis and P.-C. Sui, Mesoscopic modeling and characterization of the porous electrodes for vanadium redox flow batteries, *Journal of Energy Storage*, 2020, 32, 101782.
37. W. Yang, Y. He and Y. Li, Performance modeling of a vanadium redox flow battery during discharging, *Electrochimica Acta*, 2015, 155, 279-287.
38. M. Haghayegh, M. H. Eikani and S. Rowshanzamir, Modeling and simulation of a proton exchange membrane fuel cell using computational fluid dynamics, *International Journal of Hydrogen Energy*, 2017, 42, 21944-21954.
39. M. Ghasabehi, M. Ashrafi and M. Shams, Performance analysis of an innovative parallel flow field design of proton exchange membrane fuel cells using multiphysics simulation, *Fuel*, 2021, 285, 119194.
40. D. Cheddie and N. Munroe, Parametric model of an intermediate temperature PEMFC, *Journal of Power Sources*, 2006, 156, 414-423.

41. P. Hong, L. Xu, J. Li and M. Ouyang, Modeling of membrane electrode assembly of PEM fuel cell to analyze voltage losses inside, *Energy*, 2017, 139, 277-288.
42. S. Zhang, S. Beale, U. Reimer, M. Andersson and W. Lehnert, Polymer electrolyte fuel cell modeling-A comparison of two models with different levels of complexity, *International Journal of Hydrogen Energy*, 2020, 45, 19761-19777.
43. Q. Xu, T. Zhao and P. Leung, Numerical investigations of flow field designs for vanadium redox flow batteries, *Applied Energy*, 2013, 105, 47-56.
44. O. C. Esan, X. Shi, X. Su, Y. Dai, L. An, and T. S. Zhao, A Computational Model of a Liquid E-fuel Cell, *Journal of Power Sources*, 2021, 501, 230023.

Tables

Table 5-1 Cell geometry properties and porous media parameters.

Symbol	Parameter description	Value	Unit	Ref.
h	Height of the cell	0.02	m	[34]
w	Width of the cell	0.02	m	[34]
δ_a	Thickness of the porous anode	0.0015	m	[34]
ε	Porosity of the anode	0.8	-	[35]
d	Fibre diameter of the anode	10	μm	[24]
a_a	Active surface area of the anode	3.5×10^5	m^2/m^3	[36]
A	Cross-sectional area of the flow channel	1.0×10^{-6}	m^2	[34]
$\sigma_{a,s}$	Electrical conductivity of the anode	1000	S/m	[37]
σ_m	Ionic conductivity of the membrane	7.0	S/m	[38]
δ_{ccl}	Thickness of the CCL	10	μm	[39]
a_{ccl}	Active surface area of CCL	5.6×10^5	m^{-1}	[40]
$\sigma_{c,l}$	Proton conductivity of CCL	3.05	S/m	[41]
$\sigma_{c,s}$	Electrical conductivity of CCL	2000	S/m	[42]
δ_{cdl}	Thickness of CDL	260	μm	[39]

Table 5-2 E-fuel parameters and operating conditions for the cell using oxygen as oxidant.

Symbol	Parameter description	Value	Unit	Ref.
$c_{V^{2+}}^0$	Initial concentration of V^{2+}	500	mol m ⁻³	[34]
$c_{V^{3+}}^0$	Initial concentration of V^{3+}	500	mol m ⁻³	[34]
$c_{H^+}^0$	Initial proton concentration at the anode	6000	mol m ⁻³	[34]
δ_m	Thickness of the membrane	200	μm	[35]
μ	Viscosity of the e-fuel solution	0.005	Pa s	[25]
ρ	Density of the e-fuel solution	1680	Kg m ⁻³	[43]
T	Operating temperature	296	K	[34]
Q_a	Volumetric flow rate of e-fuel solution	20	mL min ⁻¹	[34]

Table 5-3 Electrolyte parameters and operating conditions for the cell using hydrogen peroxide as oxidant.

Symbol	Parameter description	Value	Unit	Ref.
$c_{V^{2+}}^0$	Initial concentration of V^{2+}	1500	mol m^{-3}	[16]
$c_{H^+}^0$	Initial proton concentration at the anode	8000	mol m^{-3}	[16]
$c_{H_2O_2}^0$	Initial concentration of H_2O_2	4000	mol m^{-3}	[16]
$c_{H_2O_2}^{ref}$	Reference concentration of H_2O_2	4000	mol m^{-3}	[16]
$c_{H^+}^0$	Initial concentration of H^+ at the cathode	2000	mol m^{-3}	[16]
$c_{H^+}^{ref}$	Initial concentration of H^+ at the cathode	2000	mol m^{-3}	[16]
δ_m	Thickness of the membrane	25	μm	[16]
μ	Viscosity of the e-fuel solution	0.005	Pa s	[25]
ρ	Density of the e-fuel solution	1680	Kg m^{-3}	[43]
T	Operating temperature	333	K	[16]
Q_a	Volumetric flow rate of e-fuel solution	50	mL min^{-1}	[16]

Table 5-4 Physicochemical parameters for the cell using oxygen as oxidant.

Symbol	Parameter description	Value	Unit	Ref.
k_a	Rate constant for the anodic reaction	7.0×10^{-8}	m s^{-1}	[27]
$\alpha_{1,a}$	Anodic charge transfer coefficient	0.5	-	[18]
E_a^0	Standard potential of the anode	- 0.255	V	[18]
E_c^0	Standard potential of the cathode	1.23	V	[18]
$i_{0,c}$	Cathodic exchange current density	1.0×10^{-7}	A m^{-2}	[38]
$\alpha_{2,c}$	Cathodic charge transfer coefficients	0.85	-	Assumed

Table 5-5 Physicochemical parameters for the cell using H₂O₂ as oxidant.

Symbol	Parameter description	Value	Unit	Ref.
k_a	Rate constant for the anodic reaction	7.0×10^{-8}	m s^{-1}	[27]
k_{HPOR}	Rate constant for HPOR	1.01×10^{-3}	$\text{mol m}^{-2} \text{s}^{-1}$	[22]
$\alpha_{1,a}$	Anodic charge transfer coefficient	0.5	-	[18]
α_{HPRR}	HPRR transfer coefficient	0.6	-	Assumed
α_{HPOR}	HPOR transfer coefficient	0.9	-	[22]
E_a^0	Standard potential of the anode	- 0.255	V	[18]
E_{HPRR}	Standard potential of HPRR	1.78	V	[21]
E_{HPOR}	Standard potential of HPOR	0.69	V	[22]
i_{HPRR}	HPRR exchange current density	1.0×10^{-7}	A m^{-2}	Assumed
i_{HPOR}	HPOR exchange current density	97.45	A m^{-2}	[22]

Table 5-6 Parameters for diffusion.

Symbol	Parameter description	Value (m²s⁻¹)	Ref.
$D_{V^{2+}}$	Diffusion coefficient of V ²⁺	2.4 x 10 ⁻¹⁰	[18]
$D_{V^{3+}}$	Diffusion coefficient of V ³⁺	2.4 x 10 ⁻¹⁰	[18]
D_{H^+}	Diffusion coefficient of proton	9.31 x 10 ⁻⁹	[18]
$D_{SO_4^{2-}}$	Diffusion coefficient of sulphate ion	1.07 x 10 ⁻⁹	[18]
$D_{H_2O_2}$	Diffusion coefficient of H ₂ O ₂	3.47 x 10 ⁻⁹	[33]

Chapter 6 Simulation and optimization of e-fuel cells using oxygen as oxidant

6.1 Introduction

To further predict and optimize the performance of the e-fuel cells that employ oxygen as oxidant, the numerical simulation of the developed model, using a computational platform, is presented here. The influence of varying the operating parameters such as vanadium-ion concentration, sulfuric acid concentration, and e-fuel flow rate; structural design parameters such as anode porosity, anode thickness, membrane thickness, and cathode catalyst layer thickness; and electrochemical parameters such as anodic and cathodic exchange current densities on the cell performance are examined via the numerical simulation. The concentration distribution of the e-fuel at the anode under some designated current densities, which may not be obtained by experimental approach, are presented to further provide substantial information useful for gaining in-depth insights into the operation of the e-fuel cell and the simulation of its performance. The simulation results reveal that the cell performance improves with increasing the vanadium-ion concentration, sulfuric acid concentration, and e-fuel flow rate. As for the aforementioned structural design parameters, the cell performance increases with these parameters except the membrane thickness where performance degradation is found. The model also reveals that the performance of the e-fuel cell improves with an increase in both the anodic and cathodic exchange current densities.

6.2 Simulation tool

The numerical simulation of the two-dimensional mathematical model is conducted by using COMSOL Multiphysics package which provides computational platform not only to obtain convincing modeling results, but to also predict and present the cell performance.

6.3 Results and discussion

6.3.2 Effect of operating parameters

6.3.2.1 Effect of the vanadium-ion concentration

The effect of the vanadium ion concentrations on the cell performance is examined in this section. The simulation results, presented in Figure 6.1, clearly show that the cell performance significantly improves when the vanadium-ion concentration in the e-fuel solution increases from 0.1 M to 0.5 M. This is because local concentrations of vanadium-ion at the anode of the cell increase with its initial concentration as a result of the enhanced mass transport of the vanadium-ion [1,2]. Consequently, the electrochemical kinetics of the anodic reaction is further improved, and concentration loss is considerably minimized due to the higher concentration of V^{2+} employed [3]. The simulated cell voltage mostly shows a linear drop with increasing current density before eventually falling off to the limiting current density of approximately 160, 423, and 650 mA cm⁻² for e-fuel containing 0.1 M, 0.3 M, and 0.5 M V^{2+} , respectively, apparently due to mass transport loss. This is attributed to the concentration gradient between the bulk e-fuel solution and the e-fuel on the anode surface, particularly at high current densities [4]. As the performance of the cell is significantly influenced by the e-fuel concentration, the presentation of the

V^{2+} concentration distribution at the anode is of paramount importance towards understanding and investigating the operations of the e-fuel cell.

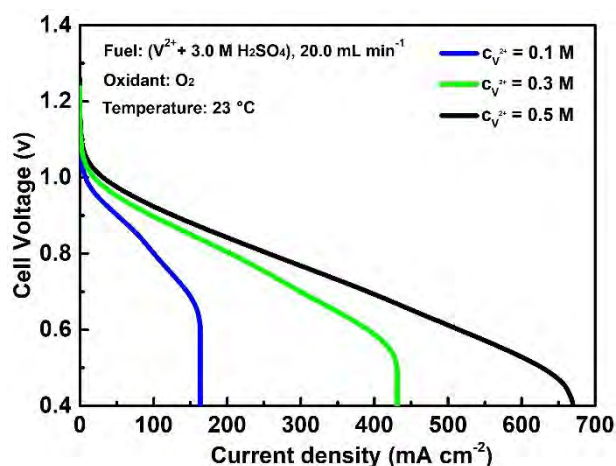


Figure 6.1 Effect of the vanadium-ion concentration on the cell performance.

To this end, the V^{2+} concentration distributions in the flow channel and the anode at designated current densities when the cell is fed with an e-fuel solution at the three different concentrations of V^{2+} are revealed. The trend and changes in the vanadium-ion concentration distributions at various current densities are presented to justify the concentration loss and the limiting current densities. While Figure 6.2a, Figure 6.3a, and Figure 6.4a show the polarization curves, Figure 6.2b, Figure 6.3b, and Figure 6.4b display the concentration distribution of the vanadium-ion at the anode compartment when the cell is fed with an e-fuel solution containing 0.1 M, 0.3 M, and 0.5 M V^{2+} , respectively.

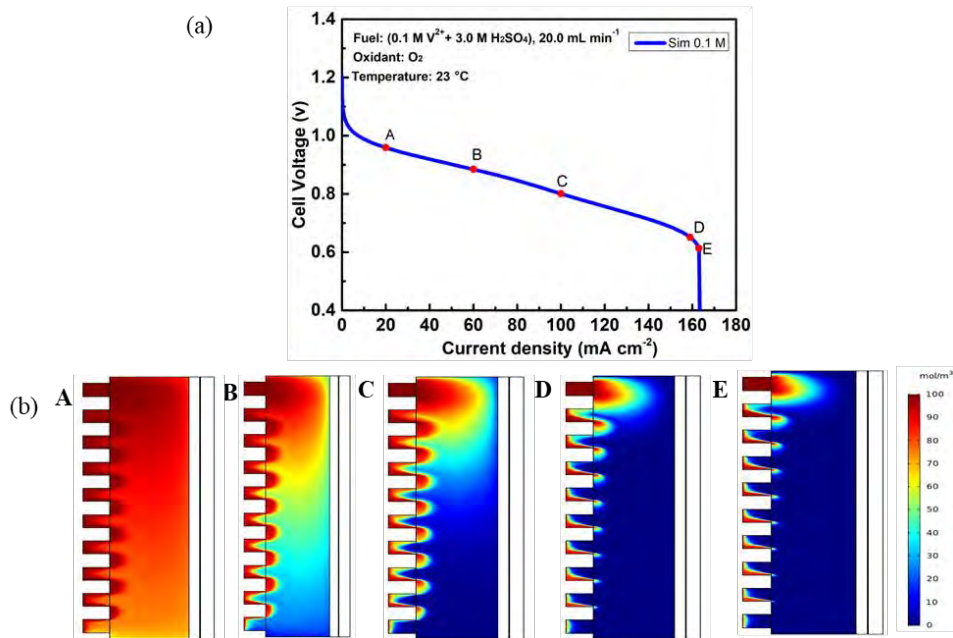


Figure 6.2 (a) Polarization curve of the cell using e-fuel of 0.1 M V^{2+} in 3.0 M H_2SO_4 . (b) Vanadium-ion concentration distributions at designated current densities – A. 20, B. 60, C. 100, D. 160, and E. 163 $mA\ cm^{-2}$.

It can be seen that at the three concentrations considered, the concentration distribution of vanadium-ion decreases in both the flow channels and the anodes with increasing current density. This is because the vanadium-ion is rapidly consumed at higher current density [5]. This therefore reveals and explains the reason the vanadium-ion is almost completely diminished when the e-fuel cell operates at current densities close to the limiting current density. Beyond the limiting current density, the concentration of the e-fuel is already extremely low or completely consumed at the anode compartment thereby leading to low reaction rate and large mass transport losses [6]. It therefore shows that a relatively high concentration of vanadium-ion at the anode is of beneficial effects on the cell performance.

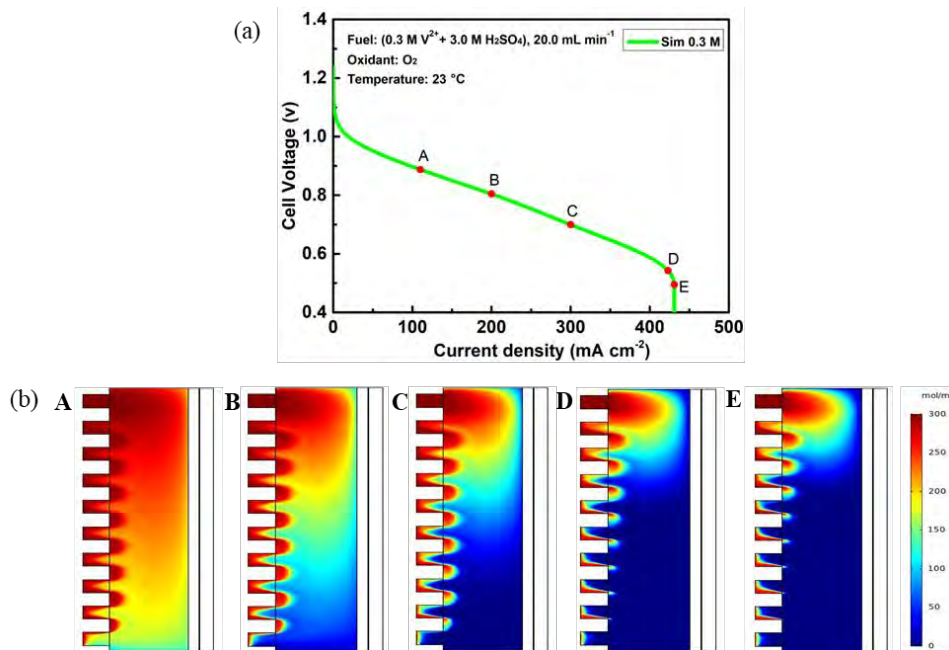


Figure 6.3 (a) Polarization curve of the cell using e-fuel of 0.3 M V^{2+} in 3.0 M H_2SO_4 . (b) Vanadium-ion concentration distributions at designated current densities – A. 100, B. 200, C. 300, D. 423, and E. 431 $mA\ cm^{-2}$.

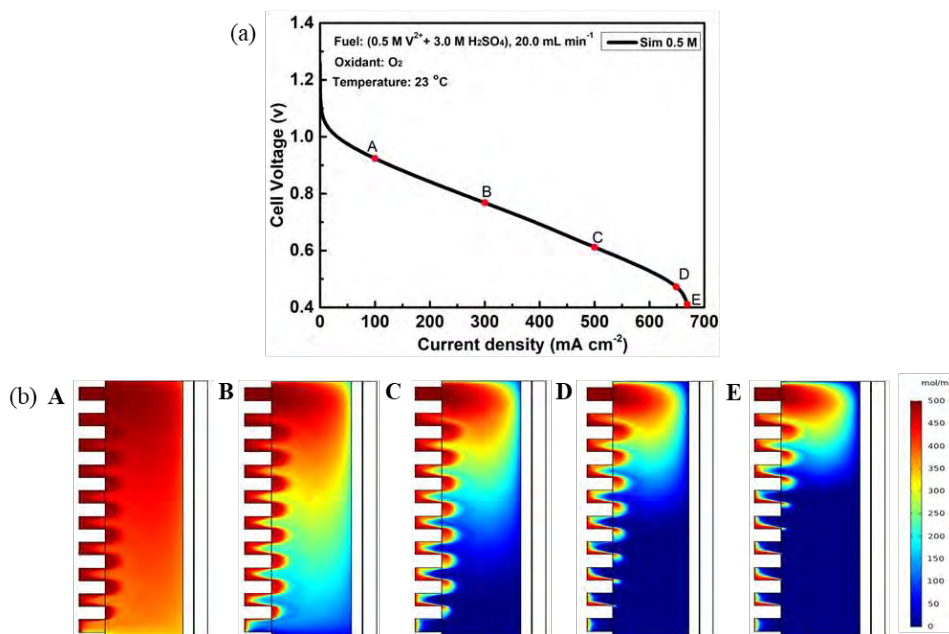


Figure 6.4 (a) Polarization curve of the cell using e-fuel of 0.5 M V^{2+} in 3.0 M H_2SO_4 . (b) Vanadium-ion concentration distributions at designated current densities – A. 100, B. 300, C. 500, D. 650, and E. 680 $mA\ cm^{-2}$.

6.3.2.2 Effect of the sulfuric acid concentration

The anode side of this e-fuel cell houses the fuel as well serves as the proton source due to the type of e-fuel solution (containing 0.5 M V^{2+} and H_2SO_4) employed in the cell operation. The sulfuric acid (H_2SO_4) functions as the supporting electrolyte, which can dissociate into H^+ and SO_4^{2-} at the anode compartment [4,7]. As mentioned earlier, the operation of the e-fuel cell involves protons (H^+) transport from the anode to the cathode and subsequently take part in the cathodic reactions. The sulfuric acid concentration in the e-fuel solution would therefore certainly influence the concentration of H^+ and thus the cell performance. Here, the effect of various concentration of H_2SO_4 on the cell performance is examined and presented in Figure 6.5. It is seen from that the cell performance improves with increasing the sulfuric acid concentration, which are more pronounced at higher current densities.

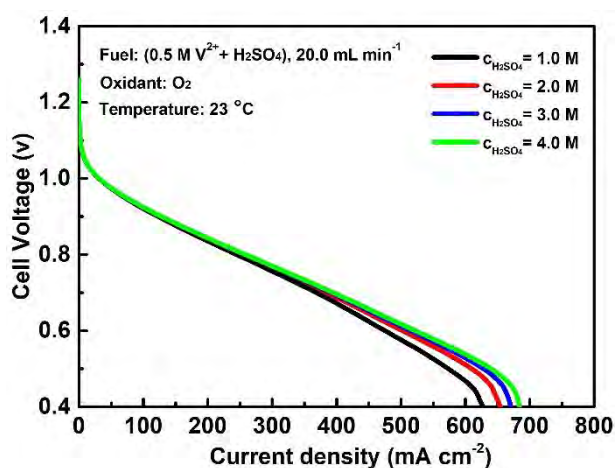


Figure 6.5 Effect of the sulfuric acid concentration on the cell performance.

For instance, at 600 mA cm⁻², the cell voltage increases from 0.461 V to 0.538 V when the sulfuric acid concentration is increased from 1.0 M to 4.0 M. In addition, the maximum current density also increases with the sulfuric

acid concentration. The performance improvement can be attributed to the fact that higher H_2SO_4 concentration leads to higher concentration distribution of H^+ at the anode and also near the membrane as evidenced in Figure 6.6. This therefore facilitates the transport of protons to the membrane thereby reducing ohmic loss [8,9]. The increase in cell voltage at high current densities indicates that a relatively high sulfuric acid concentration contributes to the upgrade of the cell performance. However, since the cell performance shows no obvious difference at the low to middle current density range with the increase of H_2SO_4 concentration, especially from 3.0 M to 4.0 M, it may not be suitable for the cell to use the e-fuel with a sulfuric acid concentration higher than 3.0 M.

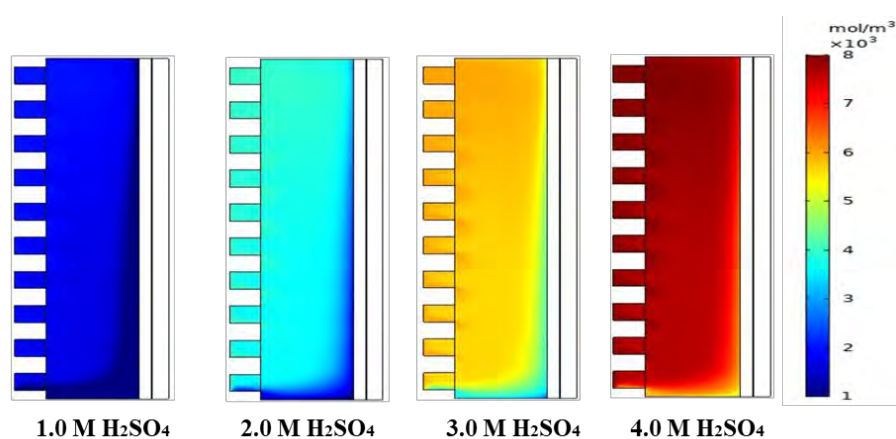


Figure 6.6 Concentration distribution of H^+ ions at the anode under various sulfuric acid concentrations at a current density of 600 mA cm^{-2} .

6.3.2.3 Effect of the e-fuel flow rate

In addition to the vanadium-ion and sulfuric acid concentration, the e-fuel flow rate is another significant operating condition which notably influences the electrochemical performance of the e-fuel cell. The e-fuel cell is energized through the circulation of the e-fuel, hence the mass transport

process as well as the performance of the cell would largely be affected by the e-fuel flow rate. In other words, the flow rate governs the magnitude of the e-fuel entering the cell and also determines the distribution of the e-fuel solution and electroactive species particularly at the anode [8,10]. In this section, the effect of different e-fuel flow rates ranging from 5.0 to 20.0 mL min⁻¹, on the cell performance are numerically examined. Considering an e-fuel solution containing 0.5 M V²⁺ and 3.0 M H₂SO₄, the cell performance obviously improves with increase in the e-fuel flow rate as shown in Figure 6.7.

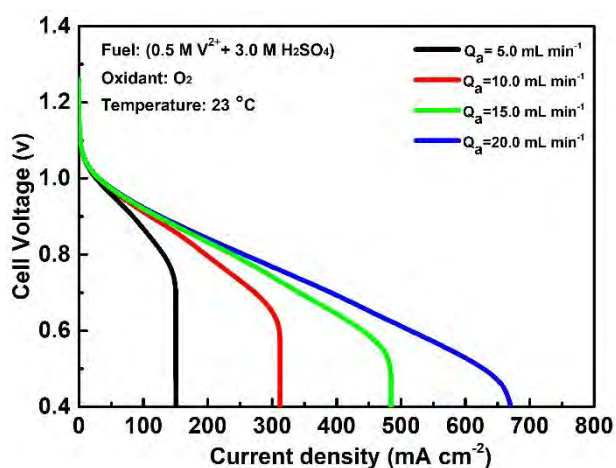


Figure 6.7 Effect of the e-fuel flow rate on the cell performance.

This is primarily as a result of the higher e-fuel flow rate that facilitates rapid and sufficient distribution of reactants at the anode as shown in Figure 6.8. It can also be seen that the limiting current density increases with the e-fuel flow rate resulting from higher flux of the e-fuel solution from the flow channel to the surface of the porous anode for rapid electrochemical reaction. In addition, higher e-fuel flow rates also favor rapid transport of protons to the cathode through the membrane [11]. However, operating the cell at higher flow rates would involve additional pump power consumption

which could deteriorates the efficiency of the e-fuel cell system [12]. This therefore highlights the need to further investigate the optimal e-fuel flow rate suitable for the operation of the cell.

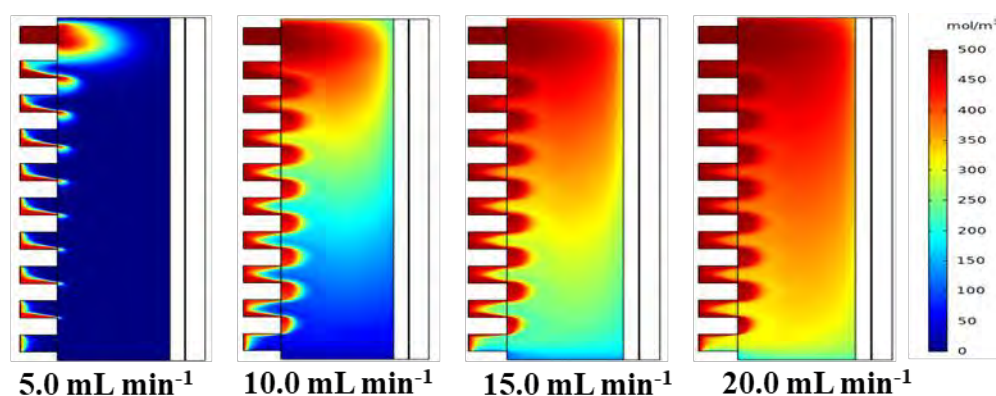


Figure 6.8 Vanadium-ion concentration distribution at the anode under different e-fuel flow rates at a current density of 150 mA cm^{-2} .

6.3.3 Effect of structural design parameters

6.3.3.1 Effect of the anode porosity

During the operation of the e-fuel cell, the electroactive species in the e-fuel solution are transferred through the pores of the anode to the active surface area of the anode for electrochemical reaction to take place. Thus, the porous structure and properties of the anode exert a considerable impact on the transport processes as well as the performance of the cell [8,13]. The effects of anode porosity, as one of the critical structural design variables, on the e-fuel cell performance is numerically examined in this section. Figure 6.9 displays the polarization curves to demonstrate the effect of various anode porosities on the cell performance. It is discovered that when the anode porosity increases from 0.70 to 0.85, the cell performance significantly improves. This is primarily because higher anode porosity promotes higher

permeability of the anode to fluid flow and further increases the supply and concentration distribution of reactant for the electrochemical reaction [14].

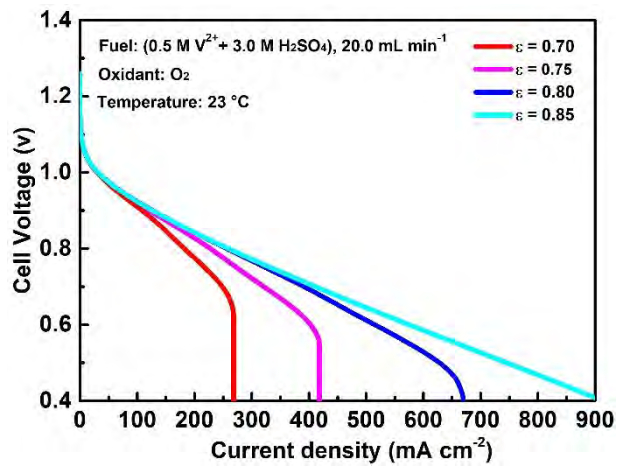


Figure 6.9 Effect of the anode porosity on the cell performance.

As a result, the depletion rate of the reactants at the anode is reduced, which is evidenced by Figure 6.10. The mass transport process is therefore improved with increase in anode porosity. Consequently, concentration polarization resulting from mass transport loss, which could limit the current density of the cell, is significantly reduced.

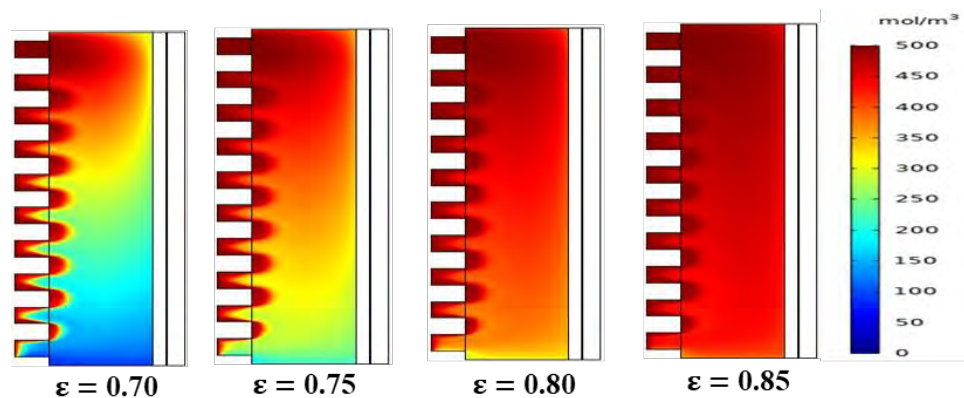


Figure 6.10 Vanadium-ion concentration distribution at the anode under different porosities at a current density of 100 mA cm^{-2} .

This is obvious at the highest anode porosity of 0.85 as no mass transport loss is observed before the cell voltage drops to 0.4 V. As a result, the overall overpotential at the anode decreases as the anode porosity increases to improve the cell performance [8]. In summary, an increase in anode porosity increases the fluid permeability and the effective diffusion coefficient of the anode which all contribute to an improvement in the overall cell performance.

6.3.3.2 Effect of the anode thickness

The thickness of anode is another significant structural design parameter that influences ionic transport pathway and thus the performance of the e-fuel cell [8]. For this reason, different anode thicknesses were employed, while the dimension of other components remain unchanged, to evaluate their influence on the cell performance. Figure 6.11 presents the simulated polarization behavior of the e-fuel cell at different anode thicknesses (1, 2, and 3 mm). This figure shows that the cell performance increases with the anode thickness. When the anode thickness is increased from 1 to 3 mm, the cell voltage is seen to increase at all the current densities. The observed improvement in the cell performance can be accredited to the fact that a thicker anode increases the total surface area of the anode, which is essential for rapid electrochemical reaction, thereby reducing activation overpotential [8,14]. The anode overpotential therefore decreases with increase of anode thickness from 1 mm to 3 mm to enhance the cell performance.

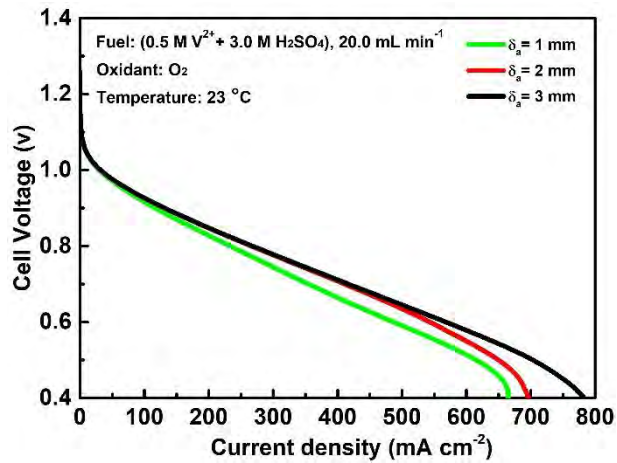


Figure 6.11 Effect of the anode thickness on the cell performance.

In addition, the increase of anode thickness is also found to alleviate e-fuel concentration loss at the anode, as demonstrated in Figure 6.12. However, a large increase of the anode thickness could elongate the charge transfer pathway in the anode which in turn would increase charge transport resistance and ohmic loss at the anode [15]. It can therefore be concluded that when a relatively thick anode is applied, the operations and performance of the cell improves.

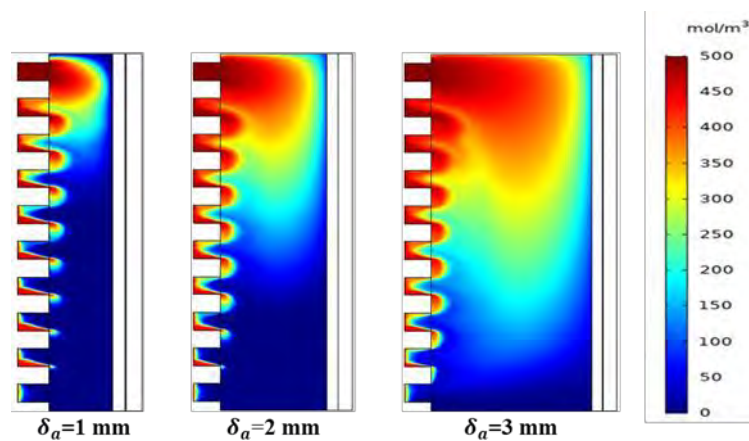


Figure 6.12 Vanadium-ion concentration distribution at the anode under different thicknesses at a current density of 650 mA cm^{-2} .

6.3.3.3 Effect of the membrane thickness

Membrane is a key component material in a typical fuel cell primarily to separate the anode and cathode compartments thereby reducing the crossover of electroactive species. Prevention of electrical short circuit within the cell is another significant function of the membrane [16-18]. Membrane properties such as thickness will heavily influence the transport of ions through the membrane and thus the overall cell performance. Therefore, the influence of membrane thickness on the e-fuel cell performance is studied in this section and the results at varying membrane thicknesses are shown in Figure 6.13. The cell voltage is found to decrease with the increase of membrane thickness at all the current density range considered. For instance, the cell voltage drops from 0.720 V to 0.469 V at a current density of 500 mA cm⁻² with respect to increase of membrane thickness from 50 μm to 400 μm.

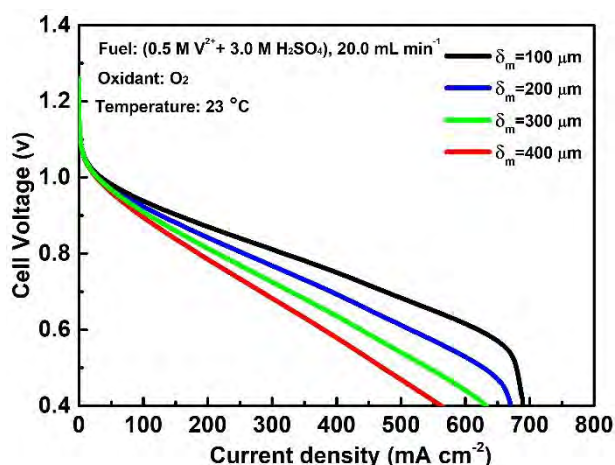


Figure 6.13 Effect of the membrane thickness on the cell performance.

The degradation of the cell performance is due to the increase in the distance of ionic transport in thicker membranes, which thereby leads to a higher membrane ohmic resistance and further increases the membrane

overpotential [19]. It is worth to mention that, at a membrane thickness higher than 200 μm , due to the large membrane overpotential induced by the increase of membrane ohmic resistance, no concentration polarization is observed before the cell voltage drops to 0.4 V. Conversely, when using thinner membranes, for instance between 50 μm and 200 μm , the cell is able to operate at current densities above 650 mA cm^{-2} due to the reduced ohmic loss. However, the drawbacks of employing thinner membranes could be its vulnerability to high crossover of species [20,21]. Although the crossover phenomena are not included this study due to the assumption that the membrane is only permeable to protons.

6.3.3.4 Effect of the cathode catalyst layer thickness

The cathode catalyst layer is one of the porous media, alongside the cathode diffusion layer, at the cathode compartment of the e-fuel cell. The cathode catalyst layer serves as the active site for the electrochemical reaction, oxygen reduction reaction, and also influences the transport of the oxidant at the cathode. The properties of the cathode catalyst layer such as its thickness will thus influence the transport process of ions, active surface area, and also affect the general performance of the cell [22,23]. Figure 6.14 displays the polarization curves of the cell when the cathode catalyst layer thickness is varied. An upgrade in the cell voltage is clearly seen throughout the whole current density range as thicker cathode catalyst layer is applied. At a high current density of 600 mA cm^{-2} , the cell voltage attained when varying the cathode catalyst layer thicknesses – 1, 10, 20, and 100 μm used for the cell simulation are 0.463 V, 0.528 V, 0.546 V, and 0.575 V, respectively.

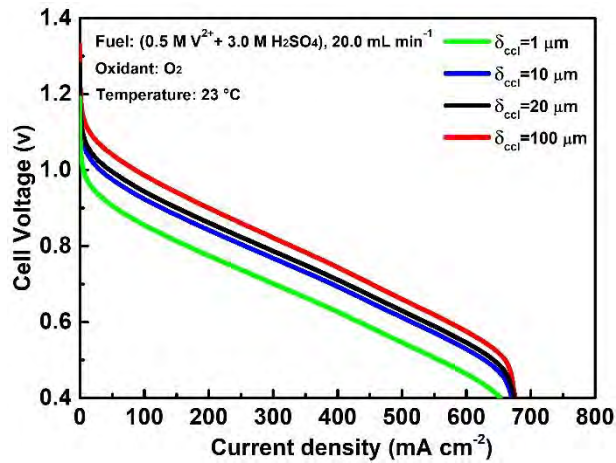


Figure 6.14 Effect of the cathode catalyst layer thickness on the cell performance.

This apparent performance improvement can be attributed to the fact that thicker cathode catalyst layer provides more surface area for the oxygen reduction reaction at the cathode which significantly reduces the cathode overpotential and therefore increases the cell voltage [24]. However, it should also be mentioned that employing a thicker cathode catalyst layer could elongate mass/charge transport process, such as the diffusion of species at the cathode, which may increase ohmic loss and charge transfer resistance to reduce the cell performance. To conclude, a relatively thick cathode catalyst layer significantly contributes to the improvement of the e-fuel cell performance.

6.3.4 Effect of electrochemical parameters

6.3.4.1 Effect of the anodic exchange current density

The performance of the e-fuel cell is also dependent on some electrochemical parameters. For instance, the exchange current density is generally incorporated to demonstrate the electrochemical activities existing at the anode. The influence of various anodic exchange current densities on

the cell performance are thus examined. It is seen in Figure 6.15 that the cell voltage improves with increase in anodic exchange current density.

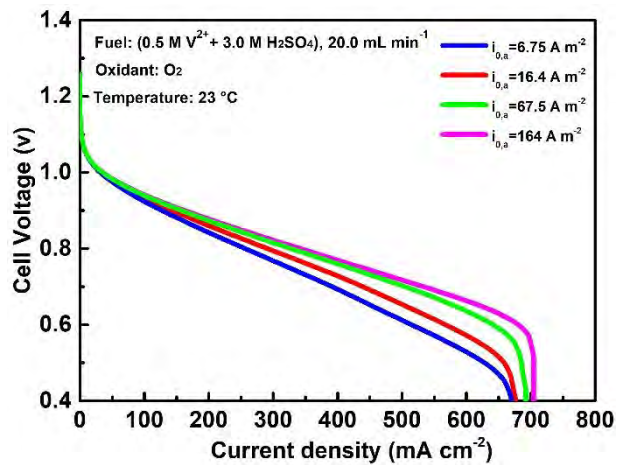


Figure 6.15 Effect of the anodic exchange current densities on the cell performance.

For example, the cell voltage rises from 0.528 V to 0.663 V at a current density of 600 mA cm⁻² following the increase of the anodic exchange current density from 6.75 A m⁻² to 164 A m⁻². This can be explained with the significant reduction of the anode overpotential as the anodic exchange current density increases [25]. The highest exchange current density yields the highest cell voltage for the entire current density range considered in this study. This therefore underscores the necessity of employing porous anodes of high electrochemical activity to enhance the exchange current densities of their electrochemical reactions.

6.3.4.2 Effect of the cathodic exchange current density

Electrochemical parameters such as the electrocatalytic activity of the cathode catalyst layer and the electrochemical reaction kinetics at the cathode also influence the overall performance of the e-fuel cell. For

example, the exchange current density is mostly used to demonstrate the electrochemical activities occurring at the cathode. At a current density of 600 mA cm^{-2} , the cell voltage is found to increase up to 0.667 V from 0.459 V when the cathodic exchange current density is increased from $1.0 \times 10^{-8} \text{ A m}^{-2}$ to $1.0 \times 10^{-5} \text{ A m}^{-2}$ as seen in Figure 6.16.

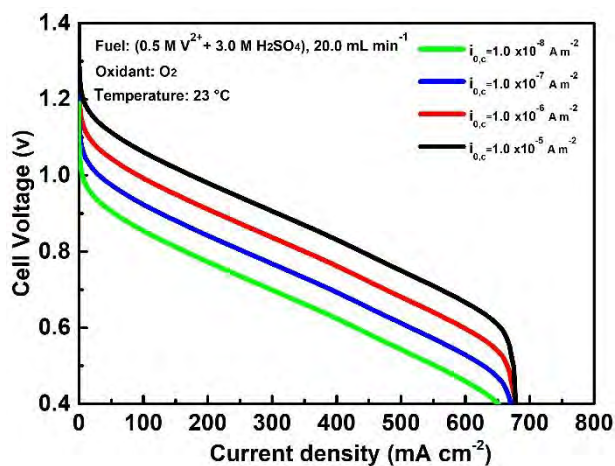


Figure 6.16 Effect of the cathodic exchange current densities on the cell performance.

This is also due to the corresponding reduction in the overpotentials at the cathode [26]. The highest exchange current density yields the highest cell voltage and superior cell performance for the entire current density range considered in this study. In comparison, the cathodic exchange current density is much lower than the anodic due to the slow reaction kinetics at the cathode. This therefore underscores the necessity of employing a catalyst material with excellent catalytic reactivity at the cathode to enhance the exchange current densities of their electrochemical reactions.

6.4 Summary

The numerical simulation of the model developed for the e-fuel cells that uses oxygen as oxidant is presented here. A computational platform is employed for the simulation process to predict and optimize the cell performance. The cell voltage is found to increase with the e-fuel concentration resulting from improved interfacial reaction kinetics and increase in the mass transport process, thereby reducing the concentration polarization. The concentration distributions of the e-fuel, which may not be obtained by experimental approach, show that a relatively high initial concentration results to high local concentration distribution of the e-fuel at the anode and that the e-fuel is rapidly consumed with increasing current density. Regarding the effects of the other operating conditions investigated, the cell performance improves with increase of the sulfuric acid concentration as well as the e-fuel flow rate. As for the structural design parameters, an increase in anode porosity, anode thickness, and cathode catalyst layer thickness all augment the cell performance, whereas the cell voltage is found to decrease as the membrane thickness increases. Furthermore, the exchange current density at the anode and the cathode was shown to markedly influence the performance of the e-fuel cell following the significant reduction in their overpotentials to improve the cell voltage as the exchange current densities increase. This study thus presents the essential basis that is invaluable for the extension and improvement of the e-fuel cell parameters towards optimizing the design and maximizing performance of the cell.

6.5 References

1. O. C. Esan, X. Shi, X. Su, Y. Dai, L. An, and T. S. Zhao, A Computational Model of a Liquid E-fuel Cell, *Journal of Power Sources*, 2021, 501, 230023.
2. A. Shah, M. Watt-Smith and F. Walsh, A dynamic performance model for redox-flow batteries involving soluble species, *Electrochimica Acta*, 2008, 53, 8087-8100.
3. X. Shi, X. Huo, Y. Ma, Z. Pan and L. An, Energizing Fuel Cells with an Electrically Rechargeable Liquid Fuel, *Cell Reports Physical Science*, 2020, 1, 100102.
4. K. Knehr, E. Agar, C. Dennison, A. Kalidindi and E. Kumbur, A transient vanadium flow battery model incorporating vanadium crossover and water transport through the membrane, *Journal of The Electrochemical Society*, 2012, 159, A1446-A1459.
5. A. Khazaeli, A. Vatani, N. Tahouni and M. H. Panjeshahi, Numerical investigation and thermodynamic analysis of the effect of electrolyte flow rate on performance of all vanadium redox flow batteries, *Journal of Power Sources*, 2015, 293, 599-612.
6. A. Tang, J. Bao and M. Skyllas-Kazacos, Studies on pressure losses and flow rate optimization in vanadium redox flow battery, *Journal of Power Sources*, 2014, 248, 154-162.
7. M. Vynnycky and M. Assunção, On the significance of sulphuric acid dissociation in the modelling of vanadium redox flow batteries, *Journal of Engineering Mathematics*, 2020, 123, 173-203.

8. X. Zhou, T. Zhao, L. An, Y. Zeng and L. Wei, Critical transport issues for improving the performance of aqueous redox flow batteries, *Journal of Power Sources*, 2017, 339, 1-12.
9. Y. Zhao, L. Liu, X. Qiu and J. Xi, Revealing sulfuric acid concentration impact on comprehensive performance of vanadium electrolytes and flow batteries, *Electrochimica Acta*, 2019, 303, 21-31
10. X. Ma, H. Zhang, C. Sun, Y. Zou and T. Zhang, An optimal strategy of electrolyte flow rate for vanadium redox flow battery, *Journal of Power Sources*, 2012, 203, 153-158.
11. F. Wandschneider, M. Küttinger, J. Noack, P. Fischer, K. Pinkwart, J. Tübke and H. Nirschl, A coupled-physics model for the vanadium oxygen fuel cell, *Journal of Power Sources*, 2014, 259, 125-137.
12. X.-Z. Yuan, C. Song, A. Platt, N. Zhao, H. Wang, H. Li, K. Fatih and D. Jang, A review of all-vanadium redox flow battery durability: Degradation mechanisms and mitigation strategies, *International Journal of Energy Research*, 2019, 43, 6599-6638.
13. K. Oh, S. Won and H. Ju, Numerical study of the effects of carbon felt electrode compression in all-vanadium redox flow batteries, *J Electrochimica Acta*, 2015, 181, 13-23.
14. E. Ali, H. Kwon, J. Choi, J. Lee, J. Kim and H. Park, A numerical study of electrode thickness and porosity effects in all vanadium redox flow batteries, *Journal of Energy Storage*, 2020, 28, 101208.
15. M. P. Manahan, Q. H. Liu, M. L. Gross and M. M. Mench, Carbon nanoporous layer for reaction location management and performance

enhancement in all-vanadium redox flow batteries, *Journal of Power Sources*, 2013, 222, 498-502.

16. X. Shi, O. C. Esan, X. Huo, Y. Ma, Z. Pan, L. An and T. Zhao, *Polymer Electrolyte Membranes for Vanadium Redox Flow Batteries: Fundamentals and Applications*, *Progress in Energy and Combustion Science*, 2021, 85, 100926.

17. X. Su, Z. Pan and L. An, Ion transport characteristics in membranes for direct formate fuel cells, *Frontiers in Chemistry*, 2020, 8, 765.

18. Y. Shi, C. Eze, B. Xiong, W. He, H. Zhang, T. Lim, A. Ukil and J. Zhao, Recent development of membrane for vanadium redox flow battery applications: A review, *Applied Energy*, 2019, 238, 202-224.

19. X. Shi, Y. Ma, X. Huo, O. C. Esan and L. An, Nafion Membranes for E-fuel Cell Applications, *International Journal of Green Energy*, 2021, 1-7.

20. S. Won, K. Oh and H. Ju, Numerical Analysis of Vanadium Crossover Effects in All-Vanadium Redox Flow Batteries, *Electrochimica Acta*, 2015, 177, 310-320.

21. H. Prifti, A. Parasuraman, S. Winardi, T. M. Lim and M. Skyllas-Kazacos, Membranes for redox flow battery applications, *Membranes*, 2012, 2, 275-306.

22. T. Zhao, C. Xu, R. Chen and W. Yang, Mass transport phenomena in direct methanol fuel cells, *Progress in Energy Combustion Science*, 2009, 35, 275-292.

23. Y. Sun, S. Polani, F. Luo, S. Ott, P. Strasser and F. Dionigi, Advancements in cathode catalyst and cathode layer design for proton exchange membrane fuel cells, *Nature communications*, 2021, 12, 1-14.

24. L. An and T. Zhao, Transport phenomena in alkaline direct ethanol fuel cells for sustainable energy production, *Journal of Power Sources*, 2017, 341, 199-211.
25. Q. Xu and T. S. Zhao, Fundamental models for flow batteries, *Progress in Energy and Combustion Science*, 2015, 49, 40-58.
26. L. An and R. Chen, Mathematical modeling of direct formate fuel cells, *Applied Thermal Engineering*, 2017, 124, 232-240.

Chapter 7 Simulation of e-fuel cells using H₂O₂ as oxidant

7.1 Introduction

One of the major targets of the current advances in the design and development of direct liquid fuel cells is to achieve high performance at low cost [1]. Considering the financial and time constraints of experimental studies to reveal and address some of the performance-limiting and performance-enhancing parameters of fuel cells, modeling and simulation have been identified as a cost-effective method to overcome these barriers [2,3]. Following the experimental investigations on the novel e-fuel/hydrogen peroxide cell discussed in Chapter 4 of this thesis, mathematical model, which has been validated with experimental data, have also been developed for this cell as presented in Chapter 5. Here, the numerical simulation of the model, using a computational platform, to predict and optimize the performance of the fuel cell is presented. It is worthy to mention that the simulation of this model incorporates mixed potential at the cathode, due to the consideration of hydrogen peroxide oxidation reaction (HPOR) in addition to hydrogen peroxide reduction reaction (HPRR) as the cathodic reactions.

7.2 Simulation tool

The numerical simulation of the mathematical model developed for the e-fuel/H₂O₂ cell is also conducted by using COMSOL Multiphysics which provides computational platform not only to obtain convincing modeling results, but to also predict and present the cell performance.

7.3 Results and discussion

7.3.1 Effect of the hydrogen peroxide concentration

In this chapter, hydrogen peroxide is employed, in lieu of gaseous oxygen or ambient, as oxidant at the cathode. Hence, H_2O_2 concentration is of crucial effect and paramount importance on the cell performance. Here, the effect of various concentration of H_2O_2 on the cell performance is examined and displayed in Figure 7.1. It is clearly shown that the cell performance improves with increasing the H_2O_2 concentration.

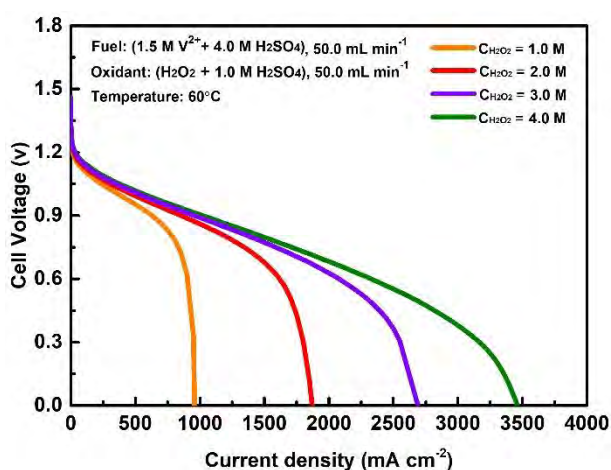


Figure 7.1 Effect of the hydrogen peroxide concentration on the cell performance.

The improvement in the cell performance with increase in the H_2O_2 concentration is majorly attributed to the enhanced mass transport of the reactive species. The presence of higher concentration of hydrogen peroxide at the active sites of the cathode catalyst layer also reduces concentration loss and further improves the cell performance. This is evidenced in Figure 7.2 where the H_2O_2 is rapidly exhausted at the cathode compartment when low concentration is employed thereby leading to low reaction rate and large mass transport loss at a current density of 900 mA cm^{-2} . In addition, the

electrochemical kinetics of the H_2O_2 reduction reaction is improved at higher hydrogen peroxide concentration [4,5]. The maximum current density of the cell also increases with the hydrogen peroxide concentration. For example, the maximum current density of the cell is observed to significantly increase from 900 to 3480 mA cm^{-2} when the H_2O_2 concentration is increased from 1.0 M to 4.0 M.

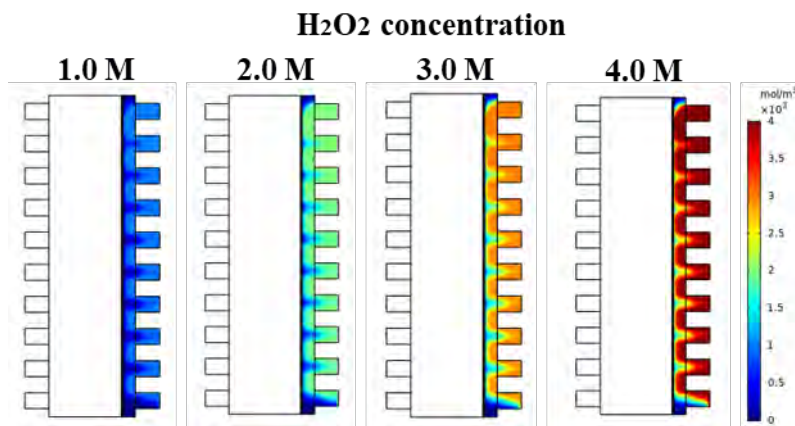


Figure 7.2 Concentration distribution of H_2O_2 at the cathode at a current density of 900 mA cm^{-2} .

7.3.2 Effect of the sulfuric acid concentration

The hydrogen peroxide solution at the cathode is considered to be acidified using sulfuric acid [6]. The influence of the sulfuric acid concentration at the cathode on the cell performance is therefore examined in this section. The simulated polarization curves of the cell when the sulfuric acid concentration is increased from 0.5 M to 2.0 M is depicted in Figure 7.3. It is seen that the cell voltage increases with increasing the sulfuric acid concentration. The increase in the cell performance is more significant when the sulfuric acid concentration is increased from 0.5 M to 1.5 M to produce

an increase in the cell voltage from 0.222 V to 0.532 V at a current density of 2800 mA cm^{-2} .

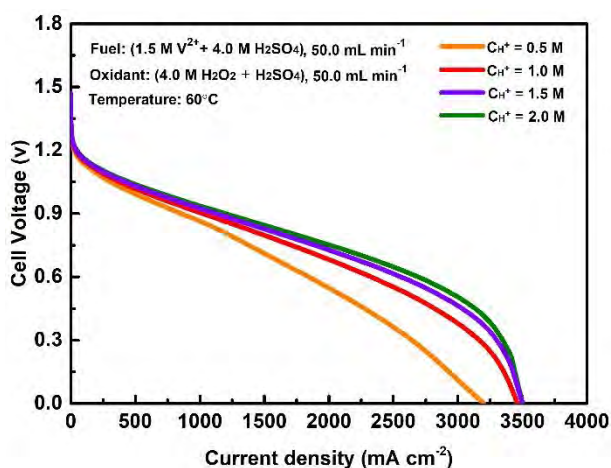


Figure 7.3 Effect of the sulfuric acid concentration on the cell performance.

The performance improvement of the cell can be attributed to the fact that higher sulfuric acid concentration produces higher concentration of H^+ at the active sites of cathode catalyst layer [7]. Following this, the electrochemical reaction at the cathode will be enhanced as H^+ is an indispensable reactant for hydrogen peroxide reduction reaction. The increase in cell voltage at high current densities indicates that a relatively high sulfuric acid concentration can significantly contribute to the improvement of the cell performance. It can be seen that increasing the sulfuric acid concentration from 1.5 M to 2.0 M does not offer significant improvement to the cell performance. The relative increase in the cell voltage at high current densities indicates that a relatively high sulfuric acid concentration at the cathode is sufficient to ensure the cell with good performance.

7.3.3 Effect of the membrane thickness

Membrane is a vital component material in this liquid fuel cell as it separates the anode and cathode sides and also provides pathways for ions transport across the two sides of the cell [8,9]. The thickness of the membrane employed in the operation of this fuel cell will definitely influence the transport of ions through the membrane and thus the overall cell performance. The influence of membrane thickness on the performance of this H₂O₂-based fuel cell is therefore examined here. The simulation results obtained from the use of different membrane thicknesses in the cell are displayed in Figure 7.4.

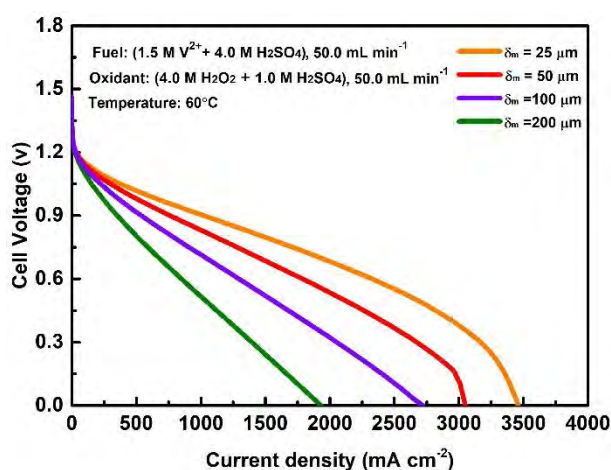


Figure 7.4 Effect of the membranes thickness on the cell performance.

The results show that the cell voltage decreases with the increase of membrane thickness at all the current density regions. For example, the cell voltage decreases from 0.797 V to 0.242 V at an operating current density of 1500 mA cm⁻² when the membrane thickness is increased from 25 μm to 200 μm. The decrease is ascribed to the elongated distance for ionic transport in thicker membrane, which leads to higher membrane ohmic resistance and further increase the membrane overpotential [10,11]. This

therefore indicates that thinner membranes are more suitable for the operation of the cell towards achieving enhanced performance. However, the use of thinner membranes in this all-liquid fuel cell could result to high crossover of the reactive species from one side to another [12]. Although crossover of the reactants are not considered in this study due to the assumption that the membrane is only permeable to protons.

7.3.4 Effect of the anode active surface area

The performance of the e-fuel cell is also dependent on the active surface area of the electrodes. This is because, during the operation of fuel cells, the electrochemical reactions occur on the electrode surface. As for this e-fuel cell, a catalyst-free electrode is employed as the anode. The effect of the active surface area of the anode on the e-fuel cell performance is numerically investigated in this section. Figure 7.5 displays the simulated polarization curves to demonstrate the effect of various active surface area of the anode on the cell performance.

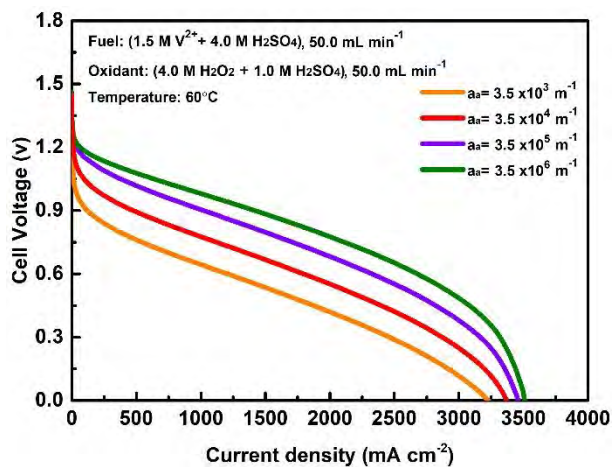


Figure 7.5 Effect of the anode active surface area on the cell performance.

It is found that the cell voltage increases at all the current density regions when the active surface area of the anode increases from $3.5 \times 10^3 \text{ m}^{-1}$ to $3.5 \times 10^6 \text{ m}^{-1}$. For instance, the cell voltage is seen to rise from 0.117 V to 0.485 V at a current density of 3000 mA cm^{-2} following the increase of the active surface area of the anode from $3.5 \times 10^3 \text{ m}^{-1}$ to $3.5 \times 10^6 \text{ m}^{-1}$. This is primarily because high active surface area enhances the electrochemical reactions at the anode which in turn reduces activation loss at the anode [13,14]. The largest active surface area of the anode yields the highest cell voltage for the entire current density range considered in this study. This therefore reveals the significance of employing anode with larger active surface area for the fuel cell.

7.3.5 Effect of the cathode active surface area

At the cathode, the electrochemical H_2O_2 reduction reactions take place on the catalyst layer. The effects of the active surface area of the cathode catalyst layer on the e-fuel cell performance is also numerically examined. Figure 7.6 presents the obtained cell voltage at different active surface area of the cathode. The figure apparently shows that the cell performance increases with the active surface area of the cathode. At a current density of 3000 mA cm^{-2} , the cell voltage is found to increase from 0.201 V to 0.380 V when the active surface area of the cathode increases $5.6 \times 10^2 \text{ m}^{-1}$ to $5.6 \times 10^5 \text{ m}^{-1}$. The improvement in the cell voltage with increase in active surface area of the cathode can be attributed to the fact that larger active surface area facilitates rapid electrochemical activity at the cathode which in turn reduces kinetic loss at the cathode [15]. The largest active surface area of the cathode produces the highest cell voltage and superior cell

performance. This therefore indicates the importance of employing cathode with larger active surface area for the fuel cell.

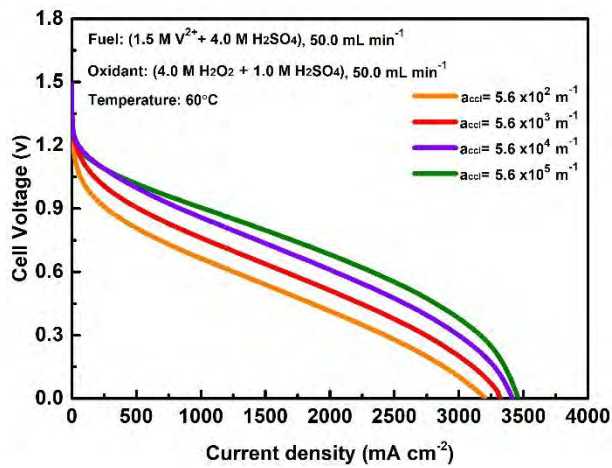


Figure 7.6 Effect of the cathode active surface area on the cell performance.

7.4 Summary

The numerical simulation of the two-dimensional mathematical model developed for e-fuel/H₂O₂ cell, using a computational platform, to predict and optimize the cell performance is presented. The simulation reveals the concentration distribution of H₂O₂ at the cathode, showing that its limited mass transport at low concentration limits the cell performance. The concentration of the sulfuric acid at the cathode on the cell performance is also studied. The simulation result shows that the cell performance increases with sulfuric acid concentration. The cell voltage is also found to increase with the use of thinner membranes. Furthermore, the active surface area of the anode and cathode are also presented to significantly influence the cell performance such that larger active surface area of the electrodes enhances electrochemical reactions which in turn reduces overpotential to improve the overall performance of the cell.

7.5 References

1. N. Shaari, S. K. Kamarudin, R. Bahru, S. H. Osman and N. A. I. Md Ishak, Progress and Challenges: Review for Direct Liquid Fuel Cell, *International Journal of Energy Research*, 2021, 45, 6644-6688.
2. O. C. Esan, X. Shi, Z. Pan, X. Huo, L. An, and T. Zhao, Modeling and Simulation of Flow Batteries, *Advanced Energy Materials*, 2020, 10, 2000758.
3. J. Desantes, R. Novella, B. Pla and M. Lopez-Juarez, A modeling framework for predicting the effect of the operating conditions and component sizing on fuel cell degradation and performance for automotive applications, *Applied Energy*, 2022, 317, 119137.
4. Z. Pan, Y. Bi and L. An, Performance Characteristics of a Passive Direct Ethylene Glycol Fuel Cell with Hydrogen Peroxide as Oxidant, *Applied Energy*, 2019, 250, 846-854.
5. Y. Li, Y. He and W. Yang, A High-Performance Direct Formate-Peroxide Fuel Cell with Palladium–Gold Alloy Coated Foam Electrodes, *Journal of Power Sources*, 2015, 278, 569-573.
6. O. C. Esan, X. Shi, Z. Pan, Y. Liu, X. Huo, L. An and T. Zhao, A high-performance H₂O₂-based fuel cell for air-free applications, *Journal of Power Sources*, 2022, 548, 232114.
7. Z. Pan, Y. Bi and L. An, Mathematical modeling of direct ethylene glycol fuel cells incorporating the effect of the competitive adsorption, *Applied Thermal Engineering*, 2019, 147, 1115-1124.

8. Z. Pan, B. Huang and L. An, Performance of a Hybrid Direct Ethylene Glycol Fuel cell, *International Journal of Energy Research*, 2019, 43, 2583-2591.
9. Y. Shi, C. Eze, B. Xiong, W. He, H. Zhang, T. Lim, A. Ukil and J. Zhao, Recent development of membrane for vanadium redox flow battery applications: A review, *Applied Energy*, 2019, 238, 202-224.
10. X. Shi, Y. Ma, X. Huo, O. C. Esan and L. An, Nafion Membranes for E-fuel Cell Applications, *International Journal of Green Energy*, 2021, 1-7.
11. X. Zhou, T. Zhao, L. An, Y. Zeng and L. Wei, Modeling of ion transport through a porous separator in vanadium redox flow batteries, *Journal of Power Sources*, 2016, 327, 67-76.
12. M. Chatenet, Tailoring membranes, *Nature Energy*, 2019, 4, 261-262.
13. X. Zhou, T. Zhao, L. An, Y. Zeng and L. Wei, Critical transport issues for improving the performance of aqueous redox flow batteries, *Journal of Power Sources*, 2017, 339, 1-12.
14. X. Zhou, T. Zhao, Y. Zeng, L. An and L. Wei, A highly permeable and enhanced surface area carbon-cloth electrode for vanadium redox flow batteries, *Journal of Power Sources*, 2016, 329, 247-254.
15. X. Su, Z. Pan, L. An and Y. Yu, Mathematical modeling of direct formate fuel cells incorporating the effect of ion migration, *International Journal of Heat and Mass Transfer*, 2021, 164, 120629.

Chapter 8 Conclusions and future work

Direct liquid fuel cells have piqued increasing research interest and applications for clean and efficient power generation due to their promising features and compelling characteristics. Towards attaining a major advancement of this fuel cell technology, this thesis presents experimental and numerical investigations on the operation and performance of direct liquid fuel cells fed with an electrically rechargeable liquid fuel at the anode while exploring various oxidants at the cathode. Detailed information on the procedures and discussion of the results obtained during the study are presented in Chapters 2-7 of this thesis. The summary of the results are as follows:

8.1 Conclusions

- 1) A direct liquid fuel cell, which eliminate the use of catalyst material at the anode and fed with an electrically rechargeable liquid fuel, is developed. The structural design of the cell consist of a proton exchange membrane sandwiched between a catalyst-free graphite-felt anode and a conventional fuel cell cathode. The operation and performance of the e-fuel cell is explored with the use of air as oxidant, while taking the use of pure oxygen at the cathode as performance benchmark. The effects of operating parameters on the performance of the cell with the use of air as the oxidant are examined. The experimental result shows that the cell attains an open-circuit voltage (OCV) of 1.25 V with the use of air at the cathode which is comparable to an OCV of 1.26 V obtained when the cathode is fed with pure oxygen. The cell is able to boost of a peak power density of 168.3 mW cm⁻², at room temperature, which outperforms a

number of conventional direct liquid fuel cells, including those fed with oxygen at the cathode. Furthermore, an energy efficiency of 26.4 % is achieved by the e-fuel cell with the use of air as oxidant which also outperforms some conventional direct liquid fuel cells that uses air as oxidant.

- 2) To further boost the performance of the e-fuel cell and more importantly realize its application in airtight environments, such as space propulsion and underwater power systems, hydrogen peroxide (H_2O_2) is considered as an alternative oxidant, in place of gaseous oxygen or ambient air. The novel e-fuel/ H_2O_2 fuel cell exhibits a peak power density of $1456.0 \text{ mW cm}^{-2}$ at $60 \text{ }^\circ\text{C}$, which is 70 % higher than the use of oxygen (857.0 mW cm^{-2}). A maximum current density exceeding 3000 mA cm^{-2} is also achieved by the cell. The performance of the cell at various operating conditions including the varying hydrogen peroxide concentration, sulfuric acid concentration, vanadium ion concentration, operating cell temperature, Nafion membrane thicknesses, and its constant-current discharge characteristics are also investigated. Furthermore, the cell achieved a stable performance even after it was refueled 10 times while discharging at a constant current of 10 mA cm^{-2} under an operating temperature of $60 \text{ }^\circ\text{C}$.
- 3) To better understand and garner more insights on the underlying theoretical and working principle of these e-fuel cells, a two-dimensional mathematical model is developed. The model incorporates fluid flow and mass/charge transport coupled with the electrochemical reactions using the actual structural domain of an e-fuel cell, eliminating

catalyst and diffusion layers at the anode. The model is first developed for the e-fuel cells using pure oxygen as oxidant. Afterwards, the modeling framework is extended to the e-fuel cells that employ hydrogen peroxide as oxidant, where mixed potential is considered in the modeling of the reactions at the cathode. The validation of the model developed for both cells through the comparison of the results with experimental data shows a good agreement. With the consideration of mixed potential in the modeling of the e-fuel/H₂O₂ cell, by including hydrogen peroxide oxidation reaction at the cathode, large voltage loss is observed at the low current densities, which makes the predicted polarization curve of the cell to be in better agreement with the experimental data. This therefore emphasizes the importance of considering mixed potential at the cathode during the modeling of e-fuel cells that use hydrogen peroxide as oxidant.

- 4) The performance of the e-fuel cells that uses oxygen as oxidant is predicted and optimized through the simulation of the two-dimensional mathematical model developed for the cell. A computational platform is employed for the numerical simulation process of the model. The cell voltage is found to increase with the e-fuel concentration. The concentration distribution of the e-fuel at the anode under some designated current densities, which may not be obtained by experimental approach, are presented to further provide substantial information useful for gaining in-depth insights into the operation and performance of the e-fuel cell. The simulation reveals that cell performance improves with increase of the sulfuric acid concentration as well as the e-fuel flow rate.

As for structural design parameters, an increase in anode porosity, anode thickness, and cathode catalyst layer thickness all boost the cell performance, whereas the cell voltage is found to decrease with increasing membrane thickness. Increase of the exchange current density at the anode and the cathode is found to improve the performance of the e-fuel cell.

- 5) The numerical simulation of the two-dimensional mathematical model developed for the e-fuel cells that uses hydrogen peroxide as oxidant to predict and optimize the performance of the cell is presented. The simulation reveals the concentration distribution of hydrogen peroxide at the cathode, showing its limited mass transport at low concentration limits the cell performance. The concentration of the sulfuric acid at the cathode on the cell performance is also studied. The simulation result shows that cell performance increases with sulfuric acid concentration. The cell voltage is found to increase with the use of thinner membranes. Furthermore, the active surface area of the anode and cathode are also revealed to significantly influence the cell performance such that larger active surface area of the electrodes enhances electrochemical reactions which in turn improve the overall performance of the cell.

8.2 Future work

Experimental and numerical studies have been conducted to investigate the operation and performance of direct liquid fuel cells fed with an electrically rechargeable liquid fuel at the anode while exploring various oxidants at the cathode. The effects of various operating conditions, structural and design parameters on the cell performance for power generation have been

revealed. In addition to these, the following works will be conducted in the future:

- i) With the use of oxygen as oxidant in the e-fuel cell, sluggish oxygen reduction reaction at the cathode side is a major limiting factor to cell performance. To further improve the e-fuel cell performance, electrocatalyst material with better catalytic reactivity for oxygen reduction reaction at the cathode will be fabricated to enhance the cell performance.
- ii) For the e-fuel cells using hydrogen peroxide as oxidant, high performance at low cost is of great importance to achieve the commercialization of this system. Therefore, a cathode with lower Pt/C loading will be fabricated and employed in the operation of the fuel cell to further reduce its fabrication cost.
- iii) Besides the transport of only protons through the membrane of the e-fuel cells, the operation of the cell in practical scenario involves inevitable transport of the reacting species across the membrane. Mathematical model will be developed to capture the crossover phenomena and numerical simulation of the model will be employed to reveal the effects of crossover on the cell performance.
- iv) Due to the wide material selectivity for e-fuel, other materials, instead of vanadium ions, will be considered and characterized for the operation of e-fuel cell. The performance of new e-fuel in the operation of fuel cells will be examined and compared to the vanadium-based e-fuel to further ascertain the flexibility and performance of the fuel cell when operated with different e-fuels.

**Appendix I Publications during PhD study at The Hong Kong
Polytechnic University**

Journal articles

1. **O. C. Esan**, X. Shi, Z. Pan, X. Huo, L. An, & T.S. Zhao. “Modeling and Simulation of Flow Batteries”. *Advanced Energy Materials*, 2020, **10**, 2000758.
2. **O. C. Esan**, X. Shi, Y. Dai, L. An, & T. S. Zhao. “Operation of Liquid E-fuel Cells Using Air as Oxidant”. *Applied Energy*, 2022, **311**, 118677.
3. **O. C. Esan**, X. Shi, X. Su, Y. Dai, L. An, & T. S. Zhao. “A Computational Model of a Liquid E-fuel Cell”. *Journal of Power Sources*, 2021, **501**, 230023.
4. **O. C. Esan**, X. Shi, Z. Pan, Y. Liu, X. Huo, L. An, & T. S. Zhao. “A high-performance H₂O₂-based fuel cell for air-free applications”. *Journal of Power Sources*, 2022, **548**, 232114.
5. X. Shi[†], **O. C. Esan**[†], X. Huo, Y. Ma, Z. Pan, L. An, & T. S. Zhao. “Polymer Electrolyte Membranes for Vanadium Redox Flow Batteries: Fundamentals and Applications”. *Progress in Energy and Combustion Science*, 2021, **85**, 100926. († Co-first author)